Harmonic Current Summation Using Probabilistic Bivariate Modelling

MAREK JARKOVOI

**TAL
TECH**
PRESS

TALLINN UNIVERSITY OF TECHNOLOGY
School of Engineering
Department of Electrical Power Engineering and Mechatronics
This dissertation was accepted for the defence of the degree 15/11/2019

Supervisor: Prof. Lauri Kütt
                            Department of Electrical Power Engineering and Mechatronics
                            Tallinn University of Technology
                            Tallinn, Estonia

Co-supervisor: Toomas Vinnal, PhD
                            Department of Electrical Power Engineering and Mechatronics
                            Tallinn University of Technology
                            Tallinn, Estonia

Opponents: Alexander Novitskiy, PhD
                            Senior Researcher
                            Faculty of Electrical Engineering and Information Technology
                            Technische Universität Ilmenau
                            Germany

                            Petr Toman, PhD
                            Head of the department
                            Department of Electrical Power Engineering
                            Brno University of Technology
                            Czech Republic

Defence of the thesis: 16/12/2019, Tallinn

Declaration:
Hereby I declare that this doctoral thesis, my original investigation and achievement, submitted for the doctoral degree at Tallinn University of Technology has not been submitted for doctoral or equivalent academic degree.

Marek Jarkovoi

                            _____
                                                    signature

Vooluharmoonikute summeerimine rakendades kahe muutujaga tõenäosuslikku modelleerimist

MAREK JARKOVOI

Contents

List of Publications

The list of author's publications, on the basis of which the thesis has been prepared:

I   Vinnal, T.; **Jarkovoi, M**.; Kütt, L. (2018). Harmonic Currents and Voltages in LV Networks of Estonia: Measurement Results, Case Studies. RTUCON2018, 59th International Scientific Conference on Power and Electrical Engineering of Riga Technical University. Riga, Latvia. November 12-14, 2018. Riga: IEEE, 1−7.

II Niitsoo, J.; **Jarkovoi, M**.; Taklaja, P.; Klüss, J.; Palu, I. (2015). Power Quality Issues Concerning Photovoltaic Generation in Distribution Grids. Smart Grid and Renewable Energy, 6 (6), 148−163.10.4236/sgre.2015.66014.

III Iqbal, M. N.; **Jarkovoi, M**.; Kütt, L.; Shabbir, N. (2019). Impact of LED thermal stability to household lighting harmonic load current modeling. 2019 Electric Power Quality and Supply Reliability Conference & 2019 Symposium on Electrical Engineering and Mechatronics: 2019 Electric Power Quality and Supply Reliability Conference, June 12 to 14, 2019 in Kärdla, Hiiumaa Island of Estonia. IEEE.

IV **Jarkovoi, M**.; Iqbal, M. N.; Kütt, L. (2019). Analysis of harmonic current stability and summation of LED lamps. 2019 Electric Power Quality and Supply Reliability Conference & 2019 Symposium on Electrical Engineering and Mechatronics: 2019 Electric Power Quality and Supply Reliability Conference, June 12 to 14, 2019 in Kärdla, Hiiumaa Island of Estonia. IEEE, 1−8.

V   **Jarkovoi, M**.; Iqbal, M. N.; Kütt, L. (2020). Probabilistic bivariate modelling of harmonic current. 2020 International Conference on Harmonics and Quality of Power, March 22-25, 2020. Dubai, UAE. IEEE (accepted).

Author's Contribution to the Publications

Contribution to the papers included in this thesis are:

I   Marek Jarkovoi is the co-author of the paper. He is responsible for data processing and statistical analysis. Marek Jarkovoi presented the paper at the 59th International Scientific Conference on Power and Electrical Engineering of Riga Technical University in 2018 (RTUCON2018), Riga, Latvia.

II   Marek Jarkovoi is the co-author of the paper. He is responsible for writing the theoretical background and discussion.

III   Marek Jarkovoi is one of the co-authors of the paper. He is responsible for the measurement setup, data acquisition, data processing and discussion.

IV   Marek Jarkovoi is the main author of the paper. He is responsible for the measurement setup, data acquisition, data processing and writing the paper. Marek Jarkovoi presented the paper at the 2019 Electric Power Quality and Supply Reliability Conference (PQ2019), Kärdla, Estonia.

V   Marek Jarkovoi is the main author of the paper. He is responsible for the measurements, data processing, method proposition, analysis and writing the paper.

Abbreviations

AC	Alternating current
BND	Bivariate normal distribution
CCS	Constant current source
CDF	Cumulative distribution function
CFAM	Crossed-frequency admittance matrix
CLT	Central limit theorem
CV	Coefficient of variation
DC	Direct current
EM	Expectation-maximization
EMC	Electromagnetic compatibility
GMM	Gaussian mixed model
HCNE	Harmonic coupled Norton equivalent
HV	High voltage
IEC	International Electrotechnical Commission
IEEE	Institute of Electrical and Electronics Engineers
ITS	Inverse transform sampling
KCL	Kirchhoff's Current Law
KDE	Kernel density estimate
LED	Light-emitting diode
LV	Low voltage
MV	Medium voltage
NLL	Nonlinear load
PC	Personal computer
PCC	Point of common coupling
PDF	Probability density function
PFC	Power-factor correction
PV	Photovoltaic
RMS	Root mean square
SD	Standard deviation
TDD	Total demand distortion
THD	Total harmonic distortion
VSD	Variable-speed drive
WG	Wind generator

Symbols

In order of appearance.

$i(t)$	Instantaneous current
$u(t)$	Instantaneous voltage
h	Harmonic order
$\underline{I}_h$	*h*-th order complex current harmonic
I_h	*h*-th order current harmonic RMS value
U_h	*h*-th order current harmonic RMS value
$I_{m,h}$	*h*-th order current harmonic magnitude
$U_{m,h}$	*h*-th order current harmonic magnitude
$\theta_{I,h}$	*h*-th order current harmonic phase angle
$\theta_{I,h}$	*h*-th order voltage harmonic phase angle
f_1	Fundamental frequency
$i_{x,h}$	Harmonic current phasor real component
$i_{y,h}$	Harmonic current phasor imaginary component
I	Current RMS
THD_I	Total harmonic distortion of the current
THD_U	Total harmonic distortion of the voltage
TDD_I	Total demand distortion of current
I_L	Rated current of the PCC
K	Total number of simultaneously connected loads
$i_{x,h,k}$	Real harmonic current component of a single load
$i_{y,h,k}$	Imaginary harmonic current component of a single load
$i_{x\Sigma,h}$	Sum of harmonic current real components at the PCC
$i_{x\Sigma,h}$	Sum of harmonic current imaginary components at the PCC
$I_{\Sigma,h}$	Resulting harmonic current RMS at the PCC
$\Theta_{I\Sigma,h}$	Resulting harmonic current phase angle at the PCC
N	Total number of measurement data points
$i_{x,h,n}$	Single *n*-th measured current harmonic real component value
$i_{y,h,n}$	Single *n*-th measured current harmonic imaginary component value
$SD_{I,x,h}$	Standard deviation of harmonic current real component
$SD_{I,y,h}$	Standard deviation of harmonic current imaginary component
$SD_{I,xy,h}$	Standard spatial deviation of harmonic current phasor
$CV_{I,h}$	Coefficient of variation of harmonic current phasor
$RSD1_{I,h}$	Standard deviation of harmonic current relative to the fundamental
$\underline{Z}_h$	Norton model impedance component
$\underline{I}_h$	Complex harmonic current
$\underline{U}_h$	Complex harmonic voltage
$\mathbf{I}$	Vector of complex harmonic current
$\mathbf{U}$	Vector of complex harmonic voltage

$\underline{\mathbf{Y}}$	Crossed-frequency admittance matrix
$\underline{Y}_{MN}$	Crossed-frequency admittance between M-th and N-th harmonic
μ_{xy}	Bivariate mean vector
Σ_{xy}	Bivariate covariance matrix
K_b	Kernel function with bandwidth b
$p_{x,y}$	Probability density of a histogram bin at positions x and y
$c_{x,y}$	Number of data samples in a histogram bin
w_x	Width of a histogram bin along the x axis
w_y	Width of a histogram bin along the y axis
$f(x)$	Probability density function
$F(x)$	Cumulative probability function
$P(x)$	Probability of value x
$\Delta I_{xy,h,\%}$	Relative mean offset of simulated and measured harmonic current
$\Delta SD_{I,xy,h,\%}$	Relative standard deviation offset of simulated and measured harmonic current

1 Introduction

Background

The electrical distribution network is always in an evolving state. New power lines are constantly built, and depreciated lines replaced while residential areas are expanding, which involves introducing new consumers. Novel technology is being implemented, and older technology is replaced while distributed local generation and use of renewable sources are becoming more popular. With energy efficiency currently being one of the main objectives, governments are setting requirements for energy efficiency targets around the world, which could not be achieved without introducing a more modern type of devices utilizing electrical power more efficiently to perform specific tasks. Since concerns have also been rising about the environment and climate change, large economic sectors like transportation are also looking into electricity-based solutions instead of using fossil fuels.

Maintaining power quality and supply reliability in low voltage (LV) distribution network is the main objective of any distribution grid operator. All the above factors will and are already having an impact on electrical power quality in LV distribution networks. One of the essential aspects of power quality is supplying mains voltage as an undistorted sine waveform at a set level and frequency, which is most commonly 230 V, 50 Hz in Europe and in many other countries around the globe, and 120 V, 60 Hz mostly in North America.

Majority of the modern electrical devices use power electronics and complex control algorithms to achieve the required energy efficiency. It is not uncommon for these kinds of loads to draw non-sinusoidal distorted current from the distribution grid. As the number of connected nonlinear loads increases, the total current distortion at the point of common coupling (PCC) will also most likely rise, which, depending on the length, quality and topology of the power lines, can introduce voltage distortions in the LV distribution network. Voltage distortion does not only affect a single customer, but it can affect all the customers who are connected to the same PCC. For the network operator to be able to provide undistorted voltage to the customers, measures must be taken to reduce, anticipate and prevent current and voltage distortions.

The distortion of any periodic quantity, i.e. waveform, can be described by its decomposition into individual sine components called harmonics using a specific set of functions. These harmonic components, described by their frequency that is an integer multiple of the fundamental frequency, the magnitude of absolute value, or relative to the fundamental component, and the phase angle shift relative to the fundamental component initial phase will be the key research targets of this thesis.

Motivation and purpose

While there has been thorough research of modelling power flow in both transmission and distribution grid, modelling nonlinear loads, including harmonic currents and voltages, is a topic of growing interest the field of electrical and power engineering. Ongoing research has shown that due to the variety and diversity of modern nonlinear loads, it is very difficult to model harmonic current emissions ranging from a single device or a group of devices to a household or a group of households. Attempts in modelling have been made either based on the devices (bottom-up) or based on a large section of the residential and industrial network, e.g. a substation feeder (top-down). Various types of models have been proposed that approximate the behaviour of nonlinear loads, but

as the technology is becoming more complex and dynamic, the simpler models are quickly becoming obsolete.

The classical approach to modelling has been to use deterministic electrotechnical models to represent various loads. However, due to the stochastic properties of modern nonlinear loads, their exact behaviour is very difficult to describe, for the load parameters may vary over time. Calculating and considering average harmonic current based on average values has been implemented commonly in previous research. However, it has been indicated to be inefficient in modelling, summation and estimation of harmonic currents of nonlinear loads which also exhibit variable operating modes.

In case of such variations, a probabilistic approach is more appropriate. Primarily, simple Gaussian models have been considered and studied in the past. However, the Gaussian distribution provides a limited representation of dispersion and not all types of variations can be described using Gaussian distributions. In case the variations have strictly unique characteristics and shape of dispersion, it may not be possible to represent the harmonic current by using the standard Gaussian methods.

While the computational power was quite limited up to the early 2000s, the rapid increase of capabilities of information technology and infrastructure in 2010s has provided fresh resources for a new type of models and methods. Research on probabilistic modelling and summation of harmonic currents is one of the prospective outputs of such developments. This provides opportunities and potential for solving several issues and difficulties in modelling nonlinear loads and associated load harmonic currents with unpredictable variations.

The objective of the thesis is to provide a universal methodological base that could be further improved and incorporated into complete solutions that can be used for estimating the expected harmonic current levels in LV distribution networks.

It should be noted that while a waveform includes the harmonics of all orders simultaneously, this research and the thesis focuses on the individual current harmonics. Assessing the extent of any harmonic current variation and finding the possible extreme values at the PCC can have a major influence on distribution network planning as it is often the extreme harmonic current values that can cause malfunctions of devices, network failures due to phenomena like resonance, or increase power losses.

Tasks and methods

Primary tasks of the thesis include the following:

- Investigate the harmonic currents in LV distribution networks and identify the sources of harmonics;
- Establish possible research targets to approach negative aspects arisen from nonlinear loads present in the network;
- Study variation characteristics of harmonic currents from nonlinear loads and to determine methods to quantify and compare the dispersion of the load current harmonics;
- Analyse the possibility of implementing novel multivariate probabilistic modelling methods for harmonic current and to determine the best approach for modelling nonlinear loads having variable current harmonics;
- Research and develop a nonparametric model which is efficient in terms of balancing accuracy and data size and could be easily used in simulations;

- Study feasibility of using probabilistic modelling and simulation methods to estimate harmonic current summation of simultaneously connected nonlinear loads.

The main methodology is to use accurate and repeatable measurements in a controlled environment as input for research, development and implementation of probabilistic harmonic current models for harmonic current summation.

For investigation and studies of harmonic currents, a large number of measurements are to be performed in various environments and scenarios.

Novelty

Main scientific novelties of the thesis include the following:
- Visualization and comparison tools for the variations of harmonic currents from nonlinear loads;
- Development of a novel and effective bivariate probabilistic data structure for modelling and summation of current harmonics.;
- Investigation and proposal of probabilistic methods for modelling harmonic currents that can represent the actual variation, including the extent and the shape of the dispersion;
- Implementation of probabilistic summation methods that are based on novel probabilistic models;
- Elaboration of the possibility to use novel methods for modelling current harmonics on many different levels, e.g. device level, household level, line feeder level, etc;

The developed and proposed methods would be used for harmonic current summation simulation to provide a probabilistic estimation of harmonic currents at the PCC. The result of the thesis provides a key foundation that, with further research and combination with other related methodologies, would make it possible to estimate the harmonic current levels in LV distribution network for planning and design.

The thesis is based on the work and scientific publications which have been presented at various international conferences, and one paper published in a scientific journal.

1.1 Characteristics of harmonics

Any time-invariant non-sinusoidal current or voltage waveform can be described by a sum of individual harmonically related sinusoidal components, called harmonics. Each harmonic has an oscillating frequency that is an integer multiple of the fundamental frequency. Such composition of harmonics is called the Fourier series and is obtained using Fourier analysis.

A periodic non-sinusoidal current waveform is defined using sine- or cosine-based functions at any point in time t for current and voltage as follows:

$$i(t) = \sum_{h=1}^{\infty} I_{m,h} \cos(2\pi h f_1 t + \theta_{I,h}), \tag{1}$$

$$u(t) = \sum_{h=1}^{\infty} U_{m,h} \cos(2\pi h f_1 t + \theta_{U,h}), \tag{2}$$

where:
$i(t)$ — instantaneous current,
$u(t)$ — instantaneous voltage,
h — harmonic order,
$I_{m,h}$ — magnitude of the current harmonic,
$U_{m,h}$ — magnitude of the voltage harmonic,
f_1 — frequency of the fundamental component,
$\theta_{I,h}$ — phase angle of the current harmonic,
$\theta_{U,h}$ — phase angle of the voltage harmonic.

In Europe, the fundamental frequency of the low voltage distribution network is 50 Hz and 60 Hz in North America. Each harmonic component is defined by its magnitude and phase angle, usually described in relation to the fundamental component, which is always considered having the phase angle as zero. The composition of the harmonic components ultimately defines the shape of the waveform.

Although the Fourier series can be specified up to infinity, for practical reasons, only harmonics up to certain order are reported and analysed. Such methods of measurement and harmonic component calculation of voltage and current can be found in recognized standards IEC 61000-4-30 [1] and IEC 61000-4-7 [2].

A current harmonic is essentially a phasor, which is a rotating vector on a complex plane. A phasor can be further decomposed into real and imaginary components that geometrically describe the harmonic phasor magnitude (i.e. amplitude) and phase angle:

$$\begin{cases} i_{x,h} = \mathrm{Re}(\underline{I}_h) = I_{m,h} \cos(\theta_{i,h}) \\ i_{y,h} = \mathrm{Im}(\underline{I}_h) = I_{m,h} \sin(\theta_{i,h}) \end{cases}, \tag{3}$$

$$I_{m,h} = |\underline{I}_h| = \sqrt{i_{x,h}^2 + i_{y,h}^2}, \tag{4}$$

where:
$i_{x,h}$ — real component of the current harmonic,
$i_{y,h}$ — imaginary component of the current harmonic,
$\underline{I}_h$ — complex value of the current harmonic.

Since phasor magnitudes can also be represented using the root mean square (RMS) values and vice versa, the resulting harmonic RMS and the total RMS current is equal to:

$$I_h = \sqrt{\frac{i_{x,h}^2 + i_{y,h}^2}{2}} = \frac{I_{m,h}}{\sqrt{2}}, \tag{5}$$

$$I = \sqrt{\sum_{h=1}^{\infty} \frac{I_{m,h}^2}{2}}. \tag{6}$$

The amount of waveform distortion can be evaluated by using an index of total harmonic distortion (THD). THD represents the ratio of the sum of the RMS (or magnitude) values of harmonic components to the fundamental component and is usually described up to the specified harmonic order H as a percentage. The THD can be calculated for the current (THD_I) and the voltage (THD_U) as follows:

$$THD_I = \frac{1}{I_1} \sqrt{\sum_{h=2}^{H} I_h^2} \cdot 100\% = \sqrt{\frac{I^2}{I_1^2} - 1} \cdot 100\%, \tag{7}$$

$$THD_U = \frac{1}{U_1} \sqrt{\sum_{h=2}^{H} U_h^2} \cdot 100\% = \sqrt{\frac{U^2}{U_1^2} - 1} \cdot 100\%. \tag{8}$$

THD value of 10% means that the harmonic components make up one-tenth of the fundamental component, a 100% means that the RMS values of the fundamental component and the harmonics are equal, and a value of 200% means that the harmonics have an RMS value of twice the fundamental components. A value of THD_I between 100% and 200% is not uncommon with modern unfiltered nonlinear loads (NLL).

To characterize the amount of harmonic distortion in relation to the line current, the total demand distortion factor TDD_I is used:

$$TDD_I = \frac{1}{I_L} \sqrt{\sum_{h=2}^{H} \frac{I_h^2}{2}} \cdot 100\%, \tag{9}$$

where I_L is the maximum demand load current at the PCC, taken as the sum of the currents corresponding to the maximum demand during each of the twelve previous months divided by 12 [3].

When a load, either residential or industrial, draws current with a non-sinusoidal waveform, it also causes current harmonics to be present. When many loads are connected to a PCC, the Kirchhoff's current law (KCL) states that, at any point in time, the sum of currents toward or from a single node is equal to zero. This means that according to the superposition principle, the resulting current at the PCC is the sum of the individual harmonics originating from all connected loads. To calculate the vector sum of the current, all the individual real and imaginary components must first be added using:

$$\begin{cases} i_{x\Sigma,h} = \sum_{k=1}^{K} i_{x,h,k} \\ i_{y\Sigma,h} = \sum_{k=1}^{K} i_{y,h,k} \end{cases}, \tag{10}$$

where:
$i_{x,h,n}$ − real harmonic current component of the individual load k,
$i_{y,h,n}$ − imaginary harmonic current component of the individual load k,
K − total number of connected loads at the PCC.

The resulting harmonic current magnitude and the RMS value at the PCC are:

$$I_{m\Sigma,h} = \sqrt{i_{x\Sigma,h}^2 + i_{y\Sigma,h}^2}, \tag{11}$$

$$I_{\Sigma,h} = \frac{I_{m\Sigma,h}}{\sqrt{2}}, \tag{12}$$

and the phase angle is determined based on the resulting phasor quadrant:

$$\Theta_{I\Sigma,h} = \begin{cases} \tan^{-1}\left(\dfrac{i_{y\Sigma,h}}{i_{x\Sigma,h}}\right), & if\ i_{x\Sigma,h} > 0 \\ \tan^{-1}\left(\dfrac{i_{y\Sigma,h}}{i_{x\Sigma,h}}\right) + \pi, & if\ i_{x\Sigma,h} < 0\ and\ i_{y\Sigma,h} \geq 0 \\ \tan^{-1}\left(\dfrac{i_{y\Sigma,h}}{i_{x\Sigma,h}}\right) - \pi, & if\ i_{x\Sigma,h} < 0\ and\ i_{y\Sigma,h} < 0 \\ \dfrac{\pi}{2}, & if\ i_{x\Sigma,h} = 0\ and\ i_{y\Sigma,h} > 0 \\ -\dfrac{\pi}{2}, & if\ i_{x\Sigma,h} = 0\ and\ i_{y\Sigma,h} < 0 \end{cases} \tag{13}$$

The resulting phase angle in this format is in the range of -π…+π or -180°…+180°.

1.2 Overview of harmonics in low voltage distribution networks

To assess the nature and behaviour of current and voltage harmonics in LV distribution networks, the present situation and what the most important issues are regarding the harmonics are observed an analysed. Harmonic voltage levels in low voltage networks represent an important factor of power quality. From the aspect of the electromagnetic compatibility (EMC), voltage distortion in LV public network must be kept within the compatibility levels to enable satisfactory operation of all the equipment supplied by the network.

For the member states of the EU, general requirements for supply voltage quality are stated in the standard EN 50160 [4]. According to the standard, the THD factor of the supply voltage must be kept below 8%. Limit values for each individual harmonic voltage have also been set. The limit values are, for example, 6% for the 5th harmonic, 5% for the 7th harmonic, 3.5% for the 11th, and 3% for the 13th. It should be noted that the

EN 50160 presents the THD_U limit values for any 10-minute observation periods, where during 95% of this time interval the THD_U should remain under the stated limits.

The EN 50160 standard itself is based on the EMC standard IEC 61000-2-2 [5], adapted and implemented for use in the EU member states, in which distribution network operators use it as a network policy for providing voltage power quality. The EMC standards also include the IEC 61000-3-2 [6], which sets limits for the harmonic current emission of a single device to be used in public LV network. Compliance to this standard is one of the requirements for marketing and selling products in the EU and testing according to this standard is part of the procedures required to obtain the CE conformity marking.

Presently, requirements for limiting the current harmonics is only implemented at the device level. Limits for the summation of harmonic current from devices, i.e. general harmonic current levels in public LV networks are not imposed by the EU. However, some standards like the IEEE 519 [3] do define the limits for the harmonic current TDD at the PCC, which is implemented in some EU member states. The limit depends on the short-circuit ratio at the PCC, which is 5% for the smallest short circuit ratio (< 20) and 20% for the largest short circuit ratio (>1000). Individual current harmonics are also limited up to the 50th order.

Mapping and analysing harmonic currents and voltages in the LV distribution network has been of growing interest. For the initial approach, some qualitative results can be brought out from extensive power quality monitoring studies performed in Estonia during the 2010s in the industrial LV networks [I].

Measurements were carried out using dedicated power-quality analysers like Fluke 434, LEM Memobox and Fluke 1745, which are capable of reporting harmonic current and voltage component levels. The individual observation periods were at least one week and either 1- or 10-minute recording intervals were used. The probability density and the cumulative distribution of THD_U for all measurements are presented in Figure 1 and Figure 2.

The most often occurring THD_U 95th percentile value was around 3%. Based on the cumulative distribution, it was also the median value, which means that in half of the cases the values were below and half above 3%. The most occurring maximum value was also 3% with values of less than 3% in 40% of cases.

The 95th percentile THD_U value of 5% was exceeded in 25% of cases and the maximum value of 5% was exceeded in 30% of cases. The 95th percentile THD_U value of 8% was exceeded in 9% of cases and absolute maximum value in 15% of cases.

The maximum 95th percentile value of THD_U was up to 11%, with maximum THD_U measured value reaching over 14%. In 4% of cases, the maximum THD_U values exceeded 10%.

The minimum THD_U value was around 1%, which occurred mostly with low loads during weekends and night hours. In some cases, the minimum level of THD_U was around 4.5%, which indicates continuous high harmonic voltage levels.

From the harmonic spectrum of voltages, 5th harmonic was the most dominating. Other prominent harmonics were 7th, 11th, 13th, 17th, 19th and 23rd. Triple harmonics like 3rd, 9th and 15th were also high in several cases. Harmonic voltages of order higher than 23rd were less than 0.2%.
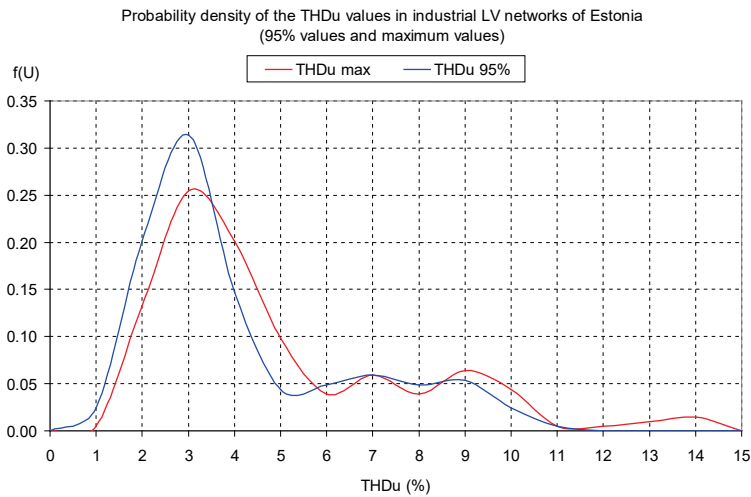
Figure 1. Probability density of measured voltage THD (95th percentile and maximum values) for all measurements.
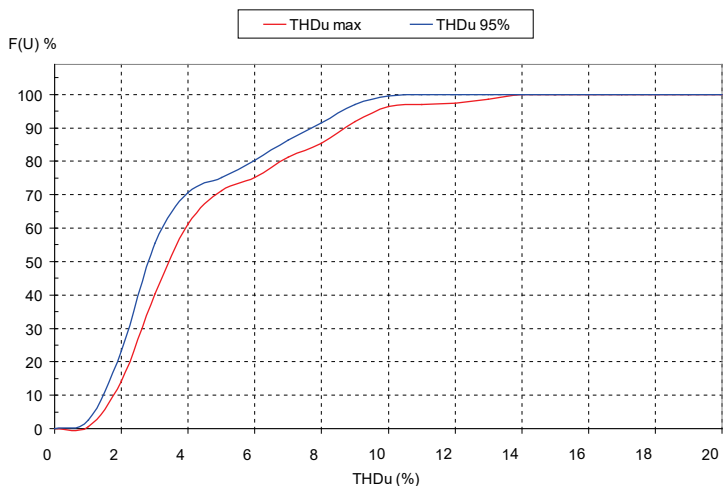

Figure 2. Cumulative distribution of measured voltage THD (95th percentile and maximum values) for all measurements.

The current harmonics varied extensively from case to case and in time. Thus, for a more descriptive insight, it is necessary to monitor currents with recording intervals below 1 minute, down to 1 second depending on the LV network.

Harmonic currents can be rather high in industrial networks, exceeding the level of 20% and reaching up to 80…90% during starting and stopping operating modes of high-power electrical drives.

An example of high current distortion levels in an industrial factory can be seen in Figure 3. The baseline for THD_I was between 10…20%, but during working hours the value fluctuated between 20…40% with peak values reaching 90% during equipment startup.

Maximum harmonic distortions of the supply current from the supply transformer in each 1min interval during one week period in a mechanical factory
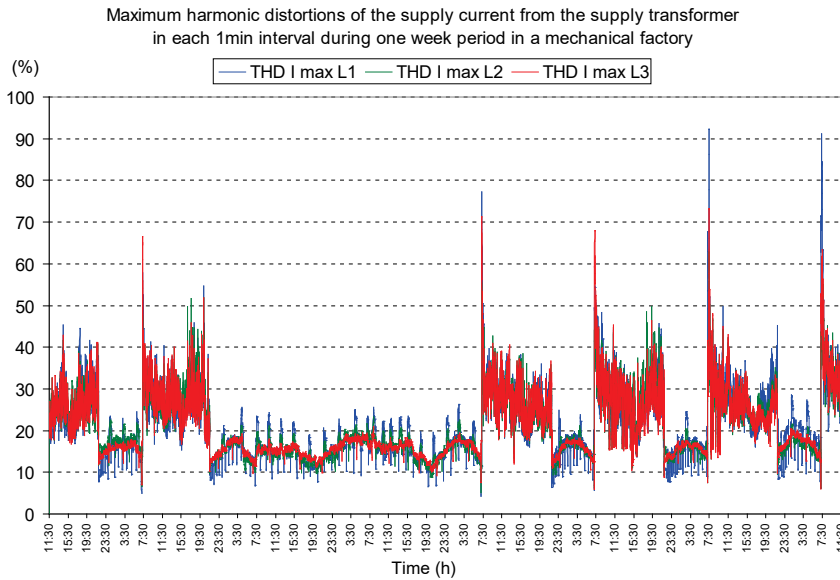
Figure 3. Supply current THD during a 1-week interval in an industrial factory.

An example of a highly distorted current and voltage waveforms can be seen in Figure 4. The 10-minute time series for THD_U for the same case is shown in Figure 5. While most of the time the voltage distortion levels were below 8%, a rise to 11% can be observed at times. The THD_U varied considerably between 1% and 10% during a one-week interval.
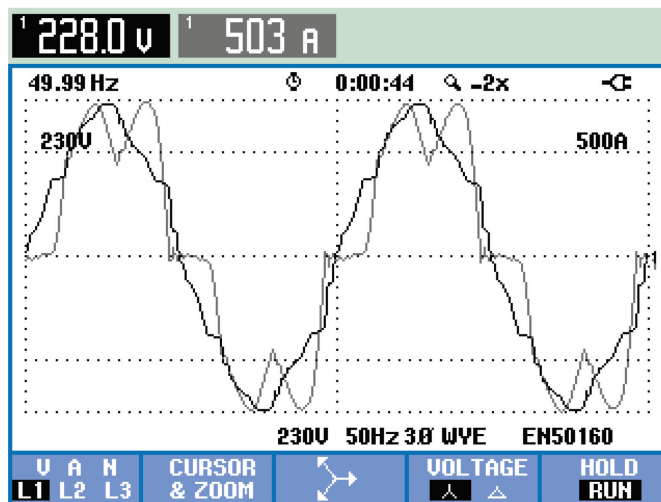
Figure 4. Supply voltage and current waveforms in an industrial LV network.

Total harmonic distortion of the supply voltage in an industrial network,
1 min average values during one week period
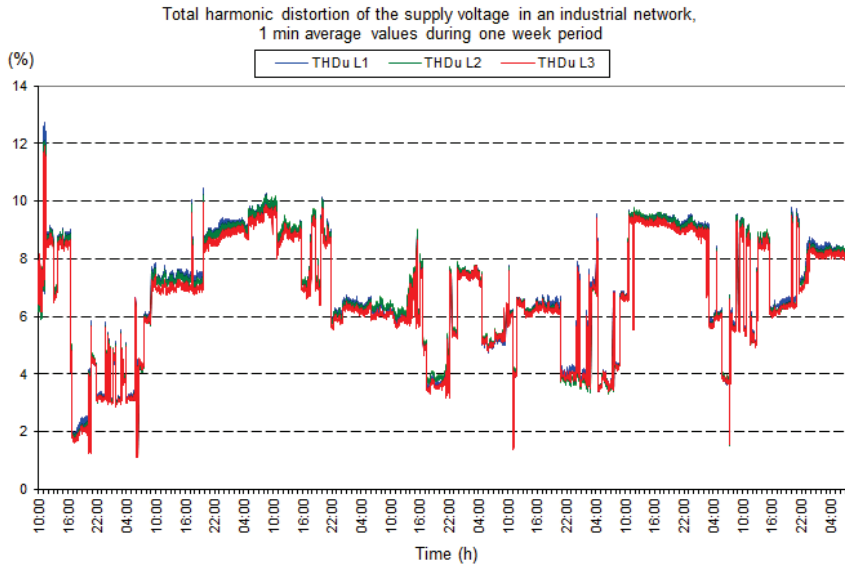
Figure 5. Supply voltage THD in an industrial LV network.

Based on the long-term measurement surveys, it can be stated that the current distortion can be high. The current harmonics can also affect the voltage with nonlinear voltage drop, causing distortion, i.e. voltage harmonics in the network. This means that one of the root causes of the voltage distortion is the presence of the current harmonics and they should be monitored with detail in LV networks. LV networks are more sensitive to current distortions due to larger impedance values than the medium voltage (MV) and high voltage (HV) transmission networks. Mapping harmonic current sources and estimating harmonic currents should be implemented to develop planning levels for power supply agreements between LV customers and LV/MV network operators.

An extensive case study on individual harmonic currents was also reported in [7]. The harmonic currents and voltages were monitored during a half-year time period. Daily patterns of harmonic current magnitudes were analysed and the effect of outside temperature on current harmonics was also studied. It was found that the harmonic current variance in LV distribution network is very high and a more complex modelling is required to provide an adequate estimation of the harmonic current.

A significant portion of studies focuses on evaluating the harmonic current magnitude. There are extensive studies available on the harmonic current of domestic loads and their effect on the LV distribution network, which also consider the harmonic current phase angles [8], [9].

1.3 Issues concerning nonlinear devices

For the year 2030, there are energy efficiency targets set, for example by the EU, to have overall improvements by at least 32% compared to the year 1990 [10]. One aspect to achieve this is by using specialized power supply units, which convert the distribution network voltage to the desired parameters using power electronic circuitry with the aim of achieving highest possible efficiency even for small-power loads. These types of units would provide a contribution to the harmonic currents in the network. Since energy efficiency is becoming a more central topic in residential households, and with the

requirements of nearly net-zero energy buildings (NZEB) by the EU directive on energy performance of buildings [11], it is not surprising that, for example, more energy-efficient LED lamps are rapidly replacing traditional incandescent and fluorescent lamps, variable-speed drives (VSD) using inverter-technology are replacing traditional electric motors, and electric vehicles (EVs) are becoming more popular. Introduction of distributed renewable power generation units in the form of photovoltaic (PV) inverters and wind generators (WG) is also growing rapidly in LV networks, especially in the rural residential areas, [IV].

It has been determined that nonlinear equipment is the main source of the current harmonics since devices like LED lamps, VSDs, EV chargers, PV and WG inverters, all draw or generate current with a non-sinusoidal waveform. Increasing market share and usage of such devices presents a new challenge in terms of modelling and estimation of current and voltage distortion in LV networks. Although most widely used nonlinear loads are low-power and may not cause any problems as single units, the joint operation of a large number of nonlinear equipment can cause a significant effect on the power quality of the local area LV network. Even networks which are operating close to the limit values will be unfavourable for the customer. Additional heating of the equipment and resulting power losses, reduction of service time, and extra costs may occur. Based on the study, in some cases, even the limit values of harmonic voltages are exceeded.

Based on the published research [II], it has been correlated that current harmonics are dependent on the PV generation power. Three different PV inverters, one single-phase and two three-phase, were measured. It has been found that the amount of current and voltage distortion also depends on the topology of the PV inverters. Figure 6 to Figure 8 present the measurement results of a 15-hour solar cycle for the respective PV inverters. At solar peaks, the THD_I stays below 10%, but when the generation is low (during morning and evening), the THD_I peaks can be up to 100%.
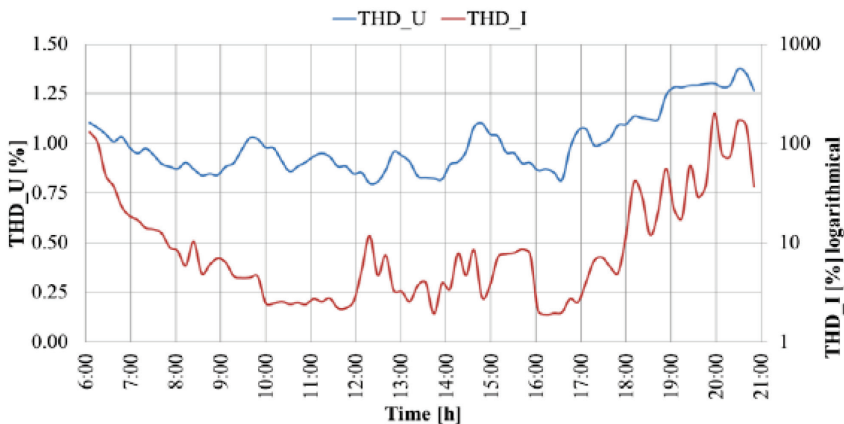

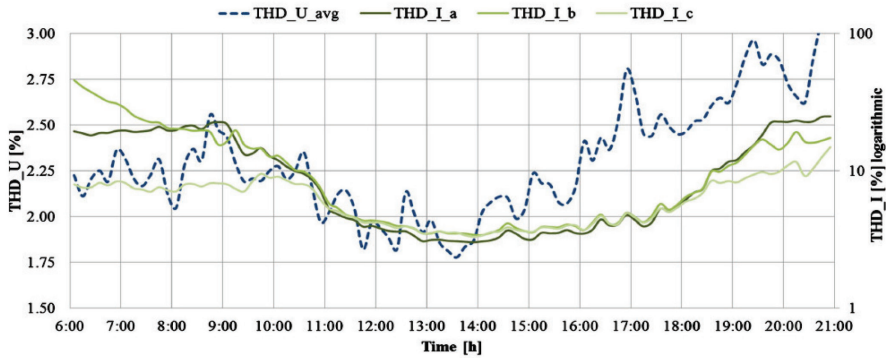Figure 6. Measured voltage and current THD of the single-phase PV inverter.

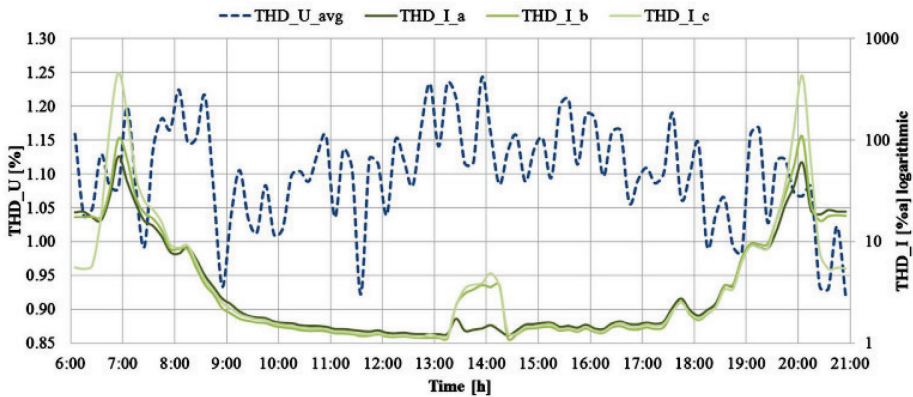*Figure 7. Measured voltage and current THD of the first three-phase PV inverter.*

Figure 8. Measured voltage and current THD of the second three-phase PV inverter.

To estimate the effect of harmonics on the LV distribution network, a residential household was modelled using DIgSILENT Power Factory software. The aim of the model was to determine the impact of PV generation. The model included various nonlinear loads at 0.4 kV voltage level distributed among three phases, an overhead line that connected the residential network to an MV/LV substation, which included a transformer, and a 10 kV slack bus. Measurement data and averaging were used to determine the model parameters of individual network components.

Results from the network simulations based on three different PV inverters are presented in Figure 9. The effect of introducing PV inverters to the network on THD_U varies from -3% up to +16% at peak power, depending on the topology and line phase.

It should be noted that at different power levels, the current harmonic spectrum changes, which in turn affect the network voltage differently. As harmonic levels change considerably due to the weather patterns, it is very difficult to assess the long-term evolution of harmonic levels only from measurements carried out over a short period of time. Modelling PV generation is still a complicated task to accomplish even with today's tools and standards.
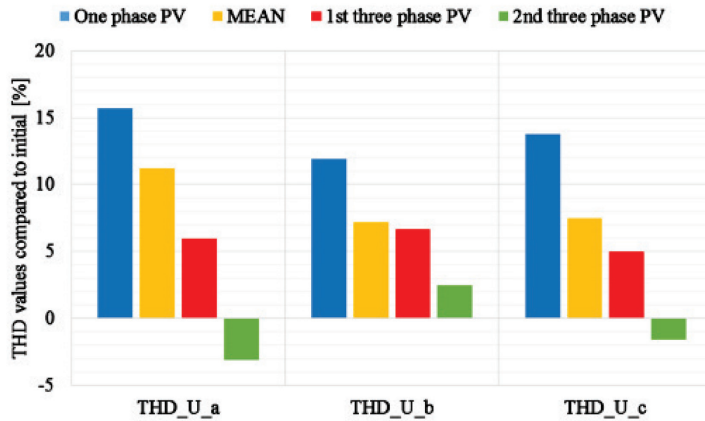
Figure 9. Simulation results of 0.4 kV bus for three different PV inverters compared to the initial condition at peak power.

Harmonic phenomena are often not so intense to cause any direct breakdown of components other than power factor correction (PFC) capacitors. However, harmonic currents affect supply voltage quality and power losses in the whole LV network, particularly, in induction motors, transformers, lines and capacitors. Supply voltage quality can lead to malfunctions in electrical equipment and may introduce additional losses. Harmonic power losses are usually not estimated because the losses are neither measured nor calculated.

Misapplication of PFC capacitors can also introduce parallel resonance in the LV network. This results in amplification of specific current and voltage harmonics, which depend on the resonance frequency. The resonance frequency depends on the capacitance, inductance and resistance present in the LV network circuit. The resonant intensity is mostly affected by the parameters of the transformer, the amount and spectrum of harmonic currents, and the type of converters installed (6-pulse, 12-pulse, etc.).

1.4 Harmonic current variation

The harmonic current of power generation devices like PV or WG inverters will inherently depend on the availability of energy sources, i.e. sunlight and wind. The harmonic spectrum at 10% nominal power and 100% nominal power may differ significantly. The harmonic spectrum of modern household loads can also have variations. For example, a washing machine or a modern refrigerator will have many different programs and options that can be set by the user. Combined with VSD technology for motors and sensors for feedback, the harmonic spectrum can vary significantly during and between uses. An extensive and detailed study was performed to determine the harmonic current variation properties of several nonlinear household loads.

1.4.1 Measurement setup
To provide the necessary baseline input data for the harmonic variation study, a comprehensive test bench was designed and built for carrying out repeatable measurements and to provide baseline data for further research.

The test setup included a personal computer (PC) with a National Instruments data acquisition (DAQ) module capable of generating arbitrary analogue waveforms with 16-bit resolution. A Chroma 61505 4 kVA programmable power supply or a low-distortion Omicron CMS 356 linear voltage and current amplifier was used to achieve desired LV distribution network voltage waveform from the analogue input signal that was fed from the PC-controlled DAQ device. A load combination array was built with two-pole double-throw relays (DPDT or 2P2T), which could accommodate up to 16 concurrent loads in any combinations. An A-Eberle PQ-Box 200 Class A power quality measurement device was used for the measurements, which is capable of recording harmonic current and voltage magnitudes and phase angles with a minimum measurement interval of 1 second, which were aggregated from the internal 200 ms, 10-cycle measurements according to the standard requirements [1]. The complete system was controlled using the MATLAB software.

The reference waveforms were generated with a sampling frequency of 100 kHz, which equates to 2000 samples per single 50 Hz cycle. The software also controlled the load relays to achieve various load combinations that were supplied by the generated and amplified waveforms. Ideal 50 Hz sine voltage waveform with an RMS value of 230 V was selected for the tests. During the complete study, only odd harmonics up to 19th order were considered and analysed, due to even- and higher-order harmonics being close or below the acceptable measurement level. The amplifier was running for at least 30 minutes before testing to achieve its working temperature. Devices under test were powered for at least 60 minutes before testing to achieve the thermal stability. To keep the devices at working temperature between the tests, the continuous running was achieved using the double-throw relays which provided power to the devices from the power outlet in the laboratory when the relays were unengaged. When the relays were engaged, both phase and neutral line were routed to the measurement circuit. The complete overview of the setup is presented in Figure 10 [IV].
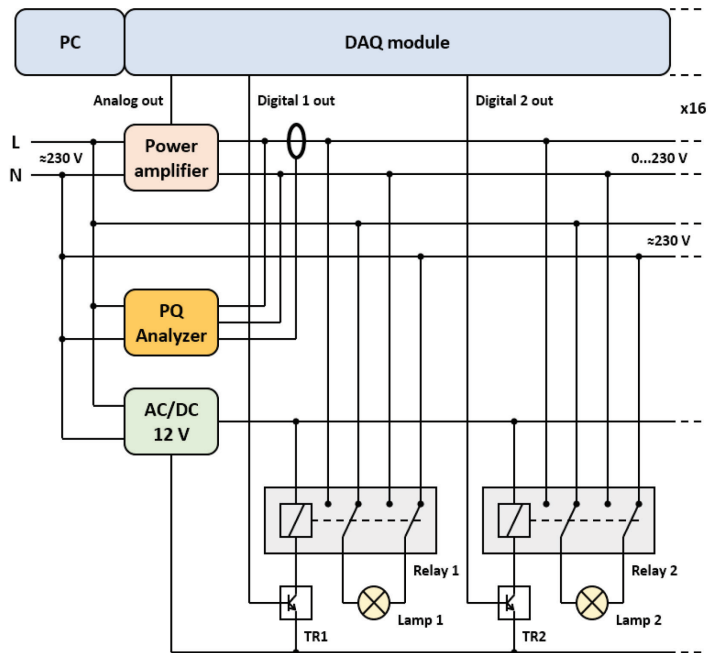

Figure 10. Measurement setup diagram.

1.4.2 Variations due to thermal effects

Research has shown that even stable loads like LED lamps can have current variations [III]. 16 randomly selected LED lamps found on the market in the year 2018 were tested. The power rating ranged from 7 W to 13 W with luminous flux between 500 lm and 1521 lm. It was found that due to the thermal stabilization during one hour, the harmonic current variations up to 20% were recorded. While most harmonic currents decreased exponentially, some harmonics of some LED lamps had an increase in magnitude during the warm-up cycle. The complete set of results are shown in Figure 11.
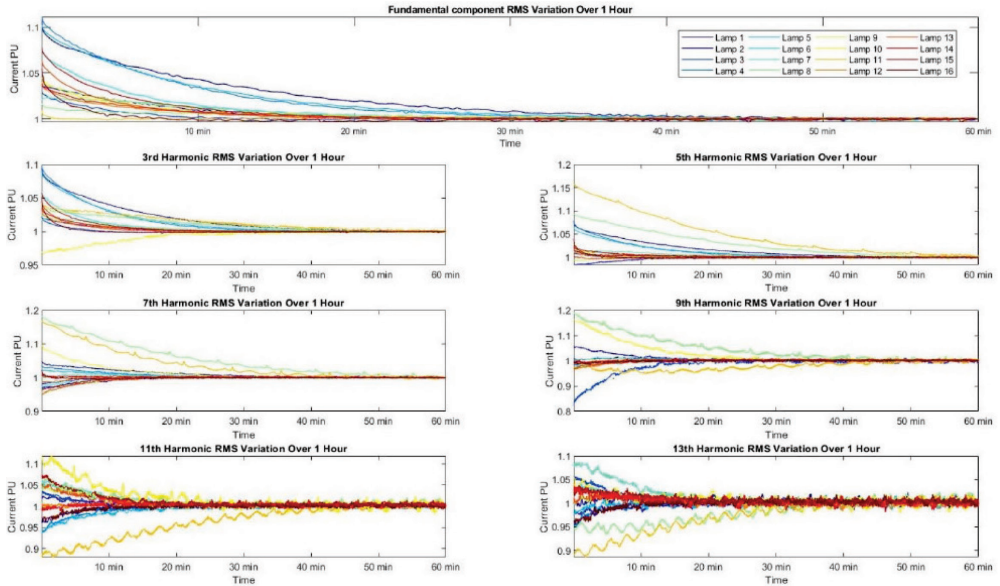
Figure 11. Harmonic current magnitude (p.u.) variation over 1 hour for LED lamps.

Changes in the phase angles were also observed. Depending on the harmonic order, phase angle differences of up to 6 degrees for low-order harmonics and differences up to 25 degrees for high-order harmonics were measured, as shown in Figure 12.
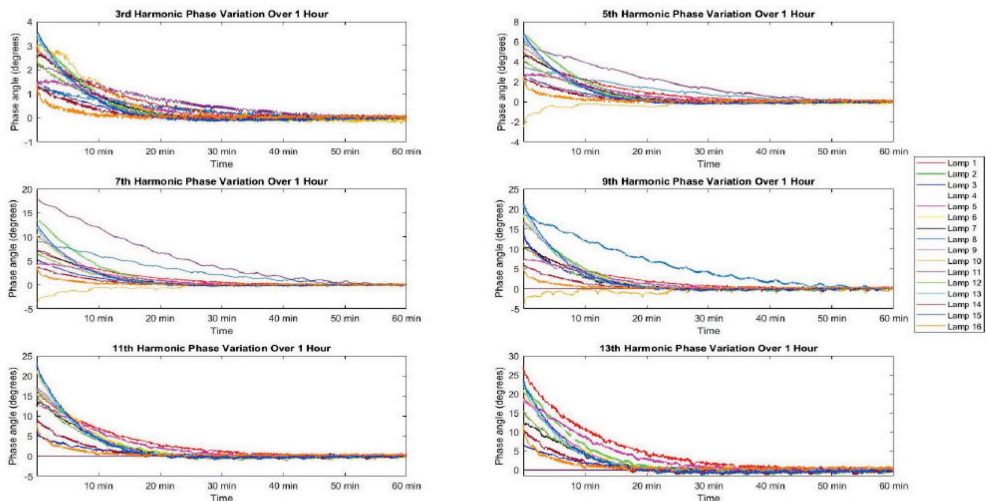
Figure 12. Phase angle variation over 1 hour for LED lamps.

1.4.3 Bivariate variations

The harmonic current variation of thermally stable loads like LED lamps, PC, PC monitor and Smart TV was also studied [IV]. Due to the complex nature of the current harmonics, the phasor variation was measured using bivariate components.

Firstly, the magnitude and the phase angle from the measurement data was converted to complex real and imaginary components using (3). Then, the average component values i_{hx} and i_{hy} were calculated from N number of measurement data points:

$$\begin{cases} i_{x,h} = \dfrac{1}{N} \sum_{n=1}^{N} i_{x,h,n} \\ i_{y,h} = \dfrac{1}{N} \sum_{n=1}^{N} i_{y,h,n} \end{cases}. \tag{14}$$

The standard deviation (SD) for both components and their geometric, or spatial SD were then found using:

$$\begin{cases} SD_{I,x,h} = \sqrt{\dfrac{1}{N} \sum_{n=1}^{N} (i_{x,h,n} - i_{x,h})^2} \\ SD_{I,y,h} = \sqrt{\dfrac{1}{N} \sum_{n=1}^{N} (i_{y,h,n} - i_{y,h})^2} \\ SD_{I,xy,h} = \sqrt{SD_{I,x,h}^2 + SD_{I,y,h}^2} \end{cases}. \tag{15}$$

To evaluate the spatial dispersion of the harmonic current, the coefficient of variation (CV) was calculated using (16). The CV shows the ratio of the standard deviation to the mean value of said harmonic current. The relative standard deviation (RSD) compared to the fundamental current component was also calculated using (17).

$$CV_{I,h} = \frac{SD_{I,xy,h}}{I_{m,h}}, \tag{16}$$

$$RSD1_{I,h} = \frac{SD_{I,xy,h}}{I_{m,1}}. \tag{17}$$

For the 16 LED lamps described above, the initially measured maximum spatial CV values for low-order odd harmonics (1-9) were between 0.4% and 1% and for high-order harmonics (11-19) between 0.7% and 1.1%. The RSD1 values, which compare the harmonic variations to the fundamental component, were only up to 0.2%. This was measured using the Chroma 61505 power supply. It was then found that the voltage sine signal output had very minor, nearly unmeasurable distortion compared to the pure sine wave, which nevertheless affected the current waveform, which in turn had an influence on the measured current harmonics. This power supply was then replaced with Omicron CMS 356 linear amplifier, which did not show any measurable voltage distortion.

The results with the improved measurement setup resulted in maximum spatial CV values between 0.1% and 0.4% for low-order harmonics and between 0.3% and 0.4%. The average values of 16 lamps were below 0.15%. The CV values are presented in Figure

13. The markers show the results for each individual lamp, the thick line shows the average values and the dashed line shows the 95th and 5th percentile values. The maximum RSD1 values were up to 0.06% and average values close to 0.01%. Such low values were expected as the LED lamps are considered to be very stable loads after reaching thermal stability. This provided a baseline for measuring devices with more variable harmonic currents.
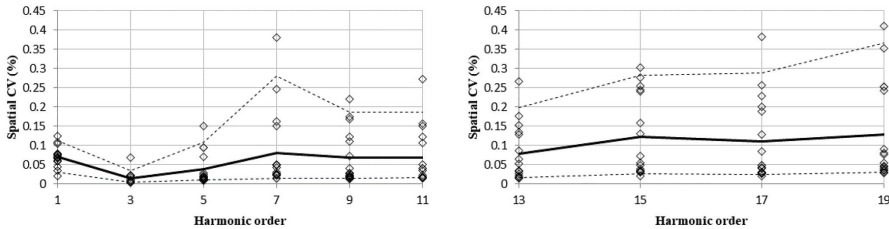

Figure 13. Spatial CV of low and high-order current harmonics for LED lamps.

The harmonic current variations of a PC monitor during 1 hour of continuous video playback over DisplayPort (DP) is presented in Figure 14. The variations were found to be very low and comparable to the LED lamps. The spatial CV was only between 0.3% and 0.35% and RSD1 values between 0.1% and 0.15%, which were decreasing with the harmonic order.
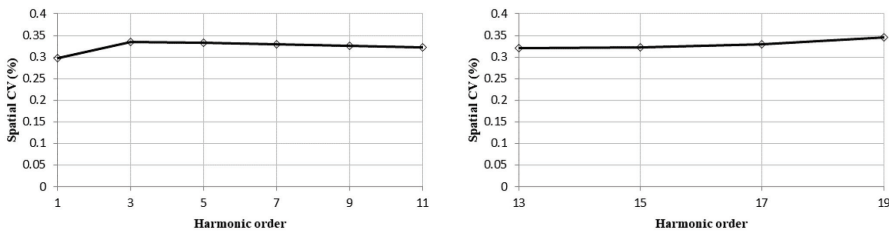
Figure 14. The spatial CV of a PC monitor during 1 hour of video playback over HDMI.

The current harmonics of a smart TV during 1 hour of continuous video playback over HDMI had a much larger variation, as shown in Figure 15. The spatial CV was measured to be between 2% and 18%, with 5th, 11th, 15th and 17th harmonic order having the highest values. Despite the high CV, the RSD1 value was below 0.5% apart from 3rd harmonic, which had an RSD1 value of about 0.8%.
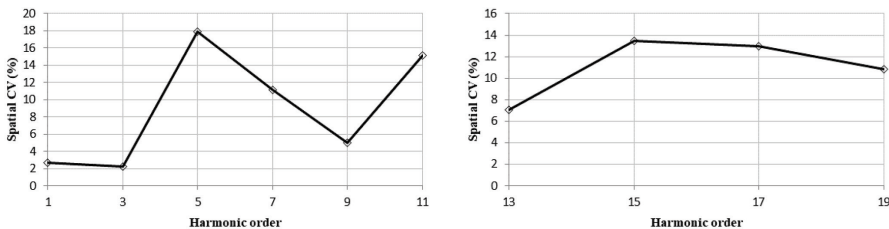

Figure 15. Spatial CV of a smart TV during 1 hour of video playback over DP.

The harmonic current variations of a PC were measured for 1 hour in two modes: video playback and dynamic system stress test.

During video playback, presented in Figure 16, the spatial CV for low-order harmonics was between 1% and 7% and for high-order harmonics between 7% and 11%. In this case, the 5th, 7th and 9th harmonics had the lowest variations up to 2% and the highest was

13th. The RSD1 values were between 0.1% and 0.3% apart from the 3rd harmonic with a value of about 0.6%.
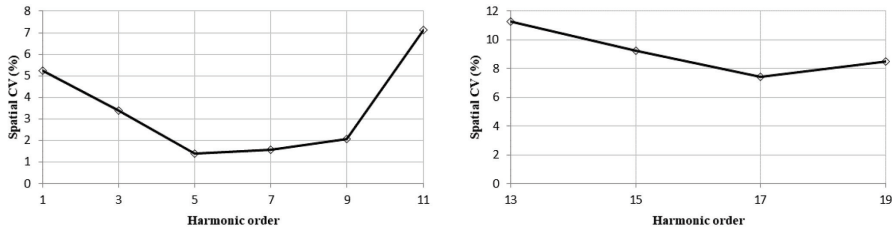

Figure 16. Spatial CV of a PC during 1 hour of video playback.

The results of the harmonic current variation of a PC during full system stress is presented in Figure 17. The maximum spatial CV values were between 4 and 14% for low-order harmonics, with 14th harmonic having the highest value. The high-order current harmonics had a much larger spatial CV value, between 20 and 40%. The RSD1 value was still low, between 0.1 and 0.5%.
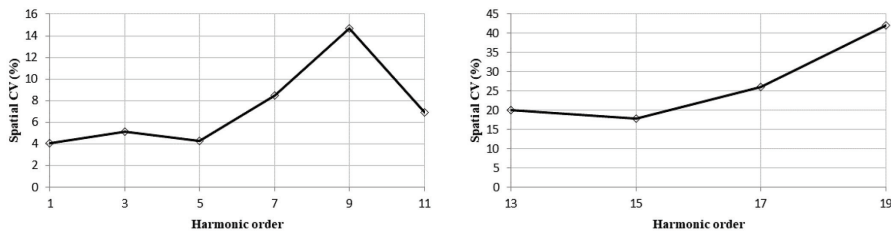
Figure 17. Spatial CV of a PC during 1 hour of a system stress test.

Table 1 presents the summary of SD values for devices under test compared to their total current RMS and the fundamental current RMS value. THD_I is also shown for reference. LED lamps with the highest and lowest THD_I are shown.

Table 1. Harmonic current SD compared to the RMS values of the current and the fundamental component.

Parameter	LED lamp #4	LED lamp #8	Monitor	Smart TV	PC (video)	PC (stress)
THD_I, %	154	22.7	203	37.6	23.4	11.1
I, mA	81.4	41.9	169	314	179	364
I_1, mA	43.3	40.9	74.1	294	174	361
$SD_{1,xy}$, mA	0.104	0.062	0.313	11.1	12.9	20.8
$SD_{3,xy}$, mA	0.084	0.004	0.301	3.41	1.50	2.24
$SD_{5,xy}$, mA	0.082	0.003	0.290	1.56	0.383	0.963
$SD_{7,xy}$, mA	0.082	0.004	0.275	1.50	0.312	1.52
$SD_{9,xy}$, mA	0.085	0.003	0.255	0.685	0.259	1.88
$SD_{11,xy}$, mA	0.089	0.002	0.233	0.935	0.567	0.648
$SD_{13,xy}$, mA	0.091	0.003	0.210	0.954	0.629	1.87
$SD_{15,xy}$, mA	0.091	0.002	0.187	0.447	0.457	1.39
$SD_{17,xy}$, mA	0.089	0.002	0.166	0.658	0.450	1.93
$SD_{19,xy}$, mA	0.088	0.003	0.148	0.699	0.451	2.65

The harmonic current variations can be very small compared to the total current RMS or the fundamental component. Considering that the current harmonic mean phasor magnitude value can also be very close to zero (i.e. variations around the zero point) the calculated CV will be greatly amplified even when the variations are very small. As in the last example, the spatial CV of the harmonic current is high, but the RSD1 value is low, in which this case the CV is not a reasonable and comparable indicator for the harmonic current variation.

The RSD1 is a more general indicator since it can be used to compare the "per unit" variation of the harmonic current. However, since it depends on the fundamental component, a heavily distorted load current (THD_I > 200%) can also affect comparability. The RSD1 value can describe, how "variable" any specific harmonic current is, but it does not provide any information about the extent of the variation.

Some examples of the variation are provided below. In each example, each black marker represents a 1-second measurement result of the harmonic current during 1 hour of testing. The blue circle represents the spatial deviation with a radius of two SD (2σ) around the mean. The red deviation ellipse is constructed using the 2SD of the real and imaginary components separately. The radial line of the red ellipse is oriented towards zero and represents the angle of the mean.

Figure 18 shows the variation of the fundamental component of the LED lamp number 8. The variation has a circular symmetric shape, but itself is very low (within 0.2 mA). This is considered a very stable current harmonic.
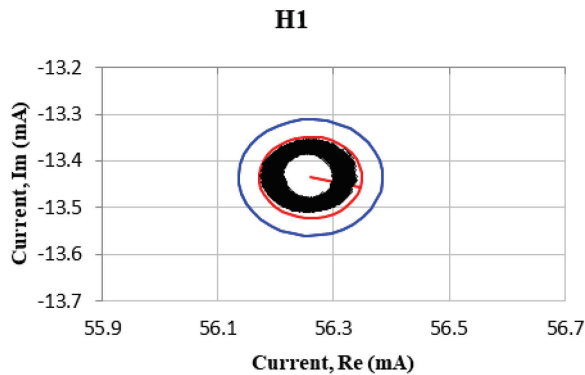

H1

Figure 18. The fundamental current of LED lamp number 8 during 1 hour.

Figure 19 shows the variation of the 5th current harmonic of a Smart TV. Most of the measurement points are clustered in a relatively small area, but for some time, the real component current variation changes significantly and even switches quadrants. Here, the spatial SD ellipses cannot properly quantify the variation of the harmonic current real and imaginary components. This is considered a harmonic current with a very wide range of variation.
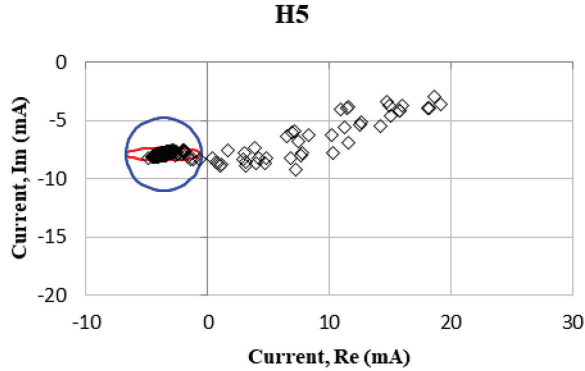
H5

Figure 19. 5th Harmonic current variation of a Smart TV during 1 hour of video playback over DP.

Figure 20 shows the variation of 9th current harmonic of a PC during a stress test. The spatial SD ellipses specify the extent of variations properly, but in this example, the variation has a unique shape, which cannot be described by the spatial SD. This is considered a harmonic current with a distinctive shape.
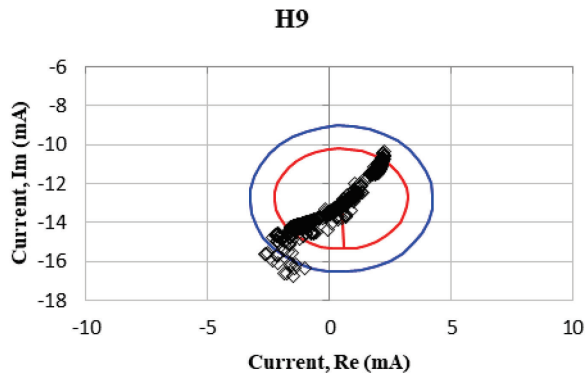
H9

Figure 20. 9th harmonic current variation of a PC during 1 hour of stress testing.

Based on the study in [IV], the variation of the current harmonics can have diverse extent, shape and direction both in case of stable and semi-stable loads. Introducing dynamic load properties to the loads (non-stable loads) can increase the variation even further and create complicated variation patterns.

In conclusion, using evaluation methods like the mean value and standard spatial deviation is not sufficient to describe the harmonic current variation range of modern variable nonlinear loads. Also, generalizing bivariate variation using only one-dimensional parameters is also ineffective due to possible distinctive variation patterns. In order to successfully asses the summation of harmonic currents, a more effective method must be implemented.

2 Nonlinear load modelling – State of the art

As the share and complexity of nonlinear loads connected to the public network are rapidly increasing, modelling load currents of these type of loads poses a significant challenge. Since nonlinear loads exhibit significant harmonic current distortion, one of the most practical methods is to decompose the load current into its harmonic components and model the harmonic content individually.

A modern household device can also exhibit different states of operation, which means the current, even at a constant voltage, will vary due to the supply circuit topology and operation, control processes and various algorithms. This kind of variation cannot be easily modelled with simple electrical parametric models. While the traditional numeric models provide an adequate representation of the stable loads, when a device or a group of devices operate at different modes with varying harmonic currents, a statistical approach is more practical. Even probabilistic models can run into difficulties, depending on the scope and characteristics of the harmonic current variation. The accuracy of any model also depends on where it is applied. For example, modelling a single device can produce different results than a group of devices, point of common coupling (PCC), or a feeder in a distribution network.

Several types of models have been proposed in the literature for modelling harmonic loads. This chapter presents an overview of common load harmonic current modelling methods, including their benefits and limitations, and analysis of several parametric and nonparametric probabilistic approaches.

2.1 Deterministic models

Deterministic load modelling is the oldest electrotechnical method of representing electrical loads. It uses electrical parameters, such as resistance, inductance, capacitance, etc. in combination to create an approximation of how the load should behave in an electrical circuit. There are various deterministic load models for modelling harmonic current. Several types that are used the most are discussed below.

2.1.1 Constant current source
The simplest harmonic load model is a constant current source model (CCS). Each current harmonic is modelled as a complex current source $\underline{I}_h$ having a fixed magnitude and phase angle. Each harmonic current is independent of the input voltage and does not vary in time. This model can be used if the load is stable and is insensitive to any external parameters.

In addition, this model is usually placed in the analysis focused on resonance, which does not consider the load dynamics. The advantage of this model is that the current harmonic spectra of numerous loads are already characterized in the literature; thus, it can be easily implemented in the harmonic analysis. However, it is not enough to analyse the interaction between the network and the nonlinear loads for non-typical operating conditions. [12]

2.1.2 Norton model
A more detailed deterministic model is the Norton model. For each harmonic order, a Norton model incorporates a harmonic complex current source in parallel with a complex impedance (Norton circuit). The parameters of a Norton model are determined experimentally using two sets of harmonic current and voltage measurements at different scenarios using (18) and (19) [13].

$$\underline{Z}_h = \frac{\underline{U}_{h,2} - \underline{U}_{h,1}}{\underline{I}_{h,2} - \underline{I}_{h,1}}, \tag{18}$$

$$\underline{I}_h = \frac{\underline{U}_{h,1}}{\underline{Z}_h} - \underline{I}_{h,1}. \tag{19}$$

The model presents a relationship between voltage and current harmonics. Although the Norton model allows for some level of network response, studies have shown that in case of highly nonlinear loads, the model can only accurately reproduce the exact scenarios that were used for calculating the Norton parameters [13]. For a wide range of test scenarios, the model showed only a slight improvement over the CSS model [12]. Additionally, this approach assumes the superposition of the harmonics and does not take into account the possibility of cross-dependency of harmonics of different orders.

2.1.3 Crossed-frequency admittance matrix

Originally proposed in the 1990s [14], the crossed-frequency admittance matrix (CFAM) takes into account the interactions between voltage and current harmonics of different orders. In general, the model consists of an *M x N*-sized matrix of complex admittances, that is multiplied by the array of complex harmonic voltages, resulting in an array of complex currents. The short form is shown in (20) and the full representation in (21). *M* and *N* represent the different harmonic orders for currents and voltages.

$$\underline{\mathbf{I}} = \underline{\mathbf{Y}} \cdot \underline{\mathbf{U}}, \tag{20}$$

$$\begin{bmatrix} \underline{I}_1 \\ \underline{I}_2 \\ \underline{I}_3 \\ \dots \\ \underline{I}_M \end{bmatrix} = \begin{bmatrix} \underline{Y}_{11} & \underline{Y}_{12} & \underline{Y}_{13} & \dots & \underline{Y}_{1N} \\ \underline{Y}_{21} & \underline{Y}_{22} & \underline{Y}_{23} & \dots & \underline{Y}_{2N} \\ \underline{Y}_{31} & \underline{Y}_{32} & \underline{Y}_{33} & \dots & \underline{Y}_{3N} \\ \dots & \dots & \dots & \dots & \dots \\ \underline{Y}_{M1} & \underline{Y}_{M2} & \underline{Y}_{M3} & \dots & \underline{Y}_{MN} \end{bmatrix} \cdot \begin{bmatrix} \underline{U}_1 \\ \underline{U}_2 \\ \underline{U}_3 \\ \dots \\ \underline{U}_N \end{bmatrix}. \tag{21}$$

In the case of linear loads, there is no interaction between different orders of harmonic voltages and currents. Thus, the size of the matrix will be *N x N* (square) and only the main diagonal of admittances $\underline{Y}_{nn}$ will remain while all the other matrix elements have zero value.

The CFAM model provides the possibility to analyse how the voltage distortions affect the current distortion, i.e. how the voltage harmonics affect the current harmonics. For example, a 3rd order voltage harmonic can affect the 3rd order harmonic current and 5th order harmonic current at the same time.

The model was further enhanced by adding the admittance matrix element dependency on the harmonic voltage phase angle [15].

A more detailed version of the original CFAM has been presented in [16], including several modifications [17]–[19] for modelling nonlinear loads. The extended short and full representation of the basic model is shown in (22) and (23).

$$\underline{\mathbf{I}} = \underline{\mathbf{Y}}^+ \cdot \underline{\mathbf{U}} + \underline{\mathbf{Y}}^- \cdot \underline{\mathbf{U}}^*, \tag{22}$$

$$\begin{bmatrix} \underline{I}_1 \\ \underline{I}_2 \\ \underline{I}_3 \\ \cdots \\ \underline{I}_M \end{bmatrix} = \begin{bmatrix} \underline{Y}_{11}^+ & \underline{Y}_{12}^+ & \underline{Y}_{13}^+ & \cdots & \underline{Y}_{1N}^+ \\ \underline{Y}_{21}^+ & \underline{Y}_{22}^+ & \underline{Y}_{23}^+ & \cdots & \underline{Y}_{2N}^+ \\ \underline{Y}_{31}^+ & \underline{Y}_{32}^+ & \underline{Y}_{33}^+ & \cdots & \underline{Y}_{3N}^+ \\ \cdots & \cdots & \cdots & \cdots & \cdots \\ \underline{Y}_{M1}^+ & \underline{Y}_{M2}^+ & \underline{Y}_{M3}^+ & \cdots & \underline{Y}_{MN}^+ \end{bmatrix} \cdot \begin{bmatrix} \underline{U}_1 \\ \underline{U}_2 \\ \underline{U}_3 \\ \cdots \\ \underline{U}_N \end{bmatrix}$$
$$+ \begin{bmatrix} \underline{Y}_{11}^- & \underline{Y}_{12}^- & \underline{Y}_{13}^- & \cdots & \underline{Y}_{1N}^- \\ \underline{Y}_{21}^- & \underline{Y}_{22}^- & \underline{Y}_{23}^- & \cdots & \underline{Y}_{2N}^- \\ \underline{Y}_{31}^- & \underline{Y}_{32}^- & \underline{Y}_{33}^- & \cdots & \underline{Y}_{3N}^- \\ \cdots & \cdots & \cdots & \cdots & \cdots \\ \underline{Y}_{M1}^- & \underline{Y}_{M2}^- & \underline{Y}_{M3}^- & \cdots & \underline{Y}_{MN}^- \end{bmatrix} \cdot \begin{bmatrix} \underline{U}_1^* \\ \underline{U}_2^* \\ \underline{U}_3^* \\ \cdots \\ \underline{U}_1^* \end{bmatrix}. \tag{23}$$

This version of the CFAM adds the dependency on the harmonic voltage complex conjugate and separating the admittances into two distinct components. The model was based on the equivalent circuit of a standard unfiltered AC/DC bridge rectifier. As this type of topology is used in most power supplies, it should be possible to apply this model to a wide range of household devices.

The difference between the two CFAM models is that the modified version does not require extensive testing to determine the admittance parameters, as they can be determined analytically using only a few measurements. However, the application is also limited by the topology used in the power supply. Despite the complicated derivation of the model parameters, the resulting linearized model for nonlinear loads provides the possibility to perform harmonic analysis on how a load behaves in a distribution network.

There have also been developments of combining CFAM model with the polynomial ZIP model to allow the modelling of nonlinear loads that undergo variable voltages with harmonic components. The model is applicable for the modelling of one or more harmonic loads in systems with the presence of other nonlinear loads, allowing to obtain some physical knowledge about the represented load [20].

2.1.4 Harmonic coupled Norton equivalent model

The harmonic coupled Norton equivalent model (HCNE) combines the properties of the Norton equivalent model and the CFAM model. The model consists of a Norton harmonic current source in parallel with a harmonically coupled admittance matrix. The representation in both short and full form is presented in (24) and (25).

$$\underline{\mathbf{I}} = \underline{\mathbf{I}_s} - \underline{\mathbf{Y}} \cdot \underline{\mathbf{U}}, \tag{24}$$

$$\begin{bmatrix} \underline{I}_1 \\ \underline{I}_2 \\ \underline{I}_3 \\ \cdots \\ \underline{I}_M \end{bmatrix} = \begin{bmatrix} \underline{I}_{s1} \\ \underline{I}_{s2} \\ \underline{I}_{s3} \\ \cdots \\ \underline{I}_{sM} \end{bmatrix} - \begin{bmatrix} \underline{Y}_{11} & \underline{Y}_{12} & \underline{Y}_{13} & \cdots & \underline{Y}_{1N} \\ \underline{Y}_{21} & \underline{Y}_{22} & \underline{Y}_{23} & \cdots & \underline{Y}_{2N} \\ \underline{Y}_{31} & \underline{Y}_{32} & \underline{Y}_{33} & \cdots & \underline{Y}_{3N} \\ \cdots & \cdots & \cdots & \cdots & \cdots \\ \underline{Y}_{M1} & \underline{Y}_{M2} & \underline{Y}_{M3} & \cdots & \underline{Y}_{MN} \end{bmatrix} \cdot \begin{bmatrix} \underline{U}_1 \\ \underline{U}_2 \\ \underline{U}_3 \\ \cdots \\ \underline{U}_N \end{bmatrix}. \tag{25}$$

The harmonic Norton current vector represents the harmonic currents at sinusoidal voltage conditions. The admittance matrix in this model describes only the influence of harmonic voltages. The full description of the HCNE model and its variations, including applications and experimental results can be found in [21]–[26]. The procedure for determining the admittance components is the same as in CFAM, by analysing interactions between the harmonic orders of voltages and currents. The difference is that the voltage harmonics are injected on top of the fundamental component, to determine the harmonic current response around the set Norton point. Test procedures have been

proposed to increase speed and uncertainty for obtaining the parameters [27]. Introducing the HCNE model significantly improved the modelling capacity and accuracy of nonlinear harmonic current producing loads. Combined with even further developments [28] it is one of the most accurate modelling methods for nonlinear harmonic current producing loads.

2.2 Probabilistic methods

Most deterministic models assume that the numerical model parameters do not vary in time. Depending on the device type, is often not the case with variable load characteristics. This means that the deterministic numerical models are suitable mostly for stable loads. Variations in load harmonic current can depend on factors like time, operating modes, usage cycling, etc. When these variations are present, a probabilistic approach should be considered. A general overview of probabilistic aspects and issues can be found in [29].

The most direct way to construct a probabilistic model is based on the empirical data, e.g. measurement results. Both harmonic current magnitudes and phase angles should be measured to produce meaningful models. The probabilistic approach can be divided into two categories. Parametric models describe probability using a fixed set of parameters that fit the data with a certain kind of distribution function. Nonparametric models describe the probability as processed empirical distributions which are calculated from the observed data set [V].

The conducted studies about the variations of the harmonic currents during operation have shown various types of patterns, which affect both the magnitude and the phase angle of the current harmonics. Due to this phenomenon, the probabilistic approaches must be bivariate, i.e. using co-dependent variables. This means that any measured harmonic current phasor is represented as a point on two-dimensional space using two variables (e.g. real and imaginary component) and only specific combinations of these components exist. Based on these preconditions, it is possible to apply probabilistic properties to a set of bivariate current phasors during load operation for each harmonic.

There are mainly two ways to represent a complex harmonic current phasor in Euclidean space: the polar coordinate system using magnitude and phase angle, and the Cartesian coordinate system using real and imaginary components. The coordinate systems can be freely translated from one to another. For the purpose of this research, and to avoid the issues arising with phase angle wrapping, the real-imaginary Cartesian coordinate system was used, indexed as x and y.

2.2.1 Parametric models

The most commonly used parametric method for probabilistic modelling is Gaussian distribution, also known as the normal distribution. The normal distribution has a specific probability curve defined using two parameters: mean value and variance (or standard deviation). The probability density function is presented in (26).

$$f(x) = \frac{1}{\sqrt{2\pi\sigma^2}} e^{-\frac{(x-\mu)^2}{2\sigma^2}}, \tag{26}$$

where:
μ – mean value of a variable x,
σ – standard deviation.

Examples of probabilistic modelling of harmonics date back to the late 1980s, where a basic concept can be found [30]. In this research, the harmonic magnitudes and phase angles were modelled as Gaussian distributions separately. It can also be applied for both the real and imaginary components and added geometrically, as it was done in previous research [IV]. However, this method only works if the variations always have an even spread on the complex plane and are independent of each other, which is very often not the case but could have been very common in the past.

To estimate the probability of the harmonic current phasors, a bivariate version of normal distribution (joint normal distribution) exists that is a generalization of Gaussian distribution to higher dimensions. Such bivariate normal distribution (BND) can be described as a probability surface defined by bivariate mean coordinates and a covariance matrix that specifies the relationship between the two variables. If, for example, a harmonic current variation has a directional shape, e.g. the variations are elongated or angled on the complex plane, the fitted BND model can describe a rotated ellipse, which defines the 95-percentile probability area.

Such bivariate normal probability distributions have been used to model harmonic current phasors in the past [31]–[33]. The mathematical representation for the mean and the covariance for joint (bivariate) normal distribution is shown in (27) and (28). The main diagonal represents the square of the variance, or SD and the other elements represent the variance between the two variables, which have opposite signs around the main diagonal.

$$\mu_{xy} = \begin{bmatrix} i_x \\ i_y \end{bmatrix}, \tag{27}$$

$$\Sigma_{xy} = \begin{bmatrix} \sigma^2(i_x) & \sigma(i_x, i_y) \\ \sigma(i_y, i_x) & \sigma^2(i_y) \end{bmatrix}. \tag{28}$$

In an example presented in Figure 21, a normal distribution is fitted to harmonic currents of a PC monitor during video playback. Here, the black markers are the 1-second measurement results during a 1-hour observation interval. The red and the blue line represents the individual probability densities of the perpendicular (real and imaginary) components. The bivariate probability density is represented as a yellow-red-black surface, with transparent and yellow colour having the smallest and black colour the largest probability density. The green ellipse on the horizontal plane represents the two-sigma (2σ or two SD) ellipse projection of the probability density distribution which accounts for the 95-percentile of values.
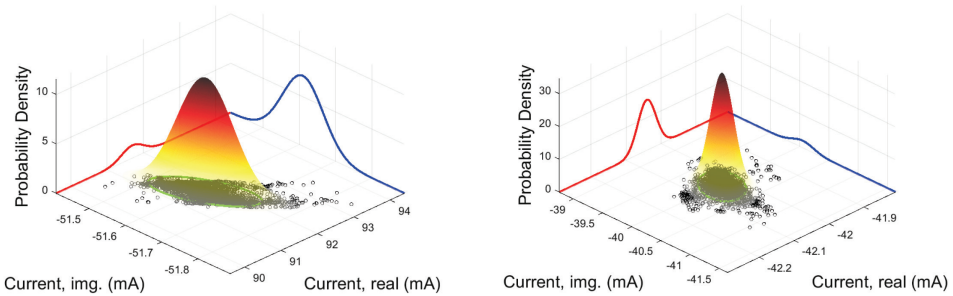
Figure 21. Bivariate normal distribution applied to the fundamental (left) and the 15th (right) current harmonic of a PC monitor during video playback.

The drawback of the BND is that it assumes the variation relationship between two components is linear on the complex plane. In case of variations with distinctive non-Gaussian shapes, spread or clustering due to multiple operating points, the normal distribution does not sufficiently represent the actual variation, as shown in Figure 22.
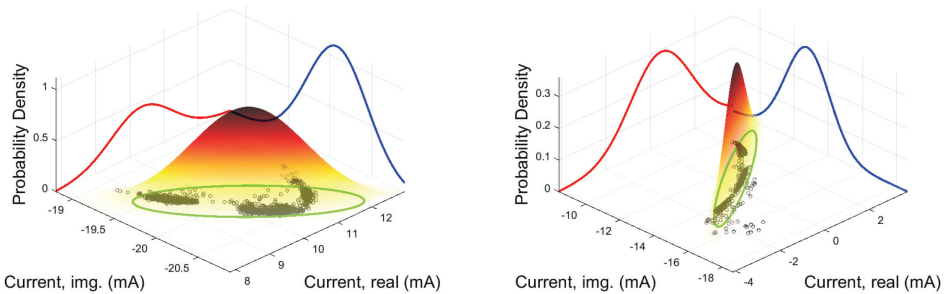

Figure 22. Bivariate normal distribution applied to the 5th (left) and 9th (right) current harmonic of a PC during a stress test.

Since the normal bivariate distribution does not distinguish clusters, there is a large number of cluster combinations which can result in identical distribution parameters. To deal with clustering issues in probabilistic analysis, various algorithms exist that are able to cluster the data into distinct groups, like the k-means, expectation-maximization (EM), etc. A probabilistic model is then applied to each cluster resulting in a total probability distribution that is composed of each individual cluster.

An example of such compound probability distribution is a multivariate normal mixture, i.e. the Gaussian mixture model (GMM) [34]. Such an approach has been reported for analysing power quality parameters, including harmonic current magnitudes and phase angles in [35], [36] as single variables. Although the GMM method is widely known and used in various scientific fields, very little research has been published on using it to model bivariate complex probabilistic load harmonic currents.

To obtain the model, the data is first clustered and the individual probabilities are then described using a set of BNDs with specified weights. The EM clustering method, for example, is iterative and convergent, which means that the result can depend on the initialization condition selection. The convergence can also be optimized, but this procedure is rather complicated and requires more iterations.

Examples of GMM are presented in Figure 23 and Figure 24. The fitted distributions represent the variations with sufficient accuracy. It is also not uncommon for the individual distributions to intersect to include the stray data points that do not fit into other cluster groups. The sub-distribution with a smaller proportion factor will contribute less to the whole distribution.
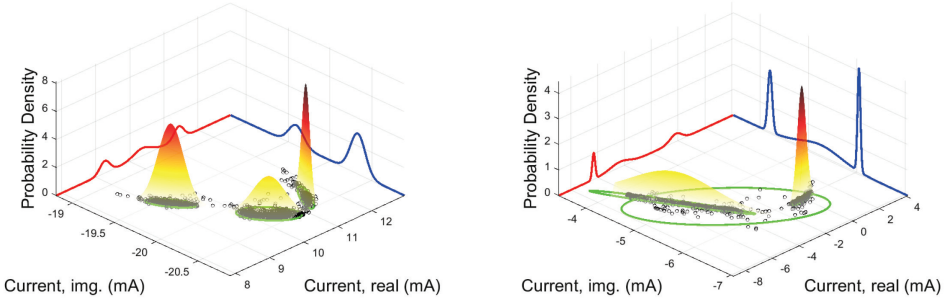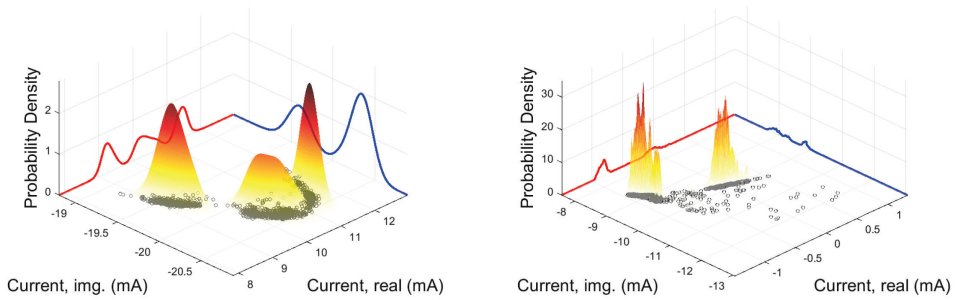
Figure 23. GMM distribution applied to the 5th (left) and 19th (right) current harmonic of a PC during a stress test.
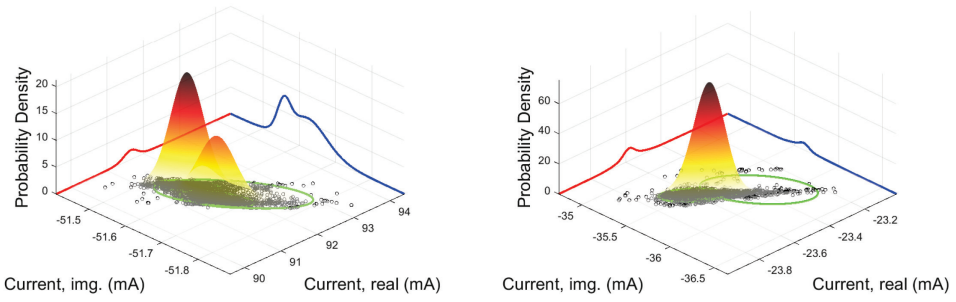
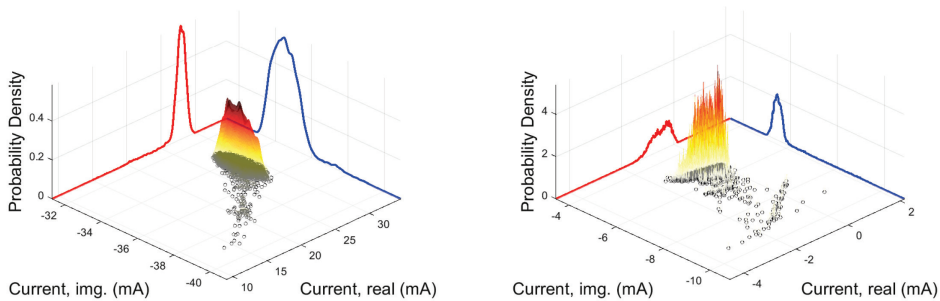*Figure 24. GMM distribution applied to the fundamental (left) and the 19th (right) current harmonic of a PC monitor during video playback.*

One of the issues with the specific GMM method is that using the standard clustering algorithms, the number of clusters must be given as an input for the algorithm. This means that to obtain the best results, GMM permutations with 1, 2, 3, etc. clusters should be calculated and the result which represents the harmonic current variation most accurately should be chosen.

2.2.2 Nonparametric models

One of the most used nonparametric approaches is the kernel density estimation (KDE). The usage of this approach under certain conditions to model harmonic current magnitudes and phase angles has been published in [37], [38]. However, as stated before, analysing the components separately will only provide information about the probability of both parameters separately, and reconstructing phasors from the said probabilities can result in inaccurate data and a bivariate version should be used instead [V].

In general, the KDE algorithm works by assigning a probability distribution for each data point using a kernel function and a smoothing parameter, called the bandwidth. The total probability is estimated by the sum of all the individual point distributions (kernels). The result of the KDE is a nonparametric curve that must be stored to represent the probability density of a variable. The general expression for kernel density estimation is:

$$f_h(x) = \frac{1}{N}\sum_{i=1}^{N} K_b(x - x_i) = \frac{1}{Nb}\sum_{i=1}^{N} K\left(\frac{x - x_i}{b}\right),$$

(29)

where:

N – total number of data points;

K – kernel function (normal distribution);

b – bandwidth.

The bandwidth in the kernel density estimation is the most important parameter. It directly influences the result as it causes smoothing of the probability density curve. Choosing a large bandwidth will result in a smoother curve that requires a smaller amount of data to be represented, but the information about specific variations can be lost with the smoothing. There are algorithms for optimal bandwidth selection, of which the most common is the mean integrated squared error (MISE) function. Overview of the utilization of the KDE, comparison of different kernel functions and bandwidth selection, and how they affect the final shape of the probability can be found in [39], [40].

The bivariate form of the formula is identical, but instead of one-dimensional variables, each parameter is a multi-dimensional vector or array. The result of a bivariate kernel density estimation is a nonparametric probability density surface. Depending on the variation extent and the desired resolution, the distribution requires a large amount of data to be stored for accurate representation.

Figure 25. KDE distribution applied to the 5th (left) and 11th (right) current harmonic of a PC during a stress test.

Figure 26. KDE distribution applied to the 3rd (left) and 13th (right) current harmonic of a PC during video playback.

Figure 25 and Figure 26 show an example of a KDE distribution applied to the harmonic currents of a PC during a stress test and video playback respectively. Despite the optimal bandwidth algorithm being used for all examples, a clear difference in the smoothness of the results can be seen depending on the variation pattern. A mesh of 200×200 points

was used for the surface. This translates to 40 000 data points that have to be stored to represent the probability of each harmonic current.

Compared to the computation-intensive KDE method, a simple nonparametric way of representing the harmonic current is to create an empirical bivariate histogram of probability. A histogram approach is grouping data into bins by counting how many data points fall inside the defined bin. The number of bins must be specified beforehand. The bivariate histogram data can then be normalized to represent the probability density of each point from a bin by using (30), resulting in a probability density mesh.

$$p_{x,y} = \frac{c_{x,y}}{N \cdot w_x \cdot w_y},$$ (30)

where:

$p_{x,y}$ – probability density of a specific bin at a specific location *(x, y)*;
$c_{x,y}$ – number of samples in a bin;
$w_x \cdot w_y$ – area of a bin;
N – total number of data points.
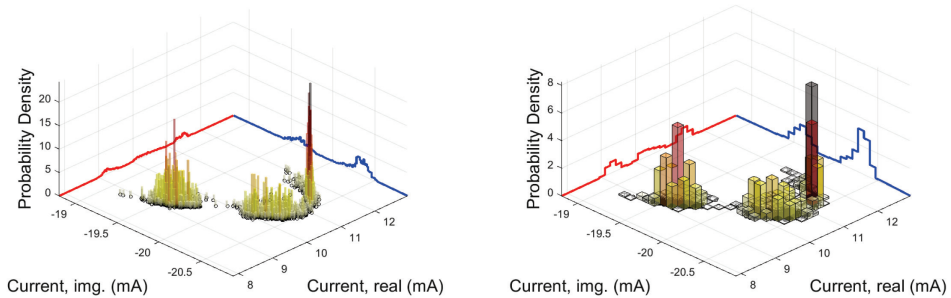
Figure 27. Histogram distribution applied to the 5th current harmonic of a PC during stress test using 100×100 (left) and 20×20 (right) bins.

Figure 27 shows an example of a bivariate histogram applied to the 5th harmonic current of a PC during a stress test using two different number of bins. Using fewer bins results in grouping more data, which results in loss of detail for small variation differences. Using more bins creates a more detailed representation of the probability distribution but the data requirement grows quadratically. The optimal number of bins is a compromise between resolution and data size and will depend on the variation spread pattern. As with the KDE, if a harmonic current has clusters that are separated from each other, there will be a lot of unused data space.

2.3 Probabilistic simulation methods

The usage of probabilistic models in simulations requires a methodology to (re)produce data samples based on the models. For bivariate probabilistic harmonic current models, each sample represents a harmonic current phasor having two components (amplitude/phase or real/imaginary). By sampling enough data points, the result should approximate the probabilistic behaviour of a load harmonic current.

One of the most universal methods for obtaining samples from any probability distribution is called inverse transform sampling (ITS), which requires the cumulative distribution function (CDF) of the probability distribution. The cumulative distribution

function F for a continuous probability of variable x can be expressed as an integral of its probability density function f:

$$F(x) = \int_{-\infty}^{x} f(x)dx, \tag{31}$$

or, for a discrete probability with points x_i, each having a probability $p_i = P(x_i)$:

$$F(x) = P(x_i \leq x) = \sum_{x_i \leq x} P(x = x_i) = \sum_{x_i \leq x} p(x_i). \tag{32}$$

When all the original data points are used to construct a CDF, it is called an empirical cumulative distribution function (ECDF). ECDF is always a stepped function that increases by $1/N$ at each sample of the N data points. ECDF can be used to validate and compare the probabilistic simulations.

The parametric and non-parametric CDFs have slight differences. A parametric distribution always results in a continuous CDF. CDF from nonparametric distribution is discrete and is based on the resolution of the probability estimation.

To sample data from a univariate distribution, a random number is generated between 0 and 1 with a uniform distribution. This number is then matched to the cumulative probability on the vertical axis of the CDF and the sample value from the horizontal axis is returned at the corresponding intersection point. The procedure for obtaining samples from an arbitrary univariate CDF is shown in Figure 28.
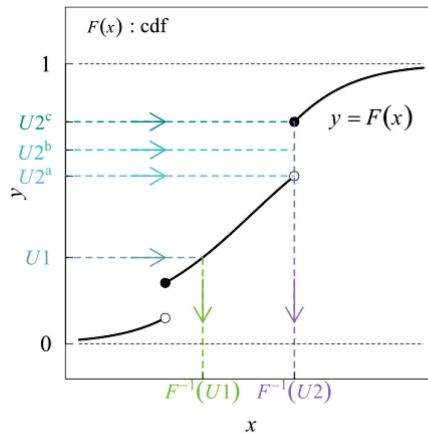
Figure 28. Inverse transform sampling examples for mixed discrete and continuous cumulative distribution function [41].

While sampling from a univariate probability distribution has many common solutions for both parametric and nonparametric cases, sampling from a multivariate distribution is still actively researched topic in the field of mathematics. There are two main issues to consider when considering bivariate sampling.

Firstly, when generating samples from a bivariate distribution, the variables must be treated as co-dependent. Using ITS on the CDFs of both variables separately may result in inaccurate data. For example, let the bivariate data of 1000 points (x, y) be clustered in different regions of the cartesian plane, with each cluster having 50% of the total number of data points. A KDE is used to create both PDF and CDF for both components separately. ITS is then used to sample data from both CDFs $F(x)$ and $F(y)$ by generating

two consecutive random numbers. The resulting data sample (x_i, y_i) is then stored. The process is repeated 1000 times to get 1000 data samples. The resulting CDF and PDF are plotted for both components and compared to the original data.

Figure 29 illustrates this process and how it leads to the generation of false data even though the CDF and PDF of original and simulated data for both components are aligned. Black and green markers represent the original and simulated data respectively. The red and blue curves represent the PDF and CDF of the original data and the magenta and cyan curves represent the simulated data.
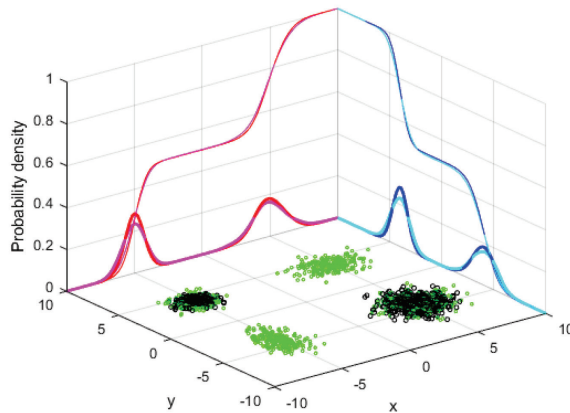
Figure 29. Example of incorrect simulation of data from KDE using CDF of both variables separately.

Secondly, while there are methods available for sampling from a multivariate normal distribution, sampling from a nonparametric bivariate (joint) distribution is a more complicated task. An example of a joint CDF is shown as a surface in Figure 30. Since the bivariate CDF is cumulative in both axes, the information about the individual marginal cumulative distributions are lost, which means the ITS method cannot be used in this context without probability transformations. Alternative methods like acceptance-rejection sampling exist, but it also has limitations in the multivariate cases.
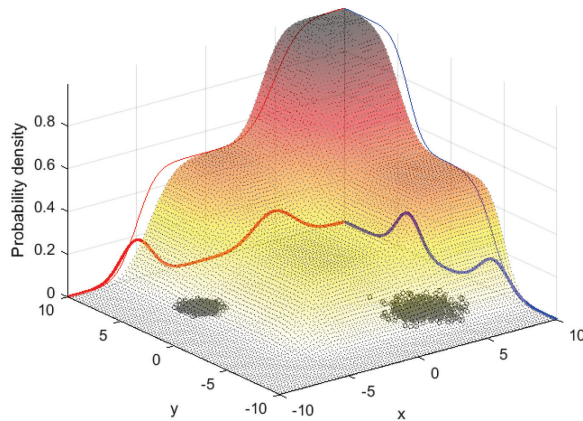
Figure 30. Joint cumulative distribution of clustered data.

3 A proposed probabilistic model for harmonic current

When dealing with the harmonic current of nonlinear variable loads, modelling harmonic currents probabilistically has the benefit of including the sporadic current variations in the model. Several probabilistic models were discussed in the previous chapter.

While the GMM provides a good approximation of the bivariate data, it still consists of fitting normal distributions to the empirical harmonic current data. Also, considering that the GMM is a convergent algorithm, it can produce different model parameters each time depending on the starting conditions.

Nonparametric models like the KDE or the histogram require bandwidth or resolution selection for the final representation of the bivariate probability distribution. The largest drawback of the traditional nonparametric surface-based probabilistic models is the required data amount for representing each harmonic current. If a harmonic current has clusters that are separated from each other, there will be a lot of empty values for the PDF and constant values for the CDF, which is inefficient. Also, sampling data from a nonparametric probability distribution is complicated and requires sophisticated and inefficient algorithms.

While taking this into account, a novel empirical approach to nonparametric probabilistic bivariate harmonic current modelling was developed for this thesis. The model describes the probabilistic distribution of a load harmonic current while maintaining a compromise between the data size and accuracy. The data representation is based on the histogram, but instead of using a mesh to represent PDF or CDF of the bivariate distribution, a set of linked CDFs arrays are used. This method reduces the data size required to represent harmonic current and allows using ITS method to correctly sample the data. The model requires a minimal amount of recalculation when used in simulations as the CDF is readily available for both variables.

One of the benefits of this type of empirical model is that the whole variation range, including extreme values, can be represented. It means that using this model in simulations can lead to the detection of potential problems in harmonic distortion levels which other models might miss.

3.1 Model definition

To construct a model for each current harmonic, a stepped CDF with a predefined resolution is created from all points of the first variable (for example, the real component of the harmonic current). The bivariate data points are then grouped based on each step of the primary CDF. Then, for each said group, a stepped CDF of the second variable (for example, the imaginary component) is constructed. This results in a total of $N + 1$ distribution curves, where N is the number of resolution groups.

Using stepped CDF functions ensures that no unnecessary points are stored where it is not needed. The resulting CDFs can be stored as a cell structure, for example, in MATLAB as a variable, or as a text file with comma-separated values (CSV), which requires more data storage, but is human-readable. The algorithm for the model construction is presented in Figure 31.
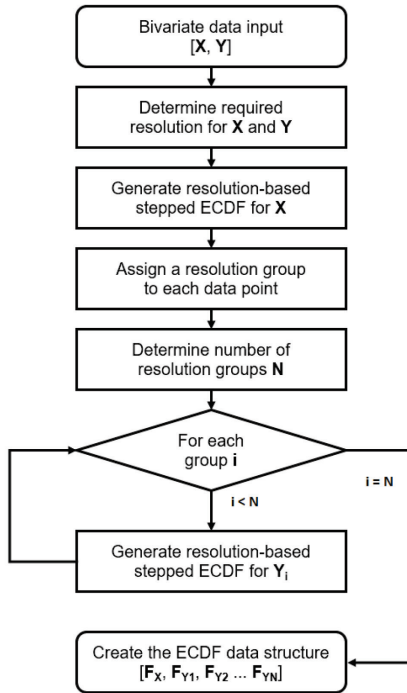
Figure 31. Algorithm for the proposed model construction.

The key factor for constructing the model is choosing the resolution of the stepped CDF. The resolution can be defined by the accuracy required to represent the current harmonics, which can be based on the harmonic current phasor magnitude. Often, a value of less than 1% is rarely needed and it is unnecessary to have too much detail of the variation because some of it can be caused by noise or the measurement setup itself. Choosing too fine resolution will result in a large number of secondary CDFs. Also, when a harmonic current has a large variation in magnitude and a 360° variation in phase (i.e. across all four quadrants), the number of secondary CDFs can also be very large.

In this study, the resolution chosen for each harmonic order was based on the minimum measured magnitude accuracy principle, according to the following sequence:

- Determine the required accuracy c as a percentage;
- Find the mean harmonic current magnitude $I_{m,h}$ of the data samples;
- Calculate the minimum magnitude threshold for excluding values very close to zero using $I_{m,h,lim} = I_{m,h} \cdot c$;
- Find the minimum current magnitude that is larger than the threshold: $I_{m,h,min} > I_{h,lim}$;
- Calculate the resolution using $D = I_{m,h,min} \cdot c$;
- If necessary, round the resolution to the nearest 10-base number;
- If necessary, limit the minimum resolution to measurement uncertainty level.

Such algorithm ensures that the maximum variation error is not more than the set accuracy of the minimum harmonic current magnitude, except in cases where the resolution is limited, and the measured harmonic current magnitude is very small. Based on extensive testing, it was found to be an optimal selection for modelling harmonic current.

3.2 Properties and examples

A compromise between the data size and resolution can reduce the number of points required to define the model. To store a very detailed representation of the harmonic load current, a resolution can be chosen that is comparable to the measurement accuracy of the system used in obtaining the measurement data, or by a specific set of rules. However, the data increases exponentially with resolution and at some point, storing the complete measurement data would be more efficient. The resolution, however, can be reduced by aggregation, where necessary.

The observation time is also a crucial factor for constructing the harmonic current model. It should be long enough to obtain enough data points and extreme values that can vary with different operating modes. For example, for a battery charging device that takes two hours to fully charge, it is not practical to measure several minutes only as the load current can vary during the cycle.

The main benefit of the model is the possibility to use the ITS method for sampling the data. First, the CDF of the first variable (for example, real component) is sampled. Then, from that matched CDF of the group, the second variable is sampled (imaginary component). The result is a data point (x, y), which is part of the defined distribution. By sampling enough points, a distribution will be reconstructed which approximates the original distribution. The model works with all kinds of variations, including clustering, which means that the model is suitable for modelling variable current harmonics.

Another benefit of this type of model is that it is universal and can be used on many different layers of the distribution network. It is possible to represent current harmonics for a single load, group of loads, PCC, network feeder or even a transformer. However, this model is mainly suitable for a single load or a group of loads as other factors such as usage patterns, time of day, week and seasonal changes are present at higher layers. By aggregating the model in time, e.g. by measuring longer intervals, which might result in loss of resolution and phasor accuracy due to averaging, it would be possible to represent a longer time cycle, such as a day or a week.

A drawback of the model is that it can only represent a specific scenario. It cannot distinguish the effects of outside factors such as voltage levels, voltage distortion, network state, etc. In order to consider such variables, measurements should be performed for each specific scenario that represents the corresponding situation.

The visualization of the model is presented in Figure 32. The red curve, in this example, represents the CDF of the real current component, and each blue curve represents the CDF of the imaginary current at each primary variable group.
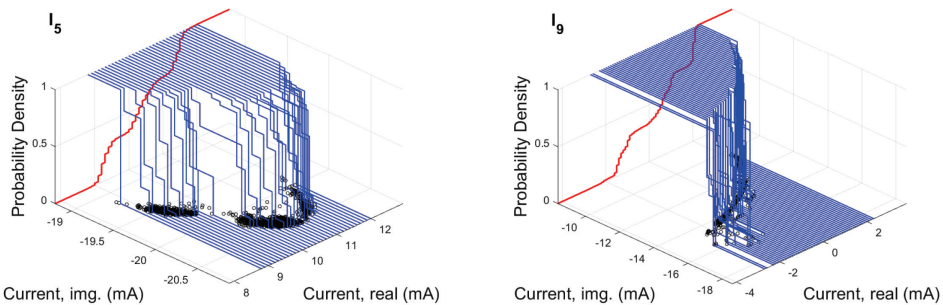

Figure 32. Visualization of the proposed bivariate probabilistic model of the 5th (left) and 9th (right) harmonic of a PC during a stress test.
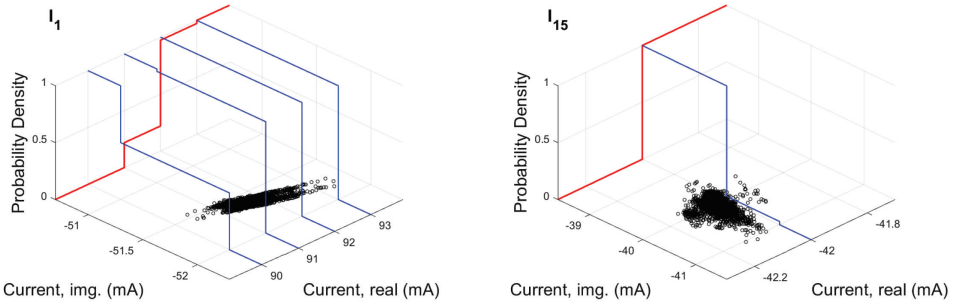
Figure 33. The proposed bivariate probabilistic model of the fundamental (left) and 15th harmonic (right) of a PC monitor during video playback.

The resolution was selected based on the accuracy of 1% of the minimum harmonic current magnitude., limited to 0.1 mA. Figure 33 shows an example of when it is not necessary to use a large number of data points to achieve 1% accuracy. The maximum relative variation error for both cases is 0.6% and 0.9% respectively.

It might be counter-intuitive to think that the resolution is finer when the harmonic currents are small, but it is essential when considering load aggregation (i.e. many loads of the same type connected simultaneously) as this will increase the accuracy of the harmonic current summation when the individual harmonic currents are small.

3.3 Probabilistic simulations

Simulations were carried out for comparing the GMM and the proposed nonparametric model since they provided the best results from the harmonic current variation perspective. In total, 1000 random data points were sampled from the bivariate probability distributions of each model and compared to the original data. To assess the model accuracy, full ECDFs for the original and simulated data were constructed for both bivariate components.

Figure 34 to Figure 37 present the harmonic current simulation results for various loads. Black markers are the measured harmonic current, green markers are the simulated harmonic current obtained from probabilistic models. Red and blue curves represent the full ECDF of the measured current real and imaginary components, and the magenta and cyan represent the ECDF of simulated current respectively.
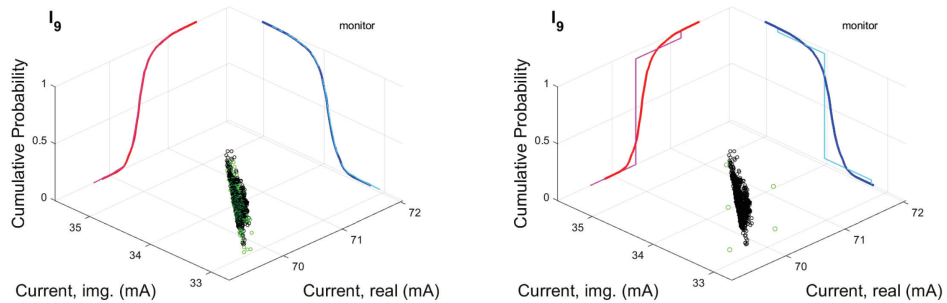
Figure 34. A data simulation comparison of GMM (left) and proposed model (right) for 9th harmonic current of a PC monitor during video playback.

45
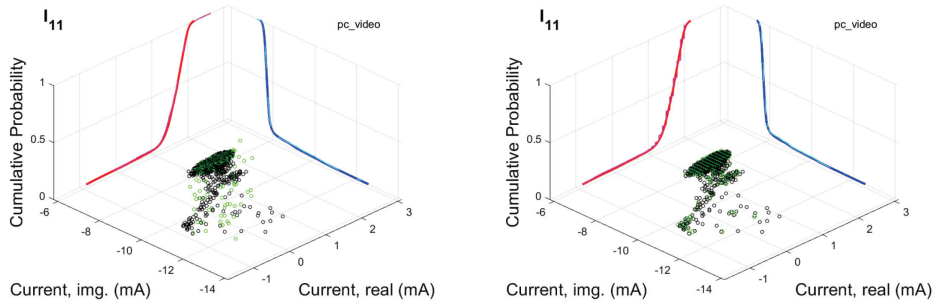
Figure 35. A data simulation comparison of GMM (left) and proposed model (right) for 11th harmonic current of a PC during video playback.
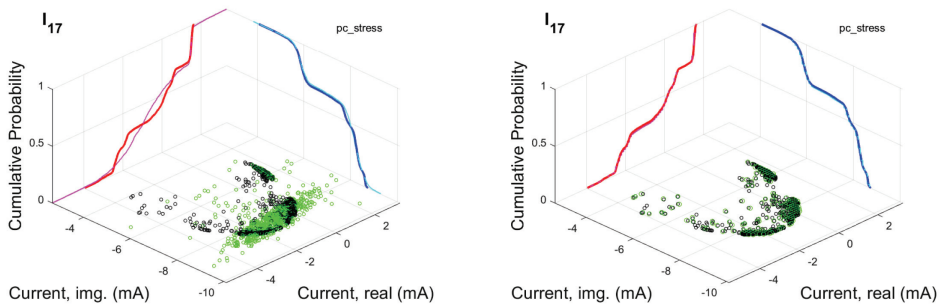
Figure 36. A data simulation comparison of GMM (left) and proposed model (right) for 17th harmonic current of a PC during a stress test.
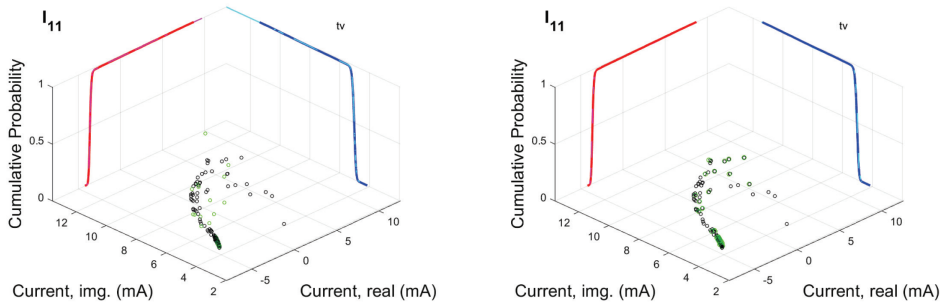
Figure 37. A data simulation comparison of GMM (left) and proposed model (right) for 17th harmonic current of a smart TV.

It is difficult to assess and validate the probabilistic simulation results analytically, thus a mix of visual inspection of the data point distribution and comparison of the individual ECDFs was conducted. Based on the research findings, both models showed good results for modelling harmonic current. Since the GM model is based on mixed normal (Gaussian) distributions, it provides continuously distributed sample points, which result in a smooth line.

The GMM matches the distribution of the simulated data almost in every case, except when the model could not be fitted perfectly due to the specific variation pattern of the harmonic current. In some cases, the model also did not converge on the first run.

46

This is one issue of the EM or other converging algorithms used for fitting models that rely on the initial condition selection. The proposed model, on the other hand, is based on resolution and it will always result in a stepped ECDF with the same result, provided the resolution remains unchanged.

The proposed model will fit the source data regardless of the variation pattern and it is only limited by the resolution. In Figure 34, in the case of the proposed model, the simulated data ECDF shows a visible difference from the original data ECDF. However, the variation in this example is very small compared to the magnitude and the maximum sample variation error is just below 1%, as was the precondition of the resolution calculation.

The main advantage of the GM model is that small amount of data is required to store the model as the definition of the BND requires only the mean value vector and the covariance matrix, combined with the weight of each mixture component. The disadvantage is that the fitting algorithm requires the number of mixture components to be specified beforehand. The algorithm might also produce different model results depending on the initial conditions, or "guesses". Depending on the source data variation pattern, it is also not guaranteed that the algorithm will converge 100% of the time and fit the shape of the variation perfectly.

The main advantage of the proposed non-parametric resolution-based bivariate probabilistic model is its efficacy and simplicity. With optimal resolution selection, the model can reproduce results with the desired accuracy. The data structure of the model, which is based on the array of marginal cumulative distribution functions, is perfect for the ITS algorithm for sampling random data. It is also universal and could represent any kind of variation pattern.

The main disadvantage of the proposed model is that since it is originally a fixed resolution-based model, there are situations when the size of the model can grow very large. When the variation of the harmonic current magnitude has a very large range, the resolution will be based on the smallest magnitude and the number of steps to represent variations on the largest magnitude scale grow exponentially. At the current state of the work, the algorithm limits the minimum resolution selection to the required accuracy percentage of the mean harmonic current magnitude. This means that any variations smaller than that specified value are grouped as one data point, which might be insignificant, considering that the specific current harmonics can also have very large values at some point.

It is possible and it is strongly encouraged to develop the proposed model and the resolution selection algorithm even further. Instead of the fixed resolution, it could be dynamic, and increase based on the magnitude of each data component value, for example, on a logarithmic scale.

Also, as the algorithm in its current state considers 100% of the harmonic current measurement points for the model. Depending on the randomness of any current harmonic, any stray data points which have insignificant probability could be excluded from the model to reduce the model data size.

4 Harmonic current summation

Estimating harmonic current of simultaneously connected variable loads can be a complicated task. Since current harmonics are phasors, it means that their phase angles, or their complex properties, must be considered when performing any kind of addition or subtraction, which is based on the KCL. Since the harmonic current can also change randomly in time, simply adding together the averages will not provide sufficient information about the possible harmonic current variation at the connection point.

The summation of complex harmonic phasors has been studied since the 1970s [42]. Until the 21st century, the probabilistic summation methods were based on the central limit theorem (CLT), which states that the sum of independent random variables approximates a normal distribution. Research published during this period presented analytical methods for random phasor summation [43]–[47]. These methods provided good results as long as the individual phasor were statistically independent, had either similar uniform or Gaussian distributions, and the number of loads was sufficiently large, or the loads were very similar. Recent research and measurement results have proven that the summation characteristics of harmonic current phasors from a random selection of modern non-linear loads differ from a BND, as predicted by the CLT [48]–[52]. The complex and polar plots presented in the research show harmonic current distributions that have distinct shapes and ranges, are dependent on the composition of the individual load characteristics, and cannot be generalized by the BND. In case the distribution of the individual phasors is not clearly defined, and varies in range and shape of the dispersion, approximations like the CLT may not be sufficient. More effective methods should be implemented in such cases that result in a universal solution.

The proposed method for harmonic current summation in this thesis is to use novel bivariate probabilistic models to estimate the probability of the collective impact of each current harmonic from each load at the PCC. The objective of the probabilistic summation is not to determine how the harmonic current is behaving over time, but instead to map the possible harmonic current emission levels and their extent. Estimating the range of harmonic currents and their probabilities can greatly assist in network planning and helps to use the network resources more efficiently.

To be able to evaluate the model-based harmonic current summation simulation, a study was performed in the scope of the thesis on verification of the KCL for harmonic current to assess any possible summation uncertainty.

4.1 Measurement-based harmonic current summation uncertainty

A study was conducted to investigate the possible deviation between the measured and calculated sum of the harmonic currents from various nonlinear stable loads. A set of 16 LED lamps were measured for one minute in 29 combinations of 2 and 3 to investigate the harmonic current of simultaneously connected loads. The lamps had a very small individually measured 95-percentile spatial CV of below 0.6% and average CV below 0.3%.

If many stable loads that have very little current variation are connected to a common point simultaneously, the resulting current should obey the KCL, which is also true for the individual current harmonics due to the superposition principle of the harmonic analysis. The harmonic currents from each load combination scenario were compared to their analytical sum counterparts calculated from the individual load measurements. The two resulting harmonic current phasors were compared according to principles

shown in Figure 38. The results for such comparison are presented in Figure 39 and Figure 40. Red colour represents the magnitude difference, blue colour phase angle difference and the black phasor, or spatial difference. [IV].
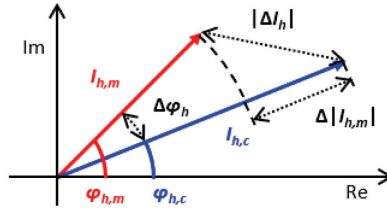

Figure 38. Diagram for determining the magnitude ($\Delta|I_h|$), phase angle ($\Delta\varphi_h$) and phasor ($|\Delta I_h|$) difference between measured (red) and calculated (blue) values.
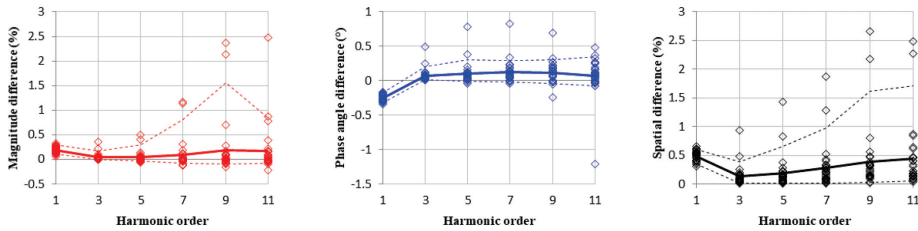

Figure 39. Differences between mean calculated and measured harmonic current parameters of summation for low-order harmonics of LED lamps.
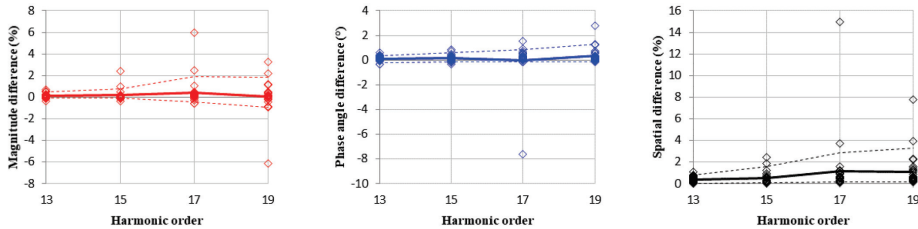
Figure 40. Differences between the calculated mean and the measured mean harmonic current parameters of summation for high-order harmonics of LED lamps.

The results from the summation study revealed that there are differences (offset) between the mean calculated and measured harmonic current even if the loads are very stable. The spatial offset also increased with the harmonic order. For low-order current harmonics up to 11th, the 95-percentile spatial difference was between 0.5 and 2%, and for high-order harmonics up to 4%. The average difference was below 1%. The magnitude component had a difference up to a range of -1% and +2%, and the phase angle up to a range of -0.5 and 2 degrees.

The 95-percentile CV values for the combinations were only up to 1% (0.4% change from the individual loads) and the maximum SD of the current harmonics for all combinations was only measured to be up to 0.1 mA, which means that the difference could not have come from the harmonic current variation, but from an actual offset of the phasors.

This means that the summation evaluation uncertainty for the measurement setup increases with harmonic order can be up to 4% or even more for the 19th harmonic order. This must be considered when performing harmonic current simulations.

The uncertainty of the harmonic current summation could come from many aspects of the measurement setup like cables, connections, layout, measurement equipment, etc., which all can affect the impedances of the circuit, which can affect both current and voltage. As the impedances depend on the frequency, the increasing uncertainty with harmonic order is in accordance with the theoretical background. The exact reason for the deviations should be studied in the future work to improve uncertainty and validation capability of the test setup.

4.2 Monte-Carlo based summation simulation

When a load harmonic current is defined by a probabilistic model, random values can be sampled from its probability distribution. By generating a large number of samples using specific algorithms, the probability distribution of the resulting data should match the original probability distribution, as was discussed in the previous chapter.

Generating samples of current harmonic phasors randomly from bivariate probabilistic distributions from multiple sources with variable current and adding them together results in one probable outcome of the sum of the harmonic current. Repeating this process large number of times results in many possible outcomes for the harmonic current combinations. The probability distribution of the resulting collective data points will represent the estimation of the total harmonic current at the PCC. This process of obtaining possible outcomes from probabilistic data is called the Monte-Carlo method.

Such simulations were performed with recorded data from a PC and a PC monitor during video playback for one hour. The harmonic current emissions of loads were measured separately and while simultaneously connected. Bivariate probabilistic models were generated from the individually measured data, and the Monte-Carlo method was used to generate probabilistic data for the sum of both loads.

The GMM and the proposed model was used in the simulations and compared since they had the best results in harmonic current representation while having feasible methods to sample data form their respective probability distributions.
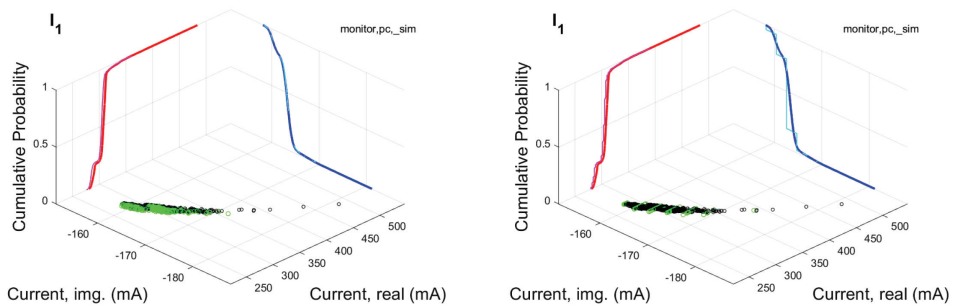
Figure 41. Summation simulation comparison of GMM (left) and proposed model (right) for the fundamental current of a PC and PC monitor during video playback.
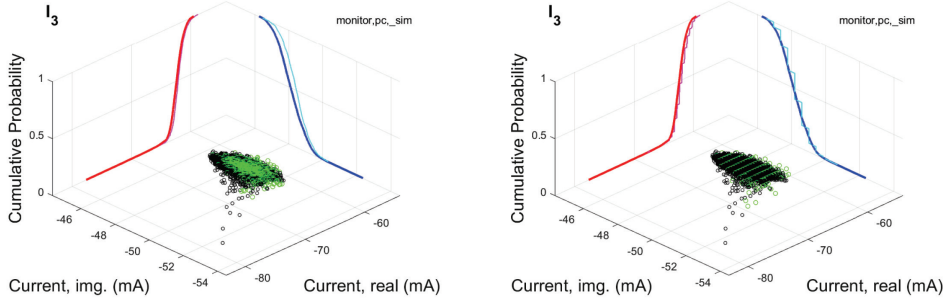
Figure 42. Summation simulation comparison of GMM (left) and proposed model (right) for 3rd harmonic current of a PC and PC monitor during video playback.
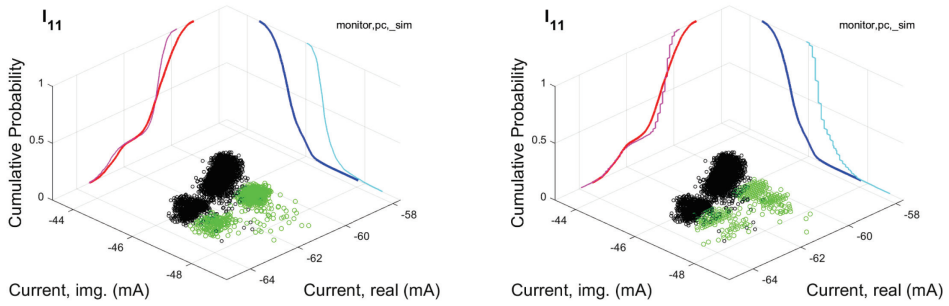

Figure 43. Summation simulation comparison of GMM (left) and proposed model (right) for the 11th harmonic current of a PC and PC monitor during video playback.

Some of the results from summation simulations are presented in Figure 41 to Figure 43. Both models show exceptional results for low-order harmonic summation estimation. The wide variation range of the fundamental component of simultaneous loads is also present in the simulated results from individual loads. The distinctive variation shapes and clusters are also preserved for high-order harmonics.

To analytically compare the simulation results, the relative spatial mean offset and standard deviation offset was calculated according to (33) and (34) respectively:

$$\Delta I_{xy,h,\%} = \frac{\sqrt{\left(i_{x,h,sim} - i_{x,h,meas}\right)^2 + \left(i_{y,h,sim} - i_{y,h,meas}\right)^2}}{\sqrt{i_{x,h,meas}^2 + i_{y,h,meas}^2}} \cdot 100\%, \qquad (33)$$

$$\Delta SD_{I,xy,h,\%} =$$
$$= \frac{\sqrt{\left(SD_{I,x,h,sim} - SD_{I,x,h,meas}\right)^2 + \left(SD_{I,y,h,sim} - SD_{I,y,h,meas}\right)^2}}{\sqrt{i_{x,h,meas}^2 + i_{y,h,meas}^2}} \cdot 100\%. \qquad (34)$$

Since the comparison uses Gaussian approximation, it cannot compare the distinctive variation patterns, but it is an adequate general tool to compare the overall spatial

position and the dispersion of data points. The results for the offset of mean values and the differences between SD values are presented as percentages in Table 2.

Table 2. Harmonic current summation simulation results.

Harmonic order	GMM		Proposed model	
	$\Delta I_{xy,h,\%}$	$\Delta SD_{I,xy,h,\%}$	$\Delta I_{xy,h,\%}$	$\Delta SD_{I,xy,h,\%}$
1	1.05	0.33	1.18	0.41
3	0.66	0.08	0.52	0.07
5	0.67	0.04	0.67	0.19
7	0.77	0.09	1.04	0.18
9	1.32	0.27	1.18	0.15
11	1.61	0.20	1.39	0.14
13	2.53	0.56	2.66	0.52
15	2.55	0.56	2.43	0.46
17	3.96	1.47	3.74	1.52
19	3.90	1.77	3.79	1.55

Although using this evaluation method, the standard normal distribution would also achieve similar results since both are based on the Gaussian distribution. However, Figure 44 shows that a normal distribution is not able to reproduce the clustered variation of the harmonic current and thus was not considered for the summation simulation.
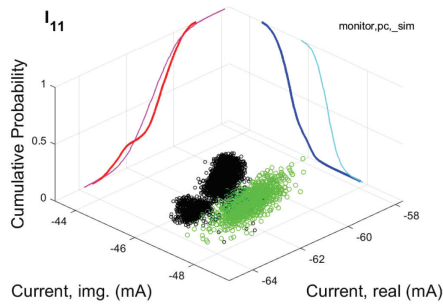
Figure 44. Summation simulation using a bivariate normal distribution model for the 11th harmonic current of a PC and PC monitor during video playback.

Based on the simulation results, a slight deviation, or offset, of the harmonic current distribution compared to the measured value was visible. The deviation of the mean harmonic current increased with the harmonic order and was up to almost 4% for both models. This was investigated and a difference between the arithmetic sum of the harmonic currents measured from individual loads, and the simultaneous operation of loads was found, as stated in the previous chapter. The difference of standard deviation was also observed, but this was expected and was under 1.8% even for the worst case. Some variation shape dissimilarities were visible in the graphical representation, but it could have also been caused by the summation uncertainty.

A summation simulation was also performed using synthesized empirical data based on the KCL analytical summation the individual measurements while ignoring any line

impedances. The synthesized data was obtained by adding each 1-second harmonic current measurement data from two devices at the same time intervals. While this is purely theoretical, it can be considered as a reasonable analytical approach because all three tests, which included the combination of the two loads, were carried out in identical operating conditions. The difference between synthesized and measured harmonic current data is shown in Figure 45. Not only is there an offset, but also a difference in the variation shape is visible. The offset contributes to the difference of the mean and the shape variation contributes to the difference of the SD.
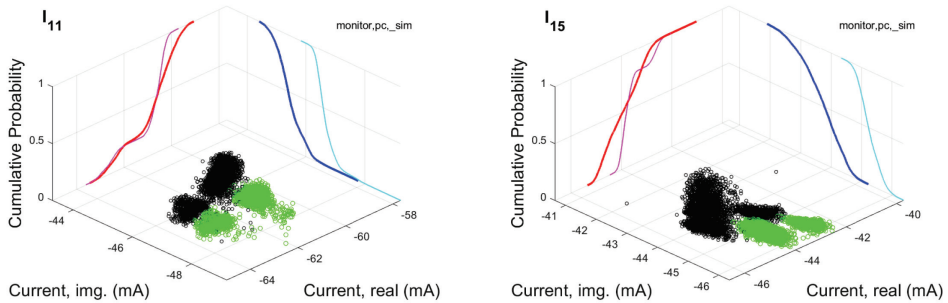
Figure 45. Differences between measured data (black) and the synthesized data (green) of harmonic current for the 11th (left) and 15th (right) harmonic current of a PC and PC monitor during video playback.

The model-based summation simulation was performed again and compared to the synthesized data. Using the synthesized data, the GMM model had a maximum mean and SD difference of 0.2% and 0.1% respectively. The proposed model had a maximum mean and SD difference of 0.3% and 0.25%. As an example, the comparison of the morel performance for the 11th current harmonic is presented in Figure 46.
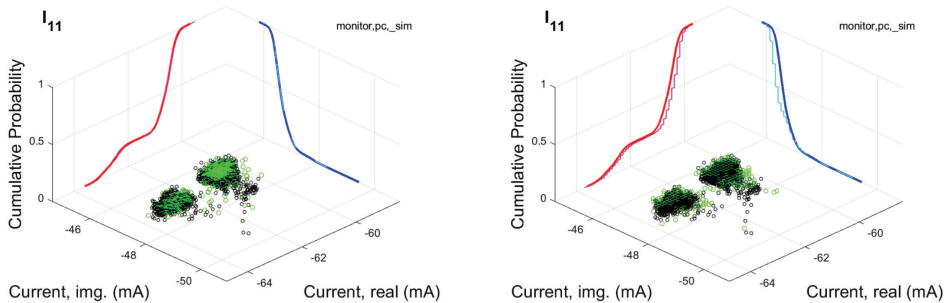
Figure 46. Summation simulation comparison based on synthesized data for GMM (left) and proposed model (right) for the 11th harmonic current of a PC and PC monitor during video playback.

Based on the results, the bivariate probabilistic modelling of harmonic current proves to be an effective method for estimating probabilistic harmonic current When the variation of load harmonic current is measured, it can be modelled using bivariate probabilistic models like the GMM and the proposed nonparametric resolution-based model. Using the models in Monte-Carlo based summation simulation, an accurate estimate of the resulting sum of the harmonic currents can be provided.

4.3 Scenario-based modelling and simulations

Measuring harmonic emissions at different scenarios will produce an "image" or a "fingerprint" for each harmonic current of a specific load or load combination for each scenario. The measured data is then converted to the probabilistic representation with a defined resolution. When enough scenarios are obtained, the harmonic current model for the specific scenario can be chosen based on the situation.

It is important to distinguish if the harmonic variations are caused by the internal operating modes or by user selection. For a static load, the time required should be enough to record any internal variations, which are usually small. For variable loads, a typical usage cycle can be recorded and then represented. If some operating modes can be distinguished based on the purpose of the operation, it could be viewed as a separate scenario. However, a single electrical device usually performs a specific task for a specific purpose. There are models available [53], [54] that can simulate when and how often a device is used, i.e. when it is on and when it is off. This is not considered as an operating cycle and it is usually influenced by the external factors and should be viewed separately.

Coupled with the load usage models and network state models, it would be possible to use the Monte-Carlo simulation to produce an estimation of the harmonic emission levels at any PCC based on different scenarios.

While the model represents the harmonic current at a fixed scenario, it is possible to group the situations with similar specific parameter ranges as one scenario and create sub-models for different scenarios. For example, where the voltage level is high, the voltage distortion is high, or both. To simulate a network scenario, a measurement can be carried out using a predefined voltage magnitude and waveform. When enough scenarios are modelled, the opportunity arises to choose the correct scenario model for simulating harmonic emission levels.

5 Conclusions

5.1 Summary

This thesis introduces a novel approach to harmonic current modelling by using bivariate probability distributions. Since harmonic currents are defined as rotating vectors, i.e. phasors, modelling just the magnitude does not have much application in the field of estimating harmonic currents in low voltage distribution networks. Adding the magnitudes without the phase angle data in case of harmonic current summation can give incorrect results if there is a phase angle diversity. The correct way of harmonic current summation is to use the vector sum of each individual harmonic phasors. Including phase angles in the models provides the ability to analyse and estimate the interference, or summation of the individual current harmonics. However, treating the phase angle as a separate variable can limit the ability to model the phasor variation in case of a variable nonlinear load. To model harmonic currents that can have any type and shape of variation, the magnitude and phase angle, or the complex current using the real and imaginary components should be considered as joint variables that are co-dependent. The bivariate probabilistic modelling and simulation method proposed in the thesis can provide many benefits compared to the previous approaches and is a one step closer to solving the issues regarding variable harmonic current modelling.

The thesis also presents a developed novel and unique nonparametric model for representing variations of harmonic current as an array of co-dependent resolution-based stepped cumulative probability functions. The model is in a way a further development of a histogram but constructed using specific criteria and having a structure which is simple and effective from which random data can easily be sampled using standard methods.

Of the existing multivariate distribution models, the GMM was found to be the most promising that can represent the harmonic current variations of household devices. The GMM is a parametric continuous function which can provide bivariate data with infinite resolution when used in random sampling. However, issues with the model include the requirement of specifying the number of mixtures to be included in the model which are fitted using the EM algorithm. While also having a converging algorithm, the resulting model parameters may vary depending on the selection of initial condition, which can cause the modelling process to be nonrepeatable.

To be able to perform the measurements and verification of the models, a test bench was designed and constructed which can accommodate up to 16 loads in any combination, including the possibility of warming the loads when not used for the measurements. The switching of the loads is controlled digitally, and power to the loads can be fed from any type of power source.

Both models were used in the harmonic current simulation, which was based on the Monte-Carlo method. The purpose of the simulation was to verify the harmonic current estimation method of simultaneously connected loads. The results showed a difference of under 4% in the worst case between the modelled and measured harmonic currents by using simple analysis. The error increased with the harmonic order and was comparable to the measurement setup uncertainty which was also determined. Such summation method with bivariate probabilistic models can be used to not only estimate the average values of the current harmonics but to also study the extent of the total harmonic current variation of connected loads, and the probability of where a certain

harmonic phasor might be found, which can provide valuable information for the network planning and design.

While the research for the thesis is focused on modelling harmonic currents of single devices, the method provided is not necessarily limited to a device level. The bivariate probabilistic modelling, simulation and analysis can be applied to many distribution network layers. One such example of the useful applications would be to use the method to model harmonic currents in a feeder of a substation. The feeder current would be measured for a 24-hour period at certain condition (day of the week, month, temperature, etc.) and a bivariate probabilistic model would be constructed from the measurement data. If many feeders are measured at the same conditions, the models constructed from the data could be used in studying possible loading of the transformer from harmonic current using feeder combination simulations. The result would be a complete probability distribution of each current harmonic present in the transformer. Parameters like the minimum and maximum harmonic current magnitude, phase angle, the most probable level, etc. could be derived from the final distribution result. Studies like this could prevent problems caused by the harmonic currents being present in the LV distribution network. Estimating harmonic currents beforehand can encourage to take precautions to eliminate possible damages caused by harmonic currents later on.

5.2 Future work

One of the primary future research topics is verifying the models and methods presented in this thesis using a more diverse selection of nonlinear loads with a wider nominal power range. As the output power of the test bench was very limited, only a few combinations of devices with small power requirement could be measured. The source of the uncertainty in summation measurements should also be identified and eliminated in order to minimize the possible errors caused by the measurement setup.

The next step would be to improve the harmonic load models. The GMM model-fitting algorithm should include an automatic optimal selection of the number of mixture components and reduction of the dependency on initial condition selection caused by convergence, and the possibility of non-convergence.

The proposed model is still in its preliminary development stage and primarily requires optimizations to find a more effective balance between the resolution and the number of stored cumulative distributions in the model array. As the cumulative distributions do not necessarily have to use a fixed step width, the resolution could be made dynamic depending on the harmonic current value by having higher resolution in the lower range and lower resolution in the higher range, so that the relative variation accuracy is maintained. The resolution selection based on the minimum phasor magnitude, as it is currently suggested in the thesis, provides the necessary accuracy in the lower range, but in the higher range the resolution would be overestimated, and very fine stepping is not necessary to achieve the relative accuracy. The resolution could also be made dependant on the extent of variation and/or probability density, both of which require finer resolution to represent variation more accurately compared to the low variation and low probability density regions. To find the optimal resolution selection algorithm, extensive research, measurements and simulations should be performed as the model was originally designed to be as universal as possible.

The biggest limitation of the proposed method is that the models represent the harmonic current only at certain conditions. When the conditions like temperature, supply voltage magnitude and distortion level, line impedance, etc. change, the

distributions of the current harmonics might also change. This sensitivity is usually associated only with the deterministic models. To deal with this, a method should be developed to relate the probability distributions to the input parameters. This would be somewhat possible with the parametric probabilistic models like the GMM, since the mean values, the covariance matrices, and the mixture weights, which define the model are defined, provided the transitions are very smooth and limited. To quantify changes in nonparametric bivariate distributions, especially the one proposed in the thesis, a suitable mathematical method should be found or developed capable of performing such tasks in multidimensional space.

If this kind of approach would be possible, the resulting modelling and simulation solution would not only provide the probabilities of the harmonic currents but also consider the sensitivity to the network parameters, which will make the models compatible with the network simulations. Considering the rapidly increasing interest in the topic of harmonic current modelling, coupled with readily available computational power and advances like neural networks and machine learning, with additional research, the merging of the variation representation capability of probabilistic models, and the network sensitivity of the deterministic models could not be very far away.

List of Figures

References

[1]   *Electromagnetic compatibility (EMC) - Part 4-30: Testing and measurement techniques - Power quality measurement methods*. IEC 61000-4-30:2015, 2017.

[2]   *Electromagnetic compatibility (EMC) Part 4-7: Testing and measurement techniques - General guide on harmonics and interharmonics measurements and instrumentation, for power supply systems and equipment connected thereto*. IEC 61000-4-7:2002, 2009.

[3]   IEEE Power and Energy Society, "IEEE Recommended Practice and Requirements for Harmonic Control in Electric Power Systems," *IEEE Std. 519-2014*. 2014.

[4]   *Voltage characteristics of electricity supplied by public distribution networks*. EVS-EN 50160:2010, 2010.

[5]   *Electromagnetic compatibility (EMC) - Part 2-2: Environment - Compatibility levels for low-frequency conducted disturbances and signalling in public low-voltage power supply systems*. IEC 61000-2-2:2003, 2019.

[6]   *Electromagnetic compatibility (EMC) - Part 3-2: Limits - Limits for harmonic current emissions (equipment input current ≤16 A per phase)*. IEC 61000-3-2:2019, 2018.

[7]   L. Kütt, E. Saarijärvi, M. Lehtonen, H. Mõlder, and T. Vinnal, "Harmonic load of residential distribution network - Case study monitoring results," in *9th International: 2014 Electric Power Quality and Supply Reliability Conference, PQ 2014 - Proceedings*, 2014, pp. 93–98.

[8]   J. Niitsoo, I. Palu, J. Kilter, P. Taklaja, and T. Vaimann, "Residential load harmonics in distribution grid," in *2013 3rd International Conference on Electric Power and Energy Conversion Systems, EPECS 2013*, 2013.

[9]   J. Niitsoo, J. Kilter, I. Palu, P. Taklaja, and L. Kütt, "Harmonic levels of domestic and electrical vehicle loads in residential distribution networks," in *IEEE AFRICON Conference*, 2013.

[10]   European Commission, "A policy framework for climate and energy in the period from 2020 to 2030," 2014.

[11]   European Parliament, "Directive 2010/31/EU," *Off. J. Eur. Union*, vol. L153/13, no. 18.6.2010, pp. 13–35, 2010.

[12]   M. E. Balci, D. Ozturk, O. Karacasu, and M. H. Hocaoglu, "Experimental verification of harmonic load models," in *Proceedings of the Universities Power Engineering Conference*, 2008.

[13]   M. Rylander and W. M. Grady, "Problems in the use of Norton equivalent models for single-phase nonlinear loads," in *IEEE PES General Meeting, PES 2010*, 2010.

[14]   M. Fauri, "Harmonic modelling of non-linear load by means of crossed frequency admittance matrix," *IEEE Trans. Power Syst.*, vol. 12, no. 4, pp. 1632–1638, 1997.

[15]   J. A. Fuentes, A. Gabaldón, F. J. Cánovas, and A. Molina, "Harmonic model of electronically controlled loads," in *Proceedings of the IEEE Power Engineering Society Transmission and Distribution Conference*, 2000, vol. 3, pp. 1805–1810.

[16]   Y. Sun, G. Zhang, W. Xu, and J. G. Mayordomo, "A harmonically coupled admittance matrix model for AC/DC converters," *IEEE Trans. Power Syst.*, vol. 22, no. 4, pp. 1574–1582, 2007.

[17]   J. Yong, L. Chen, A. B. Nassif, and W. Xu, "A frequency-domain harmonic model for compact fluorescent lamps," *IEEE Trans. Power Deliv.*, vol. 25, no. 2, pp. 1182–1189, 2010.

[18]   J. Yong, L. Chen, and S. Chen, "Modeling of home appliances for power distribution system harmonic analysis," *IEEE Trans. Power Deliv.*, vol. 25, no. 4, pp. 3147–3155, 2010.

[19]   J. Molina, J. J. Mesas, N. Mesbahi, and L. Sainz, "LED lamp modelling for harmonic studies in distribution systems," *IET Gener. Transm. Distrib.*, vol. 11, no. 4, pp. 1063–1071, 2017.

[20]   M. Brunoro, L. F. Encarnação, and J. F. Fardin, "Modeling of loads dependent on harmonic voltages," *Electr. Power Syst. Res.*, vol. 152, pp. 367–376, 2017.

[21]   L. P. Frater, A. R. Wood, and N. R. Watson, "Linearisation of non-linear loads by phase dependent frequency coupling admittance matrices," in *16th Power Systems Computation Conference, PSCC 2008*, 2008.

[22]   C. F. M. Almeida and N. Kagan, "Harmonic coupled norton equivalent model for modeling harmonic-producing loads," in *ICHQP 2010 - 14th International Conference on Harmonics and Quality of Power*, 2010.

[23]   A. B. Nassif, J. Yong, and W. Xu, "Measurement-based approach for constructing harmonic models of electronic home appliances," *IET Gener. Transm. Distrib.*, vol. 4, no. 3, pp. 363–375, 2010.

[24]   A. S. Fölting, J. M. A. Myrzik, T. Wiesner, and L. Jendernalik, "Practical implementation of the coupled norton approach for nonlinear harmonic models," in *Proceedings - 2014 Power Systems Computation Conference, PSCC 2014*, 2014.

[25]   J. E. Caicedo, A. A. Romero, and H. C. Zini, "Frequency domain modeling of nonlinear loads, considering harmonic interaction," in *2017 3rd IEEE Workshop on Power Electronics and Power Quality Applications, PEPQA 2017 - Proceedings*, 2017.

[26]   A. J. Collin, J. Drapela, R. Langella, A. Testa, S. Z. Djokic, and N. R. Watson, "Harmonic Modelling of LED lamps by Means of Admittance Frequency Coupling Matrices," 2019, pp. 1–6.

[27]   D. Gallo, R. Langella, M. Luiso, A. Testa, and N. R. Watson, "A new test procedure to measure power electronic devices' frequency coupling admittance," *IEEE Trans. Instrum. Meas.*, vol. 67, no. 10, pp. 2401–2409, 2018.

[28]   S. Müller, J. Meyer, P. Schegner, and S. Djokic, "Harmonic Modeling of Electric Vehicle Chargers in Frequency Domain," *Renew. Energy Power Qual. J.*, pp. 396–401, 2015.

[29]   Y. Baghzouz, "An overview on Probabilistic Aspects of Harmonics in power systems," in *2005 IEEE Power Engineering Society General Meeting*, 2005, vol. 3, pp. 2394–2396.

[30]   Y. Baghzouz and O. T. Tan, "Probabilistic modeling of power system harmonics," *IEEE Trans. Ind. Appl.*, vol. IA-23, no. 1, pp. 173–180, 1987.

[31]   L. Wang and Y. M. Chen, "Bivariate normal distribution and direct normal distribution on randomly varying harmonic currents," in *Proceedings of International Conference on Harmonics and Quality of Power, ICHQP*, 1998, vol. 1, pp. 298–303.

[32]   A. Cavallini, R. Langella, A. Testa, and F. Ruggiero, "Gaussian modeling of harmonic vectors in power systems," in *Proceedings of International Conference on Harmonics and Quality of Power, ICHQP*, 1998, vol. 2, pp. 1010–1017.

[33]   É. Ngandui, "Characteristics of the measured current harmonics produced by clusters of variable speed drives," in *Canadian Conference on Electrical and Computer Engineering*, 2004, vol. 3, pp. 1347–1351.

[34] S. Ray and B. G. Lindsay, "The topography of multivariate normal mixtures," *Ann. Stat.*, vol. 33, no. 5, pp. 2042–2065, 2005.

[35] J. Meyer and P. Schegner, "Characterization of power quality in low voltage networks based on modeling by mixture distributions," in *2006 9th International Conference on Probabilistic Methods Applied to Power Systems, PMAPS*, 2006.

[36] F. J. Ruiz-Rodriguez, J. C. Hernandez, and F. Jurado, "Harmonic modelling of PV systems for probabilistic harmonic load flow studies," *Int. J. Circuit Theory Appl.*, vol. 43, no. 11, pp. 1541–1565, 2015.

[37] F. Nasrfard-Jahromi and M. Mohammadi, "Probabilistic harmonic load flow using an improved kernel density estimator," *Int. J. Electr. Power Energy Syst.*, vol. 78, pp. 292–298, 2016.

[38] M. Chen, C. Roberts, P. Weston, S. Hillmansen, N. Zhao, and X. Han, "Harmonic modelling and prediction of high speed electric train based on non-parametric confidence interval estimation method," *Int. J. Electr. Power Energy Syst.*, vol. 87, pp. 176–186, 2017.

[39] T. Duong, "ks : Kernel density estimation for bivariate data," *October*, no. October, pp. 1–4, 2009.

[40] S. Węglarczyk, "Kernel density estimation and its application," *ITM Web Conf.*, vol. 23, p. 00037, 2018.

[41] "File:Generalized inversion method.svg." [Online]. Available: https://commons.wikimedia.org/wiki/File:Generalized_inversion_method.svg. [Accessed: 06-Nov-2019].

[42] N. B. Rowe, "Summation of Randomly-Varying Phasors or Vectors With Particular Reference To Harmonic Levels.," *IEE Conf. Publ.*, no. 11, pp. 177–181, 1974.

[43] W. E. Kazibwe, T. H. Ortmeyer, and M. S. A. A. Hammam, "Summation of probabilistic harmonic vectors," *IEEE Trans. Power Deliv.*, vol. 4, no. 1, pp. 621–628, 1989.

[44] M. Lehtonen, "A general solution to the harmonics summation problem," *Eur. Trans. Electr. Power*, vol. 3, no. 4, pp. 293–297, 1993.

[45] Y. J. Wang and L. Pierrat, "Summation of harmonic currents produced by AC/DC static power converters with randomly fluctuating loads," *IEEE Trans. Power Deliv.*, vol. 9, no. 2, pp. 1129–1135, 1994.

[46] Y. J. Wang and L. Pierrat, "Vectorial summation of probabilistic current harmonics in power systems: From a bivariate distribution model towards a univariate probability function," *Eur. Trans. Electr. Power*, vol. 10, no. 1, pp. 13–18, 2000.

[47] Y. Baghzouz *et al.*, "Time-varying harmonics: Part II - Harmonic summation and propagation," *IEEE Trans. Power Deliv.*, vol. 17, no. 1, pp. 279–285, 2002.

[48] J. Meyer, P. Schegner, and K. Heidenreich, "Harmonic summation effects of modern lamp technologies and small electronic household equipment," in *21st International Conference on Electricity Distribution (CIRED)*, 2011, vol. 21, pp. 6–9.

[49] V. Ćuk, J. F. G. Cobben, W. L. Kling, and P. F. Ribeiro, "Analysis of harmonic current summation based on field measurements," *IET Gener. Transm. Distrib.*, vol. 7, no. 12, pp. 1391–1400, 2013.

[50] A. Gil-De-Castro, S. K. Rönnberg, M. H. J. Bollen, and A. Moreno-Muñoz, "Harmonic phase angles for a domestic customer with different types of lighting," *Int. Trans. Electr. Energy Syst.*, vol. 25, no. 7, pp. 1281–1296, 2015.

[51]   J. Meyer, A. M. Blanco, M. Domagk, and P. Schegner, "Assessment of Prevailing Harmonic Current Emission in Public Low-Voltage Networks," *IEEE Trans. Power Deliv.*, vol. 32, no. 2, pp. 962–970, 2017.

[52]   B. Peterson, J. Rens, and J. Desmet, "Harmonic emission assessment on a distribution network: The opportunity for the prevailing angle in harmonic phasors," *CIRED - Open Access Proc. J.*, vol. 2017, no. 1, pp. 668–671, 2017.

[53]   D. Salles, C. Jiang, W. Xu, W. Freitas, and H. E. Mazin, "Assessing the collective harmonic impact of modern residential loads-part I: Methodology," *IEEE Trans. Power Deliv.*, vol. 27, no. 4, pp. 1937–1946, 2012.

[54]   M. N. Iqbal, L. Kutt, and A. Rosin, "Complexities associated with modeling of residential electricity consumption," in *2018 IEEE 59th Annual International Scientific Conference on Power and Electrical Engineering of Riga Technical University, RTUCON 2018 - Proceedings*, 2018.

Acknowledgements

I would like to dedicate my thesis to my beloved daughter Clara, who has brought me joy and happiness during difficult times.

I'd like to give my deepest thanks to Mari for the patience and encouragement during all my studies at the university and for making me feel proud of what I have accomplished.

I would like to sincerely thank my parents, who have always supported me in every way possible and raising me to become the person I am today.

Special thanks go out to my friends from GNKS who have provided me with long nights of fun, deep conversations and serious discussions, and to all my other friends who I still keep in touch with since high school.

To my colleagues at Tallinn University of Technology, I give thanks for the input, ideas and discussions which have helped me improve my work and the thesis.

Last, but not least, I would like to personally give thanks and appreciation to my supervisors, prof. Lauri Kütt and Toomas Vinnal for guidance, support and contributions to the long-lasting work.

Abstract

Harmonic current summation using probabilistic bivariate modelling

Since the introduction of nonlinear loads to low voltage distribution networks, the distortion level of load current has been steadily on the rise. From the power quality aspect, high level of harmonic current emission in the network can cause issues like voltage distortions, resonances, equipment failures, power losses, etc. In order to better optimize and plan the network accordingly, it is necessary to estimate the harmonic current levels in low voltage distribution networks.

To provide necessary baseline input data for research and to validate the simulation results, a comprehensive test bench was designed and built to carry out repeatable measurements, which accommodates up to 16 concurrent loads that could be tested in any combination. The loads were tested using analogue sine voltage waveform with a 16-bit resolution fed through a low-distortion power amplifier to achieve distribution network level. A Class A power quality recorder was used for measuring that could evaluate both magnitude and phase angle of current and voltage harmonics with a minimum aggregation interval of 1 second. MATLAB software was used for test control, measurement data processing, modelling, simulations, and analysis.

The variation of harmonic currents due to control algorithms and device operating modes, especially in the case of nonlinear loads, introduces difficulties in modelling expected harmonic current levels. Standard deterministic models are not able to cope with intrinsic harmonic current phasor variations. Using only average values does not represent the variation of current harmonics, nor does the average-based summation provide a full insight as to which harmonic phasors might be present in the network and to what extent. Thus, a probabilistic approach should be considered.

Simple Gaussian distributions, both univariate and bivariate, which have been used in previous studies, are only able to represent a limited type of variations with certain dispersion shape. When a load produces harmonic currents with unique and distinctive variation patterns, more effective probabilistic models and methods should be implemented.

In the thesis, the harmonic currents in LV distribution networks were studied, the possible harmonic current sources found in residential households were analysed, and an overview of harmonic current characteristics and measurement results was given.

Harmonic current variations of several household devices were studied in fine detail to determine the possible variation patterns and provide baseline information for applying the best modelling solution. Deterministic and probabilistic state of art modelling methods were analysed and compared as a reference to find the shortcomings and ideas on how to solve the issues found in present models. A researched and developed novel and practical probabilistic modelling method was also presented and analysed. The selected best performing approaches were used and analysed in harmonic current summation simulations to determine their feasibility in the estimation of the simultaneously connected variable nonlinear loads.

Results of the thesis indicated that the proposed harmonic current models and method can perform summation simulations with accuracy that is comparable to the measurement setup uncertainty. Results provide a considerable baseline for the future work that, combined with additional research, makes it possible to estimate the extent and probability of harmonic currents in the low voltage distribution network.

Lühikokkuvõte
Vooluharmoonikute summeerimine rakendades kahe muutujaga tõenäosuslikku modelleerimist

Mittelineaarsete koormuste kasutuselevõtt madalpinge-jaotusvõrkudes on kaasa toonud koormusvoolude moonutuse pideva tõusu. Toitekvaliteedi aspektist lähtudes võib voolude harmooniliste komponentide kõrge tase elektrivõrkudes esile kutsuda probleeme nagu pingemoonutused, resonantsnähtused, seadmete rikked, toitekaod jms. Selleks, et võrku paremini optimeerida ja seda vastavalt planeerida, on tarvis hinnata vooluharmoonikute tasemeid madalpinge-jaotusvõrkudes.

Uurimistööks vajalike lähteandmete hankimiseks ja simulatsioonitulemuste valideerimiseks kavandati ja ehitati ulatuslik katsestend, mida kasutati korduvate mõõtmiste läbiviimiseks ning mis võimaldab korraga katsetada kuni 16 erinevat koormust või tarbijat mistahes kombinatsioonis. Koormusi testiti kasutades 16-bitise eraldusvõimega analoog-siinuslainekujuga pinget, mida võimendati madala moonutusega võimendiga jaotusvõrgu taseme saavutamiseks. Mõõtmiseks kasutati A-klassi elektrikvaliteedisalvestit, mis võimaldas hinnata voolu- ja pingeharmoonikute amplituudi ja faasinurka 1-sekundilise keskmistamise intervalliga. Katsete juhtimiseks, mõõtmisandmete töötlemiseks, modelleerimiseks, simulatsioonideks ja analüüsiks kasutati MATLAB tarkvara.

Voolu harmooniliste komponentide variatsioon, mis on põhjustatud seadmete töörežiimidest ja juhtalgoritmide toimest, muudab eeldatavate vooluharmoonikute tasemete modelleerimise ja hindamise keeruliseks. Traditsioonilised determinismlikud mudelid ei suuda toime tulla seadmetele omastele vooluharmoonikute faasorite iseeneslike muutustega. Keskmiste väärtuste kasutamine ei kirjelda piisavalt vooluharmoonikute variatsiooni, samuti ei anna keskmistel põhinev summeerimine täielikku ülevaadet selle kohta, millised vooluharmoonikute tasemed võivad võrgus esineda ja millises ulatuses.

Varasemates uuringutes kasutatavad lihtsad nii ühe kui ka mitme muutujaga Gaussi jaotused suudavad kirjeldada vaid kindla dispersioonikujuga piiratud tüüpi variatsioone. Kui koormus tekitab vooluharmoonikuid ainulaadse ja eristatava variatsioonikujuga, tuleks rakendada tõhusamaid tõenäosusmudeleid ja -meetodeid.

Lõputöös uuriti toitevoolu harmooniliste komponentide esinemist jaotusvõrkudes, analüüsiti elamumajapidamistes leiduvaid võimalikke harmooniliste voolude allikaid ning anti ülevaade vooluharmoonikute omaduste ja mõõtmistulemuste kohta.

Uuriti mitme majapidamisseadme vooluharmoonikute variatsiooni, et teha kindlaks võimalikud variatsioonimustrid ning anda lähteteavet parima modelleerimislahenduse rakendamiseks. Analüüsiti ja võrreldi levinud deterministlikke ja tõenäosuslikke modelleerimismeetodeid puuduste tuvastamiseks ning ideede leidmiseks, kuidas lahendada praegustes mudelites leiduvaid probleeme. Samuti tutvustati ja analüüsiti uuritud ja välja töötatud uudset ning praktilist tõenäosuslikku modelleerimismeetodit. Valitud parimate tulemustega lähenemisviise kasutati ja analüüsiti vooluharmoonikute summeerimist simulatsioonides, et teha kindlaks nende teostatavus samaaegselt toimiva muutuva mittelineaarsete koormuste hindamisel.

Lõputöö tulemused näitasid, et väljapakutud vooluharmoonikute mudelite ja meetodite abil on võimalik teostada summeerimise simulatsioone täpsusega, mis on võrreldav seadistuse mõõtetäpsusega. Tulemused pakuvad edaspidiseks tööks arvestatava lähtekoha, mis võimaldab täiendavate uuringute toel hinnata vooluharmoonikute ulatust ja esinemise tõe näosust madalpinge-jaotusvõrkudes.

Appendix

Publication I
Vinnal, T.; Jarkovoi, M.; Kütt, L. (2018). Harmonic Currents and Voltages in LV Networks of Estonia: Measurement Results, Case Studies. RTUCON2018, 59th International Scientific Conference on Power and Electrical Engineering of Riga Technical University. Riga, Latvia. November 12-14, 2018. Riga: IEEE, 1–7.

Harmonic Currents and Voltages in LV Networks of Estonia
Measurement Results, Case Studies

Toomas Vinnal, Marek Jarkovoi, Lauri Kütt

Department of Electrical Power Engineering and Mechatronics
Tallinn University of Technology (TalTech)
Tallinn, Estonia

Abstract – **The paper is focused on harmonic currents and voltages in low-voltage (LV) networks of Estonia. Measurement results throughout a longer period are described for estimating harmonic distortion levels, harmonic spectrum and related problems. The impact of power factor correction capacitors upon harmonic distortion in industrial LV networks is discussed. Measurement and simulation results of harmonics under resonance conditions in industrial networks are presented.**

Keywords – Total harmonic distortion; Harmonic distortion; Power system harmonics; Harmonic resonance; Harmonic currents; Harmonic voltages; Low-voltage networks

I. Introduction

Mapping of harmonic currents and voltages in low-voltage (LV) networks is of growing interest in Estonia, as well as in other countries [1] – [6]. There are at least two reasons for that. Firstly, growing number of electronic devices, particularly variable-speed drives (VSDs) and power converters in consumer installations. Secondly, rapidly growing micro-generation units, photo-voltaic (PV) panels and wind generators.

Supply voltage quality problems within industrial/commercial LV networks are often discussed regarding disturbances and failures (e.g. voltage disturbances, equipment malfunctions) [7] – [11]. When disturbances occur, it is evident that the case has to be studied and harmonic currents and voltages measured. Some examples of faults from VSD monitoring equipment can be seen in Fig.1.

Fig. 1. Operation failures due to high harmonic currents in a LV system.

Still, harmonic phenomena are frequently not so intense to cause any breakdown of components other than power factor correction (PFC) capacitors, but harmonic currents affect supply voltage quality and power losses in the whole LV power system, particularly in induction motors, transformers, lines and capacitors [8] – [13]. Harmonic power losses are usually not estimated because the losses are not measured nor calculated.

Since the beginning of 1990's, there has been a steady increase of nonlinear equipment in LV industrial and residential networks of Estonia. Such equipment includes all types of electronic loads, VSDs, welding converters, electronic ballasts of lamps etc. This trend has led to a growing presence of harmonic currents and consequently harmonic voltages. Moreover, industrial loads tend to operate at relatively low power factors. The widespread method for overcoming the problem of low power factor is to install controlled shunt capacitor banks on the LV customer side. This measure often increases the level of harmonics.

Misapplication of power capacitors in today's complicated industrial power systems has negative impacts on both the customer equipment (additional losses) and the utility equipment, resulting in equipment heating, additional losses as well as failures [11], [12]. A direct indicator of parallel resonance is the breakdown of recently installed capacitors as shown in Fig. 1.

Fig. 2. Capacitor breakdown (on the right) due to high harmonic voltages in a LV system.

General requirements of supply voltage quality have been stated in the standard EN 50160 [14]. Still, operating the LV network close to the limit values will be unfavorable for the customer causing extra power losses and consequently extra costs. In addition, heating of equipment and reduction of service time occurs. Moreover, in several cases even the limit values of harmonic currents and voltages are exceeded.

As shown in [1], [3], [9], [10] the dominating harmonics in LV networks are mostly the 3rd, 5th, 7th, 11th, 13th and 15th. In industrial networks 5th and 7th harmonics are dominating mostly, but in some cases the 3rd, 9th and 15th are very high.

The problems discussed in this paper are the following:

o   What is the level of harmonic currents and voltages in LV networks of Estonia?
o   What are the characteristic harmonic frequencies in LV networks?
o   What parameters should be measured to estimate the resonance condition?
o   What are characteristic harmonic frequencies that are affected by harmonic resonance?

II. BASIC CHARACTERISTICS OF HARMONICS AND STANDARDS

Harmonics are characterized with factors called total harmonic distortion (*THD*), that are calculated regarding to voltage and current respectively:

$$THD_u = \frac{\sqrt{\sum_{h=2}^{\infty}(U_h)^2}}{U_1} , \qquad (1)$$

$$THD_i = \frac{\sqrt{\sum_{h=2}^{\infty}(I_h)^2}}{I_1} . \qquad (2)$$

The rms values of voltage and current U (U_{rms}) and I (I_{rms}) could be calculated from individual harmonic values of voltage and current or from the fundamental values of voltage U_1 and current I_1 and total harmonic distortion factors correspondingly:

$$U = \sqrt{\sum_{h=1}^{\infty}U_h^2} = U_1\sqrt{1+THD_u^2} , \qquad (3)$$

$$I = \sqrt{\sum_{h=1}^{\infty}I_h^2} = I_1\sqrt{1+THD_i^2} . \qquad (4)$$

To estimate the amount of harmonic distortions it is necessary to know both parameters. Usually the THD_u values are between 1% and 10% whereas the THD_i values are between a wide range starting from several percent up to 200%.

The THD_i value of a particular device shows the distortion level from ideally sinusoidal current curve. A high THD_i value does not necessarily mean a critical situation, in case the current is very low compared to the nominal line current.

To characterize the amount of harmonic currents in relation to nominal line current the distortion factor TDD_i (*total demand distortion*) is used. The line current I_L is the maximum current throughout 15- or 30-minute intervals or the nominal current of the point of common coupling (PCC):

$$TDD_i = \frac{\sqrt{\sum_{h=2}^{40}(I_h)^2}}{I_L} . \qquad (5)$$

In practice there can be harmonics of very high order (up to 200th), but usually harmonics are measured up to the 25th or 50th order. Harmonics higher than this are very low (less than 0,1%)

Several international standards [14], [15], [16], [17], [18] and [19] determine the necessary compatibility between distribution networks, consumers and electrical products and give limits for harmonic currents and voltages. It should be noted that none of these standards is so far in a way compulsory requirement in Estonia.

As for supply voltage, the standard EN 50160 gives the main voltage parameters and their permissible deviation ranges at the customer's point of common coupling in public LV and medium-voltage (MV) distribution systems. According to EVS/EN 50160/2011 the *THD* factor of supply voltage has to be $THD_u \leq 8\%$. Also limit values for each individual harmonic voltage have been pointed out. For the 5th harmonic the limit value is 6%, for the 7th – 5%, for the 11th – 3.5%, for the 13th – 3%.

In other standards like the often referred IEEE 519, even lower harmonic levels are allowed. The total harmonic distortion factor has to be $THD_u \leq 5\%$ and the limit value for each individual harmonic voltage is 3%.

The standard IEEE 519 does not give limits for individual equipment, but for individual customers. The idea is to limit the harmonic injection from individual customers so that they will not cause unacceptable voltage distortion. The customers are categorized by the ratio of available short circuit current to their maximum demand load current at the PCC. Based on IEEE 519, the current total demand harmonic distortions TDD_i should not exceed 5% in the network with lowest short circuit capacity and 20% in the network with highest short circuit capacity.

Different measures could be used to reduce harmonic currents and voltages in the LV networks. When caused by VSDs the measures have been shown in [20].

III. Measurement Results of Harmonic Currents and Voltages

In the course of the last decade multiple monitoring studies of power quality have been performed in Estonia. These studies include measurement of harmonic currents and voltages in LV networks. The measurement point is usually at the PCC.

As measurement instruments standard power network analyzers like Fluke 434, LEM Memobox and Fluke Memobox 1745 have been used for these measurements. The measurement period was at least one week and measurement interval 10 min or 1 min.

Fig 3 shows the probability density of THD_u of all measurements in 67 network points and Fig. 4 the cumulative probability.

Harmonic voltages are mostly within the limits required by the standard EN 50160. It is rather seldom that the THD_u limit value or any individual harmonic voltage value is exceeding the limit as the 95% value. When studying the level of harmonic voltages, it is of little use to compare the measured harmonic voltages with the limit values stated in the standard EN 50160. Still, the measured harmonics exceed the limits as maximum value or 100% limit value in several cases, particularly in industrial networks, see Fig. 5 … Fig. 12.

In voltage harmonic spectrum the dominating harmonics in LV networks are mostly the 5th, 7th, 11th, 13th. In industrial networks the 5th and 7th harmonics are dominating. In residential networks the 3rd and 15th and 21st harmonics are often high. Still, the spectrum differs from case to case depending from the equipment used in the LV network, Fig. 8, Fig. 11, Fig. 12.

The characteristic waveforms of voltage and current under harmonic distortions are shown in Fig. 6. Harmonic currents can be rather high shown in Fig. 9 and Fig. 10. As could be seen the THD_i values exceed the 20% level by far and during the start of powerful VSDs reaches the level of 70% up to 90%.

When multiple DC drives and VSDs are used the spectrum of voltage harmonics includes also even harmonics, Fig. 11. When a high number of single-phase (hand) tools are used, the spectrum includes triple harmonics as shown in Fig. 12.

As a conclusion, harmonic currents and voltages are varying rapidly in time and the spectrum can be quite different depending upon LV network. Therefore, monitoring of harmonic currents and voltages is necessary, with recording intervals preferably from one second up to one minute and the overall measurement duration from 24 hours to one week.
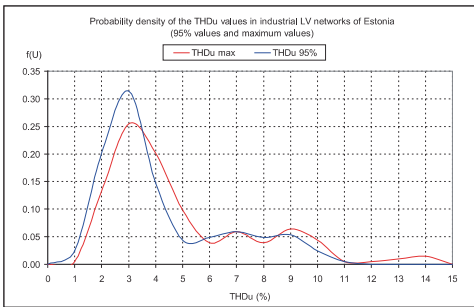

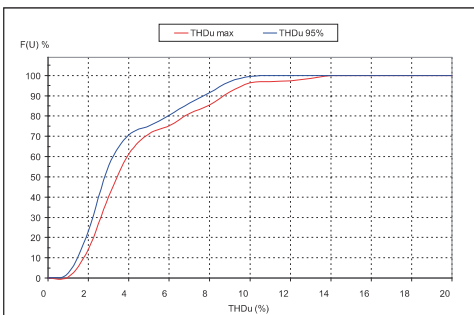Fig 3. Probability density of measured THD_u values (95% values and maximum values) of all measurements.

Fig 4. Cumulative distribution of THD_u as a percentage (95% values and maximum values) of all measurements.
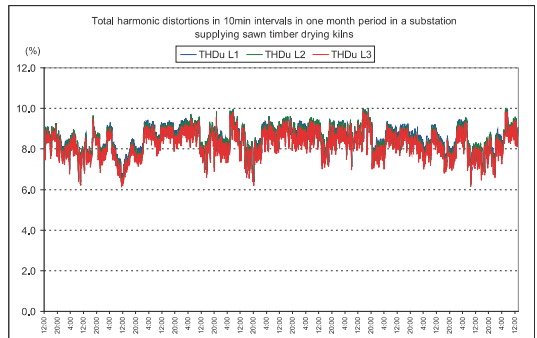
Fig. 5. Total harmonic distortion of the supply voltage, THD_u is between 6% and 10% permanently during one-month interval.
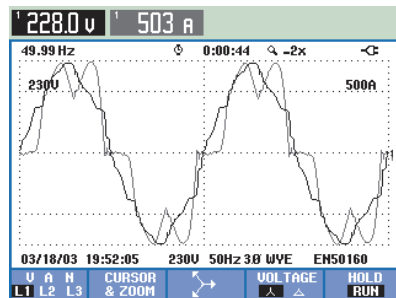
Fig. 6. The supply voltage and current curves according to the case shown in Fig. 7.
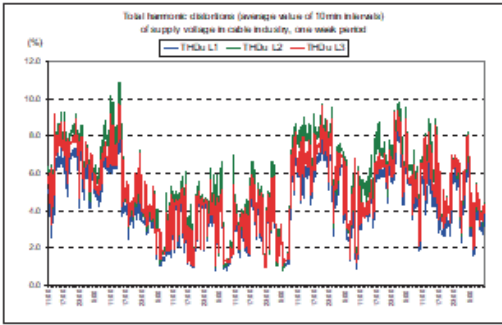
Fig. 7. Total harmonic distortion of supply voltage, THD_u is up to 11% and varying considerably during one-week interval.
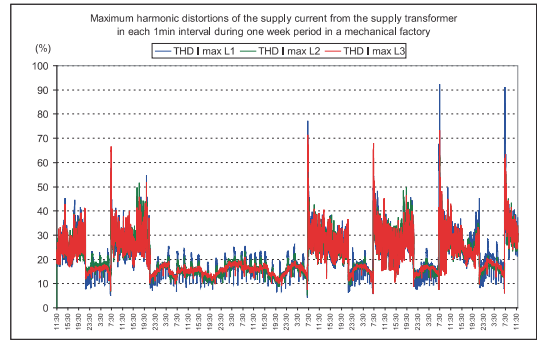
Fig. 10. Maximum total harmonic distortion of supply current, THD_i is mostly between 20% and 40% when VSDs are running (one-week interval).
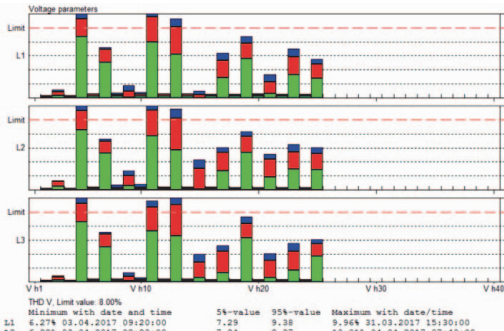
Fig. 8. The spectrum of harmonic voltages in industrial network supplying drying kilns for timber (green – 5% value, red – 95% value, blue – absolute maximum value).
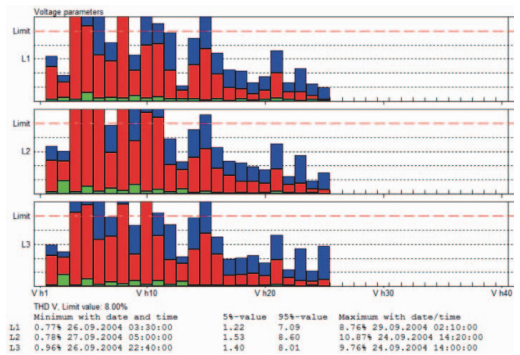
Fig. 11. The spectrum of voltage harmonics in cable industry, several harmonics exceed the limit.
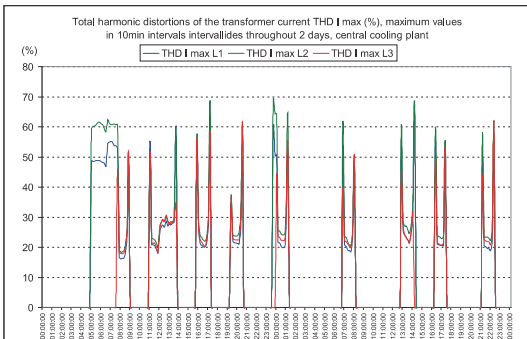
Fig. 9. Maximum total harmonic distortion of supply current, THD_i is up to 70% when starting the cooling plant.
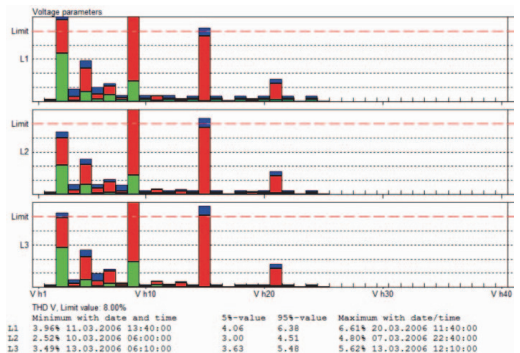
Fig. 12. Voltage harmonics in machine industry, the 3rd, 5th, 9th, 15th and 21st harmonics are highest.

IV. BASIC PRINCIPLES OF PARALLEL RESONANCE

In a simplified LV network impedance of the transformer and capacitance of the shunt capacitor form a parallel resonance circuit. To calculate the resonant frequency, one could use the equivalent circuit as shown in Fig. 13 including the inductance and resistance of the transformer, the capacitance of the capacitor and the source of harmonic currents which is in parallel to the LC-circuit, [13].

Fig. 13. The parallel resonance equivalent circuit

The resonant frequency in such a parallel circuit can be calculated from the transformer inductance L, resistance R and capacitance of the capacitor C as follows, [1]:

$$f_{res} = \frac{1}{2\pi\sqrt{LC}}\sqrt{\frac{L/C - R^2}{L/C}} \quad . \tag{6}$$

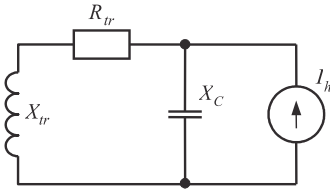The impedance of the parallel circuit at different frequencies one could calculate from, [1]:

$$Z = \frac{R + j\omega L}{1 - \omega^2 LC + j\omega RC} \quad . \tag{7}$$

The resistance R_{tr} and inductance X_{tr} of the transformer at the fundamental frequency one could calculate from well-known equations:

$$R_{tr} = \frac{\Delta P_k \cdot U_{nom}^2}{S_{nom}^2} \quad , \tag{8}$$

$$X_{tr} = \frac{u_k \cdot U_{nom}^2}{S_{nom}} \quad , \tag{9}$$

where ΔP_k – no-load losses of the transformer, (kW);
$\quad U_{nom}$ – nominal line voltage of the transformer primary side, (kV);
$\quad S_{nom}$ – nominal power of the transformer, (kVA);
$\quad u_k$ – short-circuit voltage of the transformer.

In case the resonant frequency of the parallel circuit corresponds to the frequency of the harmonic source, the harmonic currents as well as voltages in the circuit will be amplified. Problems will arise if harmonic currents are high and a controlled capacitor battery is installed. In this case, the capacitor battery will be switched step-by-step to achieve the setpoint value and the conditions of resonance appear now and then.

The effect of the capacitor battery upon the resonance frequency is characterized by impedance curves. As an example, the impedance curves $Z(\Omega) = f(h)$ of a LV network are shown in Fig. 14.

The maximum value of impedance occurs when $X_{tr} = X_C$. For a battery of 12 capacitors there will be a set of 12 curves.

In real installations, damping by resistance has a great effect upon resonance. In Fig. 14 the upper curves correspond to no resistance in the capacitor circuit and the lower curves to the resistance $R_C = 0.005\ \Omega$ in the capacitor circuit.
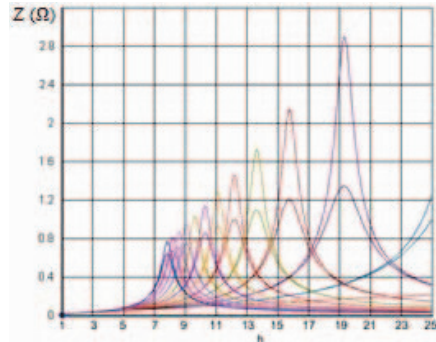
Fig. 14. Calculated impedance curves $Z(\Omega) = f(h)$ of a LV network with 12-stage capacitor battery.

As appears from measurements in industrial networks, resonances at 11th, 13th and 17th harmonic frequencies occur quite often resulting in high harmonic currents both in the capacitor battery and transformer.

The capacitor cabinet is operating automatically by switching capacitors on/off according to the PF controller setpoint value of the displacement power factor $cos\ \varphi$. The usual setpoint value of $cos\ \varphi$ is 0.98. So, the total number of capacitors switched on is varying all the time. Hence the resonance occurs only shortly now and then during some minutes. For example, a sharp increase of harmonic distortions of the capacitor current is shown in Fig. 15. Total harmonic distortions THD_i of the capacitor current reaches up to 80%.

Resonance condition at 17th harmonic frequency is shown in Fig. 16, where the time-plot of the capacitor current I_{h17} is shown. The resonance occurs for approximately 2 minutes and the current reaches as high as 74% of the

fundamental current.

Fig. 15. Total harmonic distortion of the capacitor current, during some interval the THD_i reaches 80%.

The highest harmonic currents in the capacitor are I_{h11}, I_{h13}, and I_{h17} reaching 60–65%. In this case, the most intense resonant situation occurs at the 11th harmonic frequency. In the capacitor, the current I_{h11} reaches 35% and in the transformer 25% of the fundamental values. The absolute value of these harmonic currents was 145 A and the harmonic currents are nearly equal both in the capacitor and in the transformer.
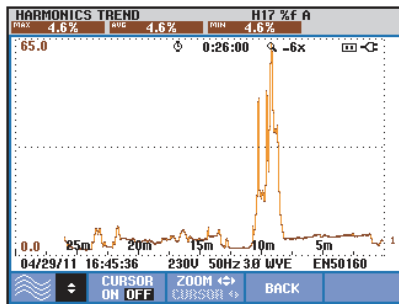
Fig. 16. Parallel resonance at the frequency of the 17th harmonic occurring during some minutes.

When studying the conditions for resonance it is of little use to measure only voltage harmonics in the LV system and to compare the harmonic voltages with the values stated in the standard EN 50160. Still, if any of these voltage harmonics is above the limit value or close to the limit value, there is a risk for resonance and the network should be studied carefully. Consequently, to ascertain the conditions and extent of resonance, measurement of harmonic currents in the LV network throughout some time interval is necessary.

V. Conclusions about Harmonic Currents and Voltages in LV Networks of Estonia

1.   The average minimum level of THD_u was 1,1%, that is characteristic to night hours and weekends during low loads. Still, there are networks with the minimum level of harmonics around 4,5% which indicates a high level of harmonics constantly.

2.   The highest value of THD_u probability density is around 3%. That means ca. 40% of measured networks have the THD_u at relatively low level.

3.   The THD_u level of 5% is exceeded in 30% of cases as a maximum value and ca. 25% of cases as a 95% percentile value.

4.   The THD_u level of 8% is exceeded in 15% of cases as a maximum value and ca. 9% of cases as a 95% percentile value. In such cases measures should be discussed to reduce the voltage harmonic level: decrease the supply impedance, increase the transformer rating, replace converters, install passive filters etc.

5.   In the harmonic spectrum of voltages, 5th harmonic is dominating mostly thus giving the biggest portion in total distortions THD_u. Other dominating harmonics are 7th, 11th, 13th, 17th, 19th, 23rd. Triple harmonics like 3rd, 9th and 15th are also high in several cases. Harmonic voltages higher than 23rd are usually less than 0,2%.

6.   The harmonic spectrum and harmonic currents are varying rapidly. Therefore, monitoring of harmonic currents and voltages is necessary, with recording intervals preferably from one second up to one minute depending upon the LV network.

7.   Harmonic currents can be rather high in industrial networks, exceeding the level of 20% and reaching up to 80…90% during the starting and closing operating modes of powerful VSDs.

8.   Parallel resonance appears in LV industrial networks often, particularly in case of powerful nonlinear loads combined with the battery of capacitors that are not equipped with detuned reactors. Parallel resonance is usually expected to occur at the 5th or 7th harmonic, as these harmonics are dominating in most cases. Still, measurements show that resonance takes place at much higher frequencies, particularly at the 11th or 17th harmonic.

9.   In order to detect parallel resonance, harmonic currents are recorded both in the transformer current and the capacitor current simultaneously, at the same time the capacitor battery is switched on and off step by step. The resonance intensity is mostly affected by the parameters of the transformer, the amount and spectrum of harmonic currents and the type of converters installed (6-pulse, 12-pulse etc.).

10.   Further mapping of current and voltage harmonics in LV networks should be implemented to develop planning levels for power supply agreements between LV customers and LV/MV network operators in Estonia.

distribution networks.

REFERENCES

[1] K. Procházka, P. Santarius, L. Pospíchal, F. Kysnar, P. Krejčí, D. Mezera, 2011, "EN 50160 Ed. 3 and voltage quality in the Czech Republic," *Proceedings CIRED Conference*, Paper 0748.

[2] F. Bastião, A. Lebre, L. Jorge, A. Blanco, A. Leiria, J. Alves, 2013, "Characterization of voltage harmonic distortion in the Portugese Medium and Low Voltage Grids," *Proceedings CIRED Conference*, Paper 1289.

[3] Leiria, F. Bastião, 2013, "Harmonic Assessment on Power Networks – Application to Portuguese Distribution Grid," *Proceedings CIRED Conference*, Paper 0605.

[4] Fröbel, R. Vick, 2013, "Chosen Aspects for Harmonic Analyses in Distribution Networks", *Proceedings CIRED Conference*, Paper 1262.

[5] Tavares, L.C. Pinto, 2013, "Power Quality of Supply Characterization in the Portuguese Electricity Transmission Grid". *Proceedings CIRED Conference*, Paper 0324

[6] Y. Ruwaida, D. Holmberg, M. Bollen, 2015, "Mapping of Harmonic Levels in the Low-Voltage Network", *Proceedings CIRED Conference*, Paper 1017.

[7] M. Bollen, J. Meyer, F. Zavoda, S. Bahramirad, R. Langella, J. Liu, A. Khodaei, J.P. Hasler, 2015, "Volt-Var Control and Power Quality (CIGRE/ CIRED C4.24)", *Proceedings CIRED Conference*, Paper 0183.

[8] J. Desmet, 2008, *Study and Analyses of Cable Losses in LV Cables Under Harmonic Conditions*, Ph.D. Dissertation, ISBN 978-90-5682-962-9.

[9] T.M. Blooming, 2006, "Capacitor failure analyses," *IEEE Ind. Applicat. Mag.*, vol. 12, No. 5, 38–48.

[10] F.L. Hoadley, 2008, "Curb the disturbance. Comparison of methods for the mitigation of line current harmonics," *IEEE Ind. Applicat. Mag.*, vol. 14, No. 5, 25–33.

[11] J.C. Attachie, C.K. Amuzuvi, 2013, "Investigating harmonic resonance and capacitor bank switching at a power distribution substation using a fixed capacitor bank," *Research J. in Engineering and Applied Sciences*, 2(4), 343–348.

[12] F.M. Fernandez, P.S.C. Nair, 2007, "Influence of power factor compensating capacitors on estimation of harmonic distortion," *Proceedings EPQU conference*, 1–4.

[13] R.C. Dugan, M.F. McGranaghan, S. Santoso, H.W. Beaty, 2003, *Electrical Power Systems Quality*, Second Edition, McGraw-Hill Professional.

[14] EVS/EN 50160/2011. Voltage characteristics of electricity supplied by public electricity networks.

[15] IEC EN 61000-3-2. Electromagnetic compatibility (EMC) - Part 3-2: Limits - Limits for harmonic current emissions (equipment input current ≤ 16 A per phase).

[16] IEC EN 61000-3-4. Electromagnetic compatibility (EMC) - Part 3-4: Limits - Limitation of emission of harmonic currents in low-voltage power supply systems for equipment with rated current greater than 16 A.

[17] IEC 61000-2-2. Electromagnetic compatibility (EMC) - Part 2-2: Environment - Compatibility levels for low-frequency conducted disturbances and signalling in public low-voltage power supply systems.

[18] IEC 61000-2-4. Electromagnetic compatibility (EMC) - Part 2-4: Environment - Compatibility levels in industrial plants for low-frequency conducted disturbances.

[19] IEEE Std 519:1992. Recommended Practices and Requirements for Harmonic Control in Electrical Power Systems.

[20] Technical guide No. 6. Guide to harmonics with AC drives. Copyright 2015, ABB.

Publication II

Power Quality Issues Concerning Photovoltaic Generation in Distribution Grids

Jaan Niitsoo[1], Marek Jarkovoi[2], Paul Taklaja[1], Joni Klüss[3], Ivo Palu[1]

[1]Department of Electrical Power Engineering, Tallinn University of Technology, Tallinn, Estonia
[2]Department of Electrical Engineering, Tallinn University of Technology, Tallinn, Estonia
[3]Department of Electrical Engineering and Automation, Aalto University, Helsinki, Finland
Email: jaan.niitsoo@ttu.ee

Abstract

Unregulated utilization of renewable generation including residential photovoltaic (PV) systems can have a significant impact on load characteristics in distribution networks. For improving PV generation capabilities, power quality aspects have to be coordinated with present load characteristics. This paper discusses the harmonic content of PV generation and the influence to power quality indicators in residential distribution networks. PV generation measurement results including current harmonic amplitude and phase angle values are presented. Results of different modelling scenarios are analysed and a simplified model of harmonics in PVs is offered. The results of the study showed a moderate additional harmonic distortion in residential load current and voltage distortion at the substation's busbar when PVs were added. Novelty of the paper is that harmonic current values at higher orders are presented and analysed. The results pointed out in this paper could be further used for modelling the actual harmonic loads of the PVs in distribution networks.

Keywords

1. Introduction

Harmonic voltage levels in low-voltage networks represent an important aspect of power quality. From the point of view of electromagnetic compatibility, they must be kept within the compatibility levels to enable satisfactory

operation of all the equipment supplied by the network. Furthermore, since electricity is also defined as a product, utility companies could be held responsible for excessively high harmonic levels and any resulting damage to customers' property [1]. As such, in Europe, the harmonic voltage limits specified in EN 50160 standard should be met.

Distorted voltage and current in the distribution system may result in undesirable effects, such as overloading, over-voltages, mechanical stress, malfunction of critical control and protection equipment, and lower the efficiency of appliances. Distortion affects all customers fed through the point of common coupling (PCC).

The development of electronics for the general public as well as industrial applications has led to a rapid increase in the number of non-linear loads. In addition to the increased number of electronic devices, also resistive devices such as incandescent lamps are ever more frequently replaced by energy saving lamps utilizing non-linear elements. For example, depending on type and brand, switching power supplies absorb distorted currents which flow through the impedances of the power distribution system and result in distortion of system bus voltage [2]. Harmonics can travel upwards within the network and affect the grid voltage waveform, which may become notably distorted, deviating extensively from a proper sinusoidal signal.

Residential photovoltaic (PV) generators are the dominant renewable energy source in urban and metropolitan areas. This technology is enjoying rapid growth due to a combination of subsidies, the abundance of sunshine, and the low impact of the technology on the urban landscape [3]. As photovoltaic systems incorporate power converters, which are harmonic generating devices, they will have an influence on the power quality of the supply network. High harmonic distortion levels have also been observed in certain remote regions such as winter sports resorts and rural areas far away from substations.

Distributed generation (DG) impacts the network. This impact is dependent on the location, characteristics of the distributed energy source, related power electronic device, network configurations, voltage level at the connection point, and the capacity of DG relative to load consumption [3]. Consequently, utilities are faced with the risk that the permissible levels defined in standard EN 50160 will be exceeded in a significant number of networks in the future [1]. It has been estimated that already in 2012, 60% of the power system loads in USA were nonlinear loads [4].

Over the past decade, power quality (PQ) issues have become increasingly important in the distribution grid with the widespread use of non-linear electronic equipment. The most cited PQ problems that may arise due to grid connected PV generation are voltage dips and fluctuations, harmonic distortion, transient phenomena and reverse power flow. These effects result in potential damaging of sensitive electronic equipment and capacitor banks, overheating of transformers and neutral conductors and additional losses in the power system. Degraded power quality entails additional costs for both the electricity distributor and its customers [3] [5].

The purpose of the present study is to demonstrate and analyse possible power quality situations in a residential distribution network by examining the impact of nonlinear domestic loads and PV inverters. For the analysis, measured power consumption and current waveforms of different home appliances and PV inverters have been used. Novelty is that magnitudes and phase angles of each harmonic up to the 50th order were applied for all modelled loads. The main purpose of this paper is to present the use of actual measurement data from different devices for modelling the effects on the residential distribution network and give an estimation of the important values for further modelling.

2. Theory

In electrical power networks, a distorted sine wave can be divided into numerous components, each having an integer-multiple frequency of the main frequency. Different waveforms have different harmonic content referring to individual harmonic magnitudes and phase shift relative to the main frequency component. Hereafter in this paper, the presented measurements of loads are all indicated as magnitudes and phase shift of each individual harmonic up to the 50th order.

Distortions can be observed individually by comparing different harmonic components and calculating harmonic distortion (HD). A more general approach to quantifying the distortions is using the total harmonic distortion level (THD). Total harmonic distortion can be expressed separately for current harmonic distortion as THD_I and for voltage distortion as THD_U. The harmonic distortion indicators can be calculated using corresponding Equations (1), (2), (3) and (4),

$$HD_I = \frac{i_i}{i_1} \qquad (1)$$

$$\mathrm{HD}_U = \frac{u_i}{u_1} \tag{2}$$

$$\mathrm{THD}_I = \frac{1}{i_1}\sqrt{i_{rms}^2 - i_1^2} \times 100 \tag{3}$$

$$\mathrm{THD}_U = \frac{1}{u_1}\sqrt{u_{rms}^2 - u_1^2} \times 100 \tag{4}$$

where i_i is current of order i, i_1 is current of 1st order, u_i is voltage of order i and u_1 is voltage of 1st order.

It has to be pointed out that THD$_I$ (total harmonic distortion of current) does not reveal the magnitudes of individual harmonics, which could still exceed the limits for specific harmonics regardless of THD$_I$ value. For the correct estimation of the harmonic levels, phase angle values of individual harmonics are also required in addition to magnitudes. It is reported that 10% smaller harmonic current magnitudes can be seen when phase angle information is included compared to the simple summing of magnitudes without phase angle values [6].

Harmonic currents in a network largely depend on the harmonic characteristics of the connected devices, their phase angles and the background distortion level of the supply voltage. Harmonic current emission spectrum information of a device (or a group of devices connected at a PCC) under different supply voltage conditions is very useful for analysing the device's influence in the network. This can be further utilised to determine the probability density profile of each order harmonic currents in the network considering their "time-varying" behaviour [7].

Some loads draw current with total harmonic distortion over 100%, but their active power consumption is not as significant when compared to other harmonic generating devices [8]. In such cases, harmonic distortion may increase significantly when numerous harmonic emitting devices are utilized in bulk. The total impact depends on the number of appliances, their power ratings, and their harmonic diversity. Harmonic angle diversity is also relevant when multiple appliances are operating simultaneously, creating either emergence or cancellation of harmonics [4]. The attenuation effect is dependent only on the phase angle, but the effect's severity is dependent on the magnitude of the harmonic voltage [9].

The harmonic generation of a PV system depends on the inverter technology, solar irradiance, temperature, loads, and the supply system characteristics. The harmonic distortion generated in PV plants can occur as a result of intrinsic and extrinsic effects. Intrinsic harmonic distortions are related to inverter deficiencies, e.g. components and control loop nonlinearities, measurement inaccuracies, and limited pulse-width modulation (PWM) resolution. Connection to a weak and distorted electrical grid can be considered an extrinsic effect on the output waveform of a PV plant. A distorted voltage acts like a disturbance in the inverter control system, causing distortion of the current waveform generated by the inverter [10].

Several factors affect the power quality characteristics of the PV inverter output current. Both the current THD and the output reactive power are related to the output active power levels, which in turn are strongly dependent on solar irradiance levels. Most of the inverters consume or feed reactive power into the network depending on their output active power and their technology. During operation at low solar irradiance levels (e.g. sunrise, sunset, cloudy days), current THD values can increase rapidly, since the THD factor is inversely proportional to the output active power of the PV inverters. Nevertheless, THD is notably reduced as the output active power of the PV Inverters increases and reaches its nominal value. The intrinsic characteristics of the control circuit and nonlinear components of PV inverters may explain the current distortion behaviour in the low power generation stages [10] [11].

Varying power density of renewable energy resources (*i.e.* irradiance level and temperature in PV conversion) potentially cause voltage and frequency variation or sag/swell patterns in the grid. Also, application of power converters as interfaces between energy sources and the grid and their interaction with other system components may cause high harmonics distortion [12].

In small and distributed or decentralized PV controlled systems, the CSIs (current source inverters) can generate highly distorted current waveforms so that their cumulative effect in high penetration PV systems can create hot spots within transformers; ultimately generating excessive eddy or copper loss [13].

The differing influences of harmonics in distribution networks are not necessarily visible/evident initially. However, harmonics can have serious long-term consequences, of which the most important ones are [14]:

- Overloading of consumer's electrical installations and power system elements by higher order frequencies of currents and voltages;
- Increased heating of neutral conductors caused by triple current harmonics (frequency multiplier of number 3). The increased level of the triple harmonics in the neutral conductor can cause serious damage and even lead to fires because the neutral conductor is not usually overload protected;
- Increased transformer heating caused by higher (order and magnitude) harmonics, as well as saturation effects in the core;
- Higher harmonics the power system can cause interference to telecommunication lines;
- Overstressing and resonant condition on the capacitors bank.

3. Methods

The residential distribution network and loads for assessing load flow were modelled using DIgSILENT Power Factory software. The model consisted of a three-phase residential load at 0.4 kV voltage level composed of different single phase loads. The schematic of the residential load model is presented in **Figure 1**.

The compiled residential load was connected to the distribution network substation via a 1.4 km long overhead line (OHL) as depicted on **Figure 2**. The distribution network substation was connected to a 10 kV network with short-circuit power of 200 MVA and short-circuit current 11.5 kA. The high voltage (HV) busbar is modelled as a slack bus. The transformer used in the distribution substation was modelled with the following parameters:
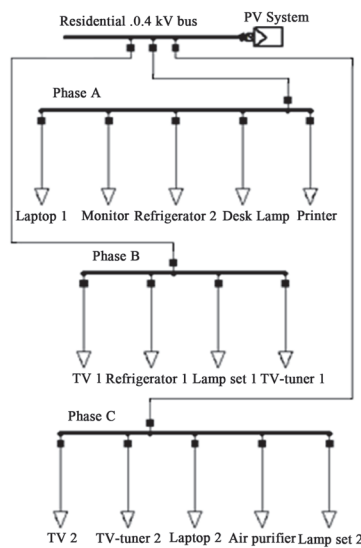
Figure 1. Schematic of residential load model.
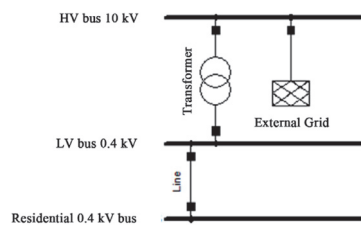
Figure 2. Schematic of distribution grid model.

- nominal power 25 kVA;
- relative short circuit voltage 4.5%;
- magnetizing impedance/ short circuit impedance ratio 3;
- vector group Yyn.

Implemented parameters in the simulation were selected based on power quality problematic issues identified in Elektrilevi's network (Estonia's main distribution grid operator) for July 1, 2013. The length of the OHL between substation and customer's PCC was defined as an average of all the lines between substations and customers with power quality problems. Similarly, the selected diameter of the line and nominal power of the transformer are the most common values for the identified problematic components.

Harmonic voltage amplitudes and phase angles up to the 50th order were obtained from measurements conducted by Elektrilevi at one of the sites where power quality issues were identified. Harmonic voltage distortion at the 10 kV bus was measured and modelled around 2%, which is a common value for this grid.

For modelling PV generation, three different commercially available PVs were measured for one week. The first measured system was single phase while the remaining were three phase systems. For all three systems, harmonic current amplitudes and angles up to 50th order were measured and used in the models in DIgSILENT. A mean load model of averaged values was composed for the single phase system and it was compared with other models composed of actual measurement results. PV inverters were connected to residential load's busbar as was described in **Figure 1**.

In order to model the network response of nonlinear loads, 14 different home appliances were measured. The results of the corresponding measured active and reactive power, harmonic current magnitudes and harmonic current phase shift angles of measured devices are presented in [15] [16]. Modelled devices were arranged in a manner where similar active power consumption was seen in every phase. The model is presumed to be the worst case scenario where all the nonlinear devices are in operation and coincidence factors are not taken into account.

4. Results

First, modelling results are given for the case where one single phase PV system was integrated to the existing grid. In the second and third case, different three phase systems were installed. All three scenarios were examined at three different power levels (stage 1—near 30%, stage 2—near 60%, stage 3—near 100%). Exact power level ratios depended on the availability of measurement data. Initial values of voltage THD in the grid before adding PV generations are presented in **Table 1**.

1) First case—single phase PV

A single phase PV inverter is connected to the residential busbar at phase C. Measurement results for the three different power levels are given at **Table 2** and **Table 3**. From the tables, it is apparent that current distortion decreases with increasing current. The same conclusion can be made by observing the power factor (PF) value which approaches unity with increasing current. Interestingly in this case, reactive power Q appears to be independent of the current level and changes polarity. In the paper the PF is the real power factor which accounts all values up to 50th order, the cos(fi) stands for displacement power factor which accounts only the main frequency components.

Table 1. Initial modelled voltage THD values [%].

Phase A	Phase B	Phase C
6.4	6.2	7.7

Table 2. Measured power values for single phase PV inverter.

Stage	Urms [V]	Irms [A]	P [W]	Q [var]	S [VA]
1—30%	233.6	3.45	739	322	807
2—60%	238.8	9.08	2125	−425	2168
3—100%	239.1	11.73	2783	−257	2805

Table 3. Measured power quality values for single phase PV inverter.

Stage	cos(fi)	PF	THD_U [%]	THD_I [%]
1—30%	1	0.92	1.01	4.27
2—60%	1	0.98	0.82	1.98
3—100%	1	0.99	1	1.67

Voltage and current distortion during a 15 h period is shown in **Figure 3**. Voltage distortion at the measurement point was notably low (around 1%) throughout the observed time period and similarly, current distortions are not greatly affected by grid disturbances.

Active power P, reactive power Q, and apparent power S are displayed in **Figure 4**. Results are in line with the prior conclusion for reactive power where Q is mainly capacitive throughout the measurement period. It can also be confirmed that reactive power is independent of current (compare with P and S).

As is evident in **Figure 5**, cos(φ) remained near unity throughout the measurement period, whereas PF varied considerably. The observed fluctuations in PF are a result of current distortion which is evident when comparing the current THD and PF curves in **Figure 3** (THD_I) and **Figure 5** (PF).

Table 4 presents the harmonic currents and phase angles up to the 21st order for the single phase PV inverter with the corresponding power levels described in **Table 4**. Phase angles are as percentages of main order current angle which is taken zero, main order current are taken 100%. Average values are also calculated and presented for modelling mean one phase PV. Even and higher order harmonics are left out due to their marginal dimension. All presented harmonic current amplitudes exhibited relatively moderate values, except for the third harmonic which was more notable.

For modelling mean PV generation, average values of the presented current harmonic amplitudes and angles (**Table 4**) were calculated. Main frequency current phase angles were defined zero as in ideal case and other angles were calculated in relation to mains current. **Figure 6** shows a graphical representation of the calculated average harmonics, where X and Y coordinates are calculated using Formulas (5) and (6). As it can be seen that the most notable component of the current is 3rd order harmonic.

$$X = A \times \cos \alpha \tag{5}$$

$$Y = A \times \sin \alpha \tag{6}$$

In the case where one single phase PV was added to the grid, voltage THD was observed to increase in all phases. Voltage distortion increased more as PV power level increased. Voltage THD for all power output stages and modelled mean PV are presented in **Table 5**. All values are given in percentages relative to initial conditions prior to the installation of PVs.

2) Second case—first three phase PV

In this case, a three phase PV inverter is connected to the existing network. Measurement results for three different power levels are given in **Table 6**. Once again, current distortion decreases when current (power) is increasing and same conclusion can be made observing the power factor (PF) value which approaches unity with increasing current. However, diverging from the first case, here total reactive power generation (Q_tot) is growing when current is increasing.

Table 7 provides reactive power and PF values for each phase. In addition to the aforementioned increase in total reactive power, observed reactive power changes were diverse for different phases. It is most probably due to different nature of specific phase load.

Harmonic currents up to 21st order of first three phase PV inverter are given in **Table 8** at the different power levels described in **Table 2**. In this case, the most notable harmonic was the 9th which exhibited values in the proximity of 2% in all phases, even at highest power level. Also the 13th harmonic had prominent values in phases B and C at highest power level. At the lower power level, most of the harmonics had significantly high values, even exceeding 6% at times.

Phase angles of harmonic current amplitudes displayed in **Table 8** are given in **Table 9**. It was observed that angles change with changing currents and as such, no mean values could be presented for this three phase PV inverter.

Voltage and current distortion of the first three phase PV inverter over a 15 hour period is shown in **Figure 7**.
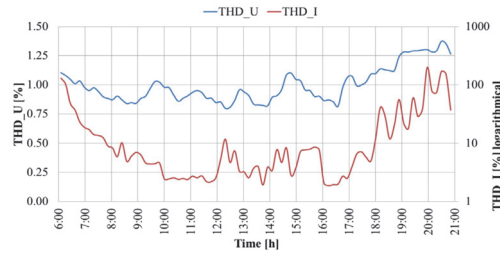
Figure 3. Measured voltage THD and current THD of single phase PV inverter.
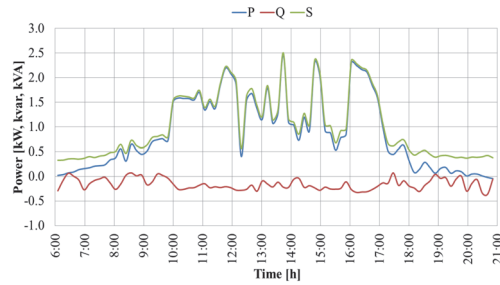
Figure 4. Measured power values of single phase PV inverter.
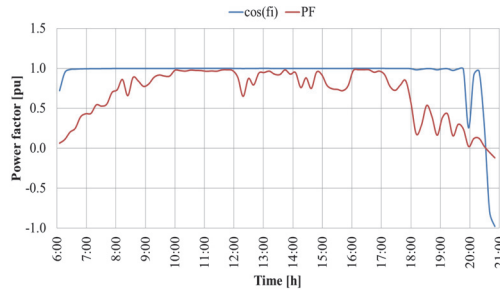
Figure 5. Measured power factors of single phase PV inverter.

Table 4. Harmonic currents [%] and phase angles [˚] of single phase PV inverter.

Order	I_1	Angle_1	I_2	Angle_2	I_3	Angle_3	I_mean	Angle_mean
1	100	0	100	0	100	0	100	0
3	1.92	28	1.20	62	1.01	52	1.38	47
5	0.48	97	0.31	146	0.26	139	0.35	127
7	1.08	175	0.27	159	0.27	164	0.54	166
9	0.88	116	0.33	145	0.35	146	0.52	135
11	0.89	104	0.38	60	0.32	52	0.53	72
13	0.69	75	0.21	73	0.20	77	0.37	75
15	0.23	109	0.08	104	0.10	107	0.14	107
17	0.35	88	0.07	145	0.06	190	0.16	141
19	0.29	287	0.10	259	0.10	271	0.16	272
21	0.63	209	0.20	205	0.17	209	0.33	208
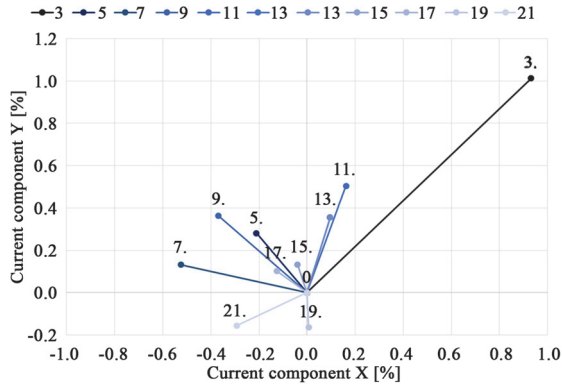
Figure 6. Mean harmonic current values of single phase PV inverter.
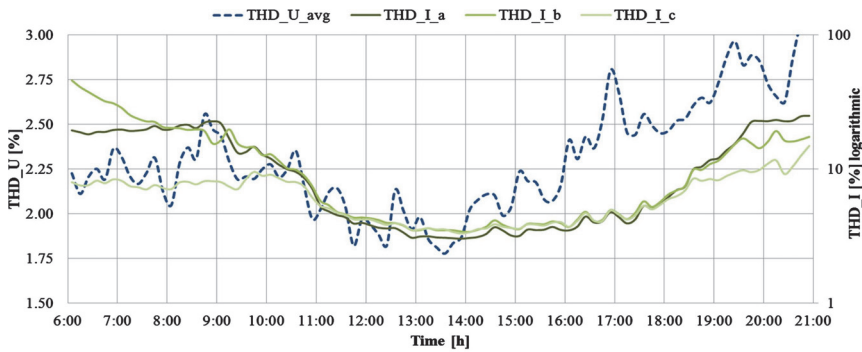
Figure 7. Measured voltage and current THD values of first three phase PV inverter.

Table 5. Measured power values for single phase PV inverter.

Stages	THD_U_a	THD_U_b	THD_U_c
1—30%	3.5	2.9	2.9
2—60%	12.9	10.2	9.7
3—100%	15.7	11.9	13.8
Mean	11.2	7.2	7.5

Table 6. Measured values for first three phase PV inverter.

Stage	1—30%	2—60%	3—100%
THD_U_avg [%]	2.33	1.98	2.03
THD_I_avg [%]	11.29	4.38	3.3
P_tot [kW]	1.06	2.78	3.88
Q_tot [kvar]	0.28	0.43	0.47
S_tot [kVA]	1.62	3.01	4.04
cos(fi)_avg	0.99	1	1
PF_avg	0.65	0.92	0.96

Table 7. Measured Q and PF values of first three phase PV inverter.

Stage	1—30%	2—60%	3—100%
Q_a [Var]	−335	−207	−104
Q_b [Var]	−104	−61	−98
Q_c [Var]	718	695	669
PF_a	0.68	0.97	1
PF_b	0.94	1	1
PF_c	0.52	0.84	0.9

Table 8. Measured harmonic currents [%] of first three phase PV inverter.

Order	Stage 1—30%			Stage 2—60%			Stage 3—100%		
	I_a	I_b	I_c	I_a	I_b	I_c	I_a	I_b	I_c
1	100	100	100	100	100	100	100	100	100
3	5.01	4.19	2.56	0.87	1.09	1.43	0.7	0.87	1.03
5	6.68	5.7	3.66	0.62	0.58	0.45	0.94	0.92	1.05
7	2.72	4.85	3.95	1.31	1.62	1.34	0.14	0.31	0.8
9	3.81	4.28	3.43	3.07	3.27	3.07	2.07	1.96	1.97
11	5.14	6.69	5.07	0.96	1.12	1.09	0.61	0.83	0.43
13	0.54	2.66	1.09	0.34	0.91	0.93	0.4	1.52	1.5
15	2.79	2.55	1.69	0.66	0.91	0.61	0.78	0.86	0.59
17	0.66	1.45	0.99	0.98	0.31	1.1	0.35	0.7	0.18
19	0.65	0.49	0.42	0.9	0.16	0.94	0.25	0.11	0.17
21	1.11	0.71	0.95	0.26	0.44	0.37	0.59	0.45	0.34

Table 9. Measured phase angles [°] of harmonic currents of first three phase PV inverter.

| Order	Stage 1—30%			Stage 2—60%			Stage 3—100%		
	Angle_a	Angle_b	Angle_c	Angle_a	Angle_b	Angle_c	Angle_a	Angle_b	Angle_c
1	0	0	0	0	0	0	0	0	0
3	275	170	262	38	26	57	281	17	271
5	214	35	220	85	303	227	278	182	340
7	11	202	344	196	226	288	91	285	17
9	143	320	139	19	31	75	166	29	171
11	181	147	219	100	145	219	124	234	51
13	39	201	76	262	326	74	42	147	110
15	314	132	286	336	18	98	205	96	218
17	227	161	43	195	254	335	118	310	98
19	65	229	58	23	233	88	23	241	27
21	268	307	255	204	98	171	264	108	243

Voltage distortion at the measurement point remained at a moderate level (around 2.25%) throughout most of the time period. Correlation with current distortion was not detected.

Reactive power generation is shown in **Figure 8**. The figure shows that while reactive power is phases A and B was moderately consumed, reactive power was generated in phase C at a much higher level.

Power indices over the 15 hour period are presented in **Figure 9**. The figure supports the previous conclusion that reactive power (Q_tot) is mainly inductive. It also confirms that reactive power is independent of current in this case (compare with active power P_tot and apparent power S_tot).

Figure 10 shows that $\cos(\varphi)$ was near unity for the entire duration, whereas PF varied more. PF in phase C was especially poor. Changes in the PF were attributed to current distortion which could be seen when comparing current THD and PF (THD_I in **Figure 7** and corresponding PF in **Figure 10**).

Results of having the first three phase PV in the grid are presented in **Table 10**. For this case, results are not uniform and voltage THD did not increase in all the stages. Slight harmonic cancellation in phases A and C could be noticed at stage 2. In other stages voltage distortion increased moderately. All values are given in percentages compared to the initial conditions where no PVs were installed.
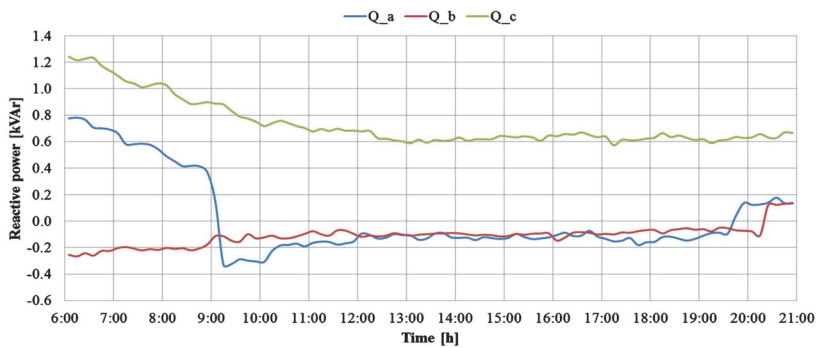
Figure 8. Measured reactive power values of first three phase PV inverter.
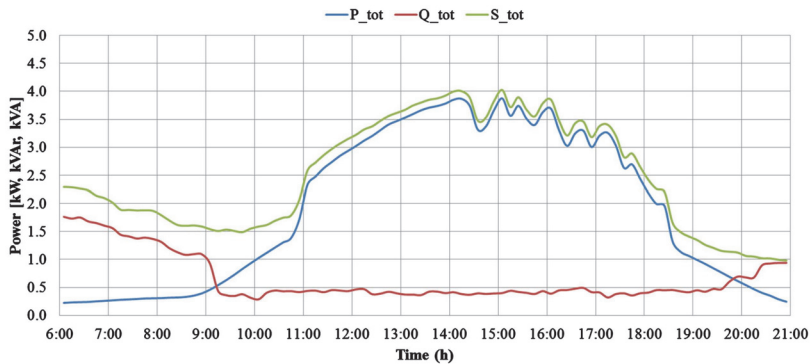
Figure 9. Measured power values of first three phase PV inverter.

Table 10. Voltage THD of grid with PV compared to grid without PV [%].

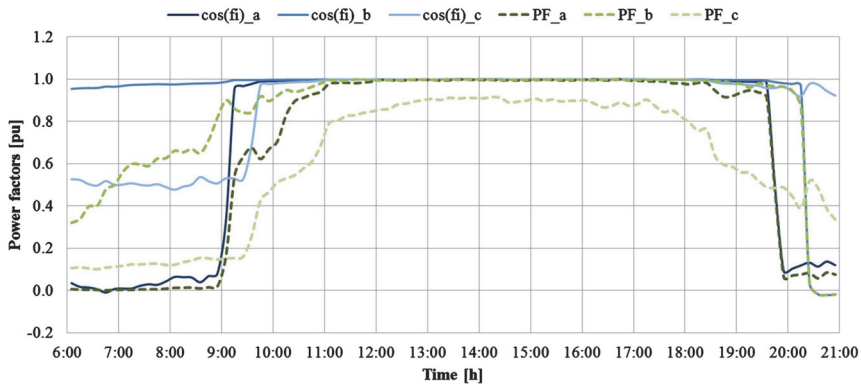| Stages	THD_U_a	THD_U_b	THD_U_c
1—30%	4.4	4.2	4.5
2—60%	−1.4	0.6	−1.7
3—100%	6.0	6.7	5.0

Figure 10. Measured power factor values of first three phase PV inverter.

3) Third case—second three phase PV

In this case, the three phase PV inverter is replaced with another inverter. Measurement results for three different power levels are given at **Table 11**. As evident from the table, current distortion decreases with increasing current and similarly, the power factor (PF) value approached unity. Only total reactive power (Q_tot) did not exhibit a linear change.

Reactive power and PF values for each phase are given in **Table 12**. In addition to the aforementioned total reactive power nonlinearity, reactive power changes were observed to differ for different phases also.

Table 13 presents harmonic currents up to 21st order of second three phase PV inverter at different power levels as described in **Table 11**. In this case harmonics were notable only at lower power levels. For the first stage, high amplitudes were seen in majority of the presented orders.

Phase angles presented harmonic current amplitudes in **Table 13** are displayed in **Table 14**. Angles were observed to change with changing currents and as such, no mean values could be presented for this three phase PV inverter.

Voltage and current distortion of second three phase PV inverter throughout the 15 h time period is shown in **Figure 11**. Voltage distortion at the measurement point was mainly low level (around 1.1%). Correlation between voltage and current distortion was not detected.

Reactive power generation is shown in **Figure 12**. Reactive power in phases A was maintained near zero, while reactive power in the other phases changed frequently in both magnitude and polarity.

Power (P, Q, and S) during the investigated time period is shown in **Figure 13** and supports the earlier observation that total reactive power oscillated around zero. A slight correlation with current could be observed in the middle of the day (compare fluctuation in Q_tot with active power P_tot and apparent power S_tot around 14:00).

Figure 14 displays how cos(φ) was maintained near unity majority of the day. Similarly, PF remained rather constant with only minor deviations. The PF curves reached unity with a slight delay and started diminish earlier. The small variation in the middle of the day was in correlation with the rise in total reactive power shown in **Figure 13** (Q_tot at 14:00).

The impact of the second three phase PV is presented in **Table 15**. Results are not uniform and voltage THD did not increased in all the cases. Higher harmonic cancellation could be noticed compared to the previous case with the first three phase PV. A definite assessment concerning distortion changes cannot be done. All values are given in percentages compared to initial conditions where no PVs were installed.

4) Comparison of results

It could be concluded that changes in voltage THD values increase as power output of PVs grows. For the one phase PV installation, it was clear that voltage harmonics increased in all three phases. For the three phase PV installations, the two cases showed different outcomes. With the first three phase PV, notable degradation was observed. However, a conclusive assessment could not be done with second three phase PV installation. Voltage THD results at the highest power level for all three cases are depicted in **Figure 15**.
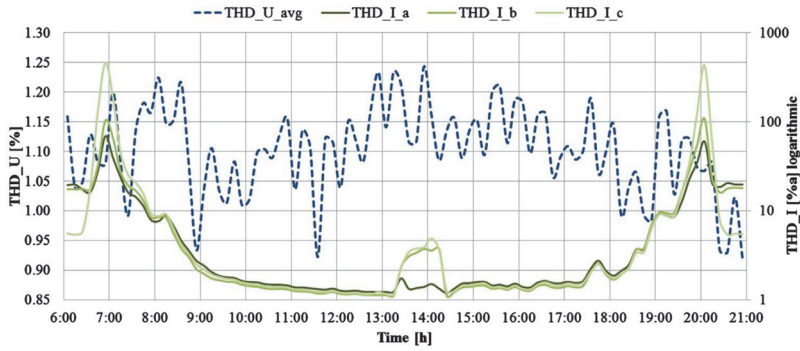
Figure 11. Measured voltage and current THD values of second three phase PV inverter.
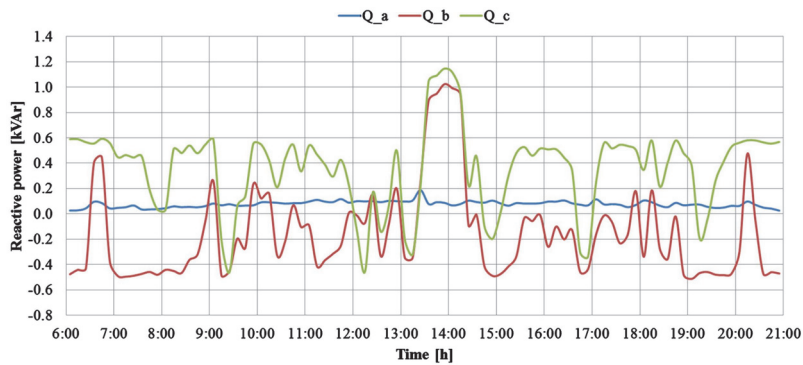
Figure 12. Measured reactive power values of second three phase PV inverter.
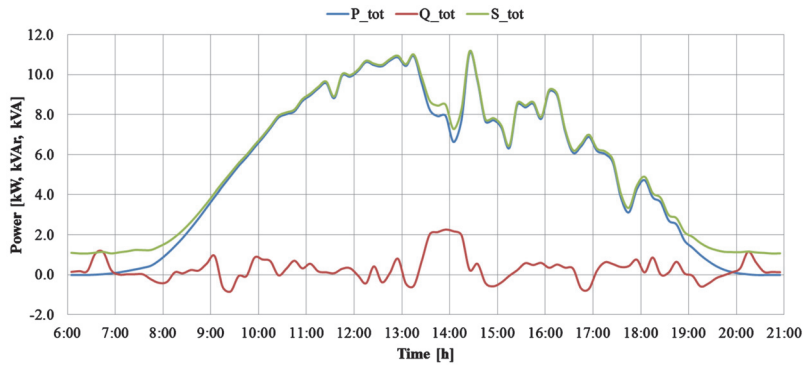
Figure 13. Measured power values of second three phase PV inverter.

Table 11. Measured values for second three phase PV inverter.

Stage	THD_U_avg [%]	THD_I_avg [%]	P_tot [kW]	Q_tot [kVAr]	S_tot [kVA]	cos(fi)_avg	PF_avg
1—30%	1.18	5.34	1.9	0.17	2.20	1.00	0.84
2—60%	1.18	1.77	5.82	−0.75	5.95	1.00	0.98
3—100%	1.07	1.19	10.19	−0.16	10.26	1.00	0.99
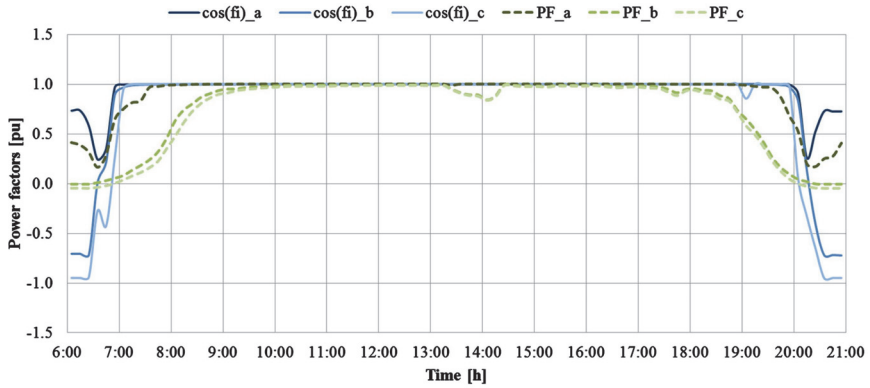
Figure 14. Measured power factor values of second three phase PV inverter.
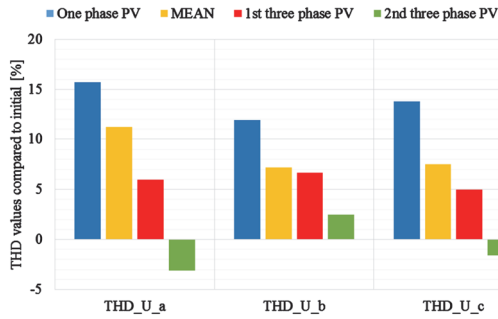
Figure 15. Voltage THD values at third stage for different PVs compared to initial conditions [%].

Table 12. Measured reactive power and PF values of second three phase PV inverter.

Stage	Q_a [Var]	Q_b [Var]	Q_c [Var]	PF_a	PF_b	PF_c
1—30%	52	−431	544	1.00	0.79	0.77
2—60%	66	−459	−360	1.00	0.97	0.96
3—100%	123	−434	149	1.00	0.99	0.99

Table 13. Measured harmonic currents [%] of first three phase PV.

| Order	Stage 1—30%			Stage 2—60%			Stage 3—100%		
	I_a	I_b	I_c	I_a	I_b	I_c	I_a	I_b	I_c
1	100	100	100	100	100	100	100	100	100
3	4.12	3.03	3.30	1.02	0.85	0.93	0.84	0.68	0.71
5	1.53	1.74	1.98	0.24	0.36	0.36	0.60	0.59	0.61
7	1.60	1.32	1.31	0.69	0.59	0.64	0.32	0.42	0.39
9	1.56	1.56	1.60	0.49	0.42	0.48	0.18	0.19	0.21
11	0.80	0.32	0.43	0.66	0.71	0.68	0.19	0.21	0.19
13	1.04	1.10	1.17	0.28	0.41	0.39	0.27	0.19	0.20
15	1.46	1.00	1.24	0.53	0.46	0.49	0.26	0.23	0.26
17	0.74	0.93	0.74	0.26	0.21	0.13	0.22	0.18	0.20
19	0.31	0.28	0.23	0.27	0.23	0.29	0.06	0.05	0.08
21	0.34	0.45	0.49	0.13	0.09	0.15	0.15	0.13	0.14

Table 14. Phase angles [°] of harmonic currents of second three phase PV.

Order	Stage 1—30%			Stage 2—60%			Stage 3—100%		
	angle_a	angle_b	angle_c	angle_a	angle_b	angle_c	angle_a	angle_b	angle_c
1	0	0	0	0	0	0	0	0	0
3	205	193	198	16	16	16	19	247	17
5	53	32	38	219	212	208	202	324	198
7	80	330	334	245	259	248	346	60	341
9	191	172	178	68	49	45	148	66	135
11	201	252	111	213	194	200	207	300	197
13	326	331	323	328	320	328	175	73	342
15	98	71	82	101	87	88	141	83	115
17	303	233	255	304	286	311	20	135	157
19	286	283	235	25	325	205	186	113	183
21	101	60	45	98	67	96	327	296	317

Table 15. Voltage THD of grid with second three phase PV inverter compared to grid without PV [%].

Stages	THD_U_a	THD_U_b	THD_U_c
1—30%	1.2	−3.2	−2.3
2—60%	−0.6	3.5	1.2
3—100%	−3.1	2.5	−1.6

5. Discussion

While the discreet disturbances of harmonic distortion may not cause immediate and easily-observed impacts, it can cause some equipment to malfunction, and result in additional power losses in both customer and network equipment [17]. As harmonic levels change considerably from one week to another, it is very difficult to assess the long-term evolution of harmonic levels only from measurements carried out over a short period [1]. This paper clearly concludes that power quality problems may occur when PV utilization is not sufficiently considered.

Harmonic current angles of small generators such as PVs are seldom considered. One aim of this paper is to draw attention to this topic which could lead to advances in modelling PV inverters with different topologies. To help mitigate harmonic distortion problems, models with appropriate harmonic current amplitudes and phase angles could be used to select most suitable devices.

This study only examines one household and one PV at time. The described effects may escalate when a larger number of devices are considered. Special attention is need in situations where devices have similar harmonic patterns and the harmonic cancellation effect is minimal. Additional measurements should be performed to obtain unified values for modelling PV generators more accurately. It would be necessary to have measurement data extending over entire years in order to acquire results independent of any disturbance. Furthermore, flicker and voltage level issues should be accounted for as they may have a significant influence in real applications.

6. Conclusions

Firstly, it can be concluded that current harmonic distortion of the PV's output is correlated with current. Distortion decreases when the PV is operating at a higher loading level. PVs function accurately under ideal conditions. Due to unstable energy availability (*i.e.*, variable solar radiation), continuous variation in power quality parame-

ters is to be expected. In the presented research, two PVs showed considerable harmonic current distortion (average THD over 5%) even at full loading. Only one PV had average current THD under 2% which was considered a very good achievement.

All of the measured PV systems had quite different harmonic patterns when compared with each other throughout their loading range. As such, it is difficult to propose simplified values for modelling without measuring and analysing a greater number of devices. Also, for more reliable harmonic current phase angle data, laboratory tests should be performed.

Secondly, contrary to theory, reactive power generation of PVs was not observed to be correlated to active power. Measured devices showed different levels and variation of reactive power in different phases. These differences may be hazardous in cases where high reactive power values and variations in one phase and zero reactive power in other another phase are not considered. It was also observed that main order reactive power was compensated more efficiently than higher order reactive power which was evident when comparing $\cos(\varphi)$ and PF.

Relative to the initial conditions where no PVs were installed, modelling one PV results in voltage distortion exceeding 10%. The influence is dependent on grid structure and topology of the PV. In case of PV with less distorted current working at high power level, minor improvement of voltage distortion was observed.

References

[1] Berthet, L., Eyrolles, P., Gauthier, J. and Sabeg, S. (2007) Harmonic Level Measurements on French Low-Voltage Networks. 19*th International Conference on Electricity Distribution*, Vienna.

[2] Aiello, M., Cataliotti, A., Favuzza, S. and Graditi, G. (2006) Theoretical and Experimental Comparison of Total Harmonic Distortion Factors for the Evaluation of Harmonic and Interharmonic Pollution of Grid-Connected Photovoltaic Systems. *IEEE Transactions on Power Delivery*, **21**, 1390-1397. http://dx.doi.org/10.1109/TPWRD.2005.860231

[3] Jayasekara, N. and Wolfs, P. (2010) Analysis of Power Quality Impact of High Penetration PV in Residential Feeders. 20*th Australasian Universities Power Engineering Conference* (*AUPEC*), Christchurch.

[4] Rawa, M., Thomas, D. and Sumner, M. (2011) Simulation of Non-Linear Loads for Harmonic Studies. 11*th International Conference on Electrical Power Quality and Utilisation* (*EPQU*), Lisbon, 17-19 October 2011, 1-6. http://dx.doi.org/10.1109/EPQU.2011.6128915

[5] Renders, B., Degroote, L., Driesen, J. and Vandevelde, L. (2007) Profits of Power-Quality Improvement by Residential Distributed Generation. 42*nd International Universities Power Engineering Conference*, Brighton, 4-6 September 2007, 377-381. http://dx.doi.org/10.1109/upec.2007.4468976

[6] Kütt, L., Saarijärvi, E., Lehtonen, M. and Niitsoo, J. (2013) A Review of the Harmonic and Unbalance Effects in Electrical Distribution Networks Due to EV Charging. 13*th International Conference on Environment and Electrical Engineering* (*EEEIC*), Wroclaw.

[7] Bhattacharyya, S., Cobben, S., Ribeiro, P. and Kling, W. (2012) Harmonic Emission Limits and Responsibilities at a Point of Connection. *IET Generation, Transmission & Distribution*, **6**, 256-264. http://dx.doi.org/10.1049/iet-gtd.2011.0376

[8] Niitsoo, J. and Palu, I. (2011) Distorted Load Impacts on Distribution Grid. *Proceedings of the* 12*th International Scientific Conference Electric Power Engineering* 2011, Kouty nad Desnou.

[9] Yong, J., Chen, L. and Chen, S. (2010) Modeling of Home Appliances for Power Distribution System Harmonic Analysis. *IEEE Transactions on Power Delivery*, **25**, 3147-3155. http://dx.doi.org/10.1109/TPWRD.2010.2051960

[10] Block, P., Salamanca, H., Teixeira, M., Dahlke, D., Shiono, O. and Dodadon, A. (2014) Power Quality Analyses of a Large Scale Photovoltaic System. *The* 5*th International Renewable Energy Congress IREC* 2014, Hammamet, 25-27 March 2014, 1-6. http://dx.doi.org/10.1109/irec.2014.6826946

[11] Kontogiannis, K., Vokas, G., Nanou, S. and Papathanassiou, S. (2013) Power Quality Field Measurements on PV Inverters. *International Journal of Advanced Research in Electrical Electronics and Instrumentation Engineering*, **2**, 5301-5314.

[12] Anwari, M., Hamid, M. and Taufik (2008) Power Quality Behavior of Single Phase Fed Adjustable Speed Drive Supplied from Grid of PV Generation. 2*nd IEEE International Conference on Power and Energy* (*PECon* 08), Bahru.

[13] Hasanzadeh, A., Edrington, C. and Bevis, T. (2012) Comprehensive Study of Power Quality Criteria Generated by PV Converters and Their Impacts on Distribution Transformers. 38*th Annual Conference on IEEE Industrial Electronics Society IECON* 2012, Montreal.

[14] Fekete, K., Klaic, Z. and Majdandzic, L. (2012) Expansion of the Residential Photovoltaic Systems and Its Harmonic

Impact on the Distribution Grid. *Renewable Energy*, **43**, 140-148. http://dx.doi.org/10.1016/j.renene.2011.11.026

[15] Niitsoo, J., Kilter, J., Palu, I., Taklaja, P. and Kütt, L. (2013) Harmonic Levels of Domestic and Electrical Vehicle Loads in Residential Distribution Networks. *Proceedings of AFRICON* 2013, Mauritius, 9-12 September 2013, 1-5. http://dx.doi.org/10.1109/AFRCON.2013.6757800

[16] Niitsoo, J., Palu, I., Kilter, J., Taklaja, P. and Vaimann, T. (2013) Residential Load Harmonics in Distribution Grid. *Proceedings of* 3*rd International Conference on Electric Power and Energy Conversion Systems* (*EPECS* 2013), Istanbul, 2-4 October 2013, 1-6. http://dx.doi.org/10.1109/epecs.2013.6713054

[17] Nicholson, G., Gosbell, V. and Parsotam, A. (2007) Analysis of Harmonic Distortion Levels on a Distribution Network. P*ower Engineering Conference*, AUPEC 2007, Perth, 9-12 December 2007, 1-7. http://dx.doi.org/10.1109/aupec.2007.4548035

Publication III

Iqbal, M. N.; Jarkovoi, M.; Kutt, L.; Shabbir, N. (2019). Impact of LED thermal stability to household lighting harmonic load current modeling. 2019 Electric Power Quality and Supply Reliability Conference & 2019 Symposium on Electrical Engineering and Mechatronics: 2019 Electric Power Quality and Supply Reliability Conference, June 12 to 14, 2019 in Kärdla, Hiiumaa Island of Estonia. IEEE

Impact of LED Thermal Stability to Household Lighting Harmonic Load Current Modeling

M Naveed Iqbal, Marek Jarkovoi, Lauri Kütt, Noman Shabbir
Department of Power Engineering and Mechatronics
Tallinn University of Technology
Tallinn, Estonia
miqbal@taltech.ee; marek.jarkovoi@taltech.ee; lauri.kutt@taltech.ee; noshab@taltech.ee

Abstract—**Global warming and high fuel prices are pushing governments and people in the direction of energy-efficient appliances. Lighting ingests almost 20% of the total electricity consumption in the residential and commercial sector. Replacing the old technology lamps with the new energy efficient light emitting diode (LED) lamps can reduce power consumption substantially. However, these nonlinear LED lamps contain circuits that can disturb the power quality by injecting current harmonics. It may affect the distribution grid power quality due to the penetration of a large number of LED lamps. This paper presents the power quality measurement data of different LED lamps available in the Estonian market. A comparison of current harmonics of thermally stable and unstable lamps are presented. The combined effect on the power quality due to the high penetration of LED lamp in the residential buildings is also presented in the paper.**

Keywords—LED lamps, power quality, thermal stability, current harmonics, residential electricity consumption model

I. INTRODUCTION

Increasing fuel prices, $CO2$ emission, and global warming are making governments and people more concerned about energy consumption. Governments and organization are working together to promote energy-saving strategies. Electrical appliances in households are becoming more energy efficient each day. Strategies to improve energy efficiency can reduce 27% energy consumption in the residential sector [1]. Lighting in the residential buildings consumes up to 20 percent of the total energy used in the building [2]. Therefore, improvement in lighting technology is playing a significant role to reduce the overall energy consumption. Incandescent lamps (IL) were replaced by energy efficient fluorescent lamps (FL) and compact fluorescent lamps (CFL) during the last decade. However, the new light emitting diode (LED) lamps are becoming much more popular because of their reduced prices and low electricity consumption. Energy policies of the state and regional level are also promoting the use of LED lamps. The European parliament regulations EC/EU No. 244/2009, 245/2009, and 1194/2012 stress the advancement in the efficiency of electrical appliances including lighting [3]. In the guidelines of these regulations, the promotion of LED lighting technology due to its effectiveness and improved life-cycle cost is emphasized. Also, the absence of mercury makes LED lamps environment-friendly [4]. The decision to select lamps by the customers is based on market price, light quality, and power ratings. A standard lamp package includes information about power ratings, energy ratings, color temperature range, estimated life span, and operating voltage and frequency range. However, LED, CFL, and FL lights contain ballasts circuit that can affect power quality. There is no information available for the customers about lamp characteristics, power quality, and design techniques used in the ballast.

Power quality and power factor are essential considerations for the network operator. The power quality expresses the quality of the voltage and the current waveform. Modern lights add current harmonics content in the grid and therefore have a significant total current harmonic distortion (THDi). The THDi corresponds to the AC currents generated by high-frequency electronic devices and causes interferences in the network. Poor power quality can cause a voltage drop. It may also result in the overheating of electrical equipment like transformers and malfunctioning of the protective devices. Moreover, resonance, losses in capacitors, and additional noise in motors or other electrical equipment are consequences of poor power quality [5]–[7]. Since lighting constitutes a significant portion of the total power consumption in the residential sector, therefore, it is essential to consider the impact of lighting on power quality. This paper is based on the measurement results of the different LED lamps available in the market. The objective is to present a power quality evaluation of existing LED lamps and when they are used in the real-time scenario in the residential building.

II. LED LAMP OVERVIEW

Incandescent lamp (IL) was a favorite light source for many years. They produce light by resistive heating but with low efficiency. Their output in terms of lumens per watt is meager as most of the energy is dissipated as heat. The life span of a typical IL is around 1000 hours. In halogen lamps, argon gas inside IL lamps was replaced with halogen gas. As a result, the lifespan of the lamp is improved considerably, and the efficiency becomes better [8]. Fluorescent lamps and compact fluorescent lamps are more energy efficient and use electromagnetic or electronic ballast. Although electromagnetic ballasts are reliable but have poor power factor and efficiency compared to the electronic ballast circuits. Therefore, CFL lights containing electronic ballasts are more energy efficient than FL. In comparison to IL, CFL lamps use 70% less energy and last 15 times longer [9].

LED lamps are based on semiconductor material coated with different luminescent materials. The LED technology has thrived over the last decade, and LED lamps are more reliable and efficient and cost-effective. They could convert electricity to light using semiconductors with near 100 percent efficiency [10]. However, LED lamp efficiency rest on the heat dissipated in the junction and design on the luminaire. Each LED lamp may contain multiple chips to make it cost-effective. It affects the temperature distribution and increases the heat confined in the lamp. As the radiation emission for LEDs is almost negligible, the heat can be only removed by convection and conduction to avoid damage. As a result, the efficiency, lifespan, and reliability of the LED lamp are reduced [11]. The

US Department of Energy (DOE) forecasted an increase in the lifespan and decrease in the prices by 2020. They predicted that lifespan of LED lamps could increase up to 50,000 hrs. During the last few years, the efficiency of LED lamps has improved significantly from 30 lm/W in 2009 to more than 90 lm/W in 2019. The average efficiency of LED lamps used in households was 76 lm/W in 2013 [6]. We have selected 150 LED lamps from 3.3 W to 23 W available in the Estonian market from different manufacturers. The average efficiency of these lamps is 92 lm/W with the highest value of 124 lm/W.

III. POWER QUALITY ASPECTS OF LED LAMPS

LED, CFL, and FL lamps have better efficiency than incandescent lamps but contain circuits that can cause poor power factor and power quality problems. A comparison of LED and CFL lamps available commercially indicates that harmonic injection depends upon the control and power supply topology [12]. Lamps from different manufacturers are equipped with different ballast topologies. The old and inexpensive lamps contain simple rectifier bridge circuits and generate more distortion. However, the new generation of LED lamps contain filters and PF correction. The performance may depend on the price as well, and the low price lamps may still not efficient. Similarly, voltage sags and distortion from the utility further affects the power quality and performance of LED lamps. The current THD values of tested LED lamps were in the range of 30 to 175 percent in [13]. Amount of current THDi depends on the filters used in the lamps. For active filters, the THDi range was recorded between 30 to 35 %. However, the THDi values were more for passive filters and were in the range of 100–175%. It was also observed that voltage sags affect the illuminance of the LED lamps and depend on sag depth and duration. In a similar study, LED lamps available in Swedish and Spanish markets were measured to observe power quality and flickering effect due to supply voltage variations [14]. The study shows that LED lamps are less sensitive to the voltage variation as compared to the CFL. They were grouped based on the light output variation due to voltage magnitude. LED lamps with low light output sensitivity generate a higher harmonic magnitude.

Dimmable LED lamps are also available in the market, and their light output can be changed using a dimmer. However, dimming operation changes the power quality and light quality of the lamps. Harmonic current levels were observed for LED lamps using dimming operation in [15]. The author observed an increase in the magnitude of harmonics when the dimming angle is increased to lower the lamp brightness.

Magnitude and phase of grid supply voltage affect the harmonics as well. In residential buildings, multiple lamps may be used at once. Therefore, harmonics generated by different lamps may have some cancellation effect. This harmonic cancellation effect is more prominent in the LED lamps as compared to the CFL. Almost all CFL lamps behave more in a similar manner and therefore less harmonic cancellation. The harmonic cancellation results of LED and CFL lamps were presented in [12]. It shows the importance of harmonic cancellation when a large number of lamps are used in the building at the same time. The cancellation depends on the voltage distortion and harmonic order. Magnitude and phase of the grid voltage also disturb the current THD.

Harmonics of the lamps also varies during the period in which they are not thermally stable. The measurement taken at the instance when they are just turned ON can be different from the measurement taken after using them for some time. In order to make a correct estimation, the measurement must be taken after the lamp became thermally stable. The high power street LED lamps were failed to achieve thermal stability even after 30 minutes of continuous usage [16]. Similarly, in [15], the measurement is taken after 10 minutes of LED lamp usage to avoid inaccuracy in the measurement procedure. We have selected 16 LED lamps from the Estonian market and measure them for their power quality evaluation. The information and ratings of the lamps are provided in Table I.

TABLE I.   LED LAMP INFORMATION

Lamps	Power ratings (W)	Energy ratings	Light output (Lumens)	Price (€)
1	7	A+	600	8.65
2	8.5	A+	810	8.90
3	9	A+	650	1.23
4	10	A+	806	4.75
5	12	A+	1050	4.92
6	8.5	A+	806	2.70
7	9	A+	806	2.70
8	9	A+	806	14.00
9	9.5	A+	806	4.90
10	9.5	A+	806	10.00
11	10	A+	1055	14.00
12	13	A+	1521	9.90
13	9.5	A+	806	4.90
14	10	A+	800	7.90
15	9.5	A+	810	5.90
16	7	A+	500	5.90

IV. MEASUREMENT SETUP

The measurement setup consists of a controllable AC Chroma 61505 4 kVA, power supply, a National Instruments data acquisition module (DAQ), a 16-lamp load module with relays, switching control box to control relays, power quality measurement device A-Eberle PQ-Box 200, and a computer as shown in Fig. 1. A MATLAB program is used to generate a reference signal for the controllable power supply. As a result, a pure sinusoidal voltage of 230V is generated by the power supply. The voltage is applied to a bus bar connected to 16 lamps through the relays in the load module. The same MATLAB program is used to generate switching signals for the relays through the DAQ module. The control box covert these digital signals to 12V DC using transistor switches. This setup has enabled to test the LED lamps automatically by turning each lamp ON for any given time. The power quality
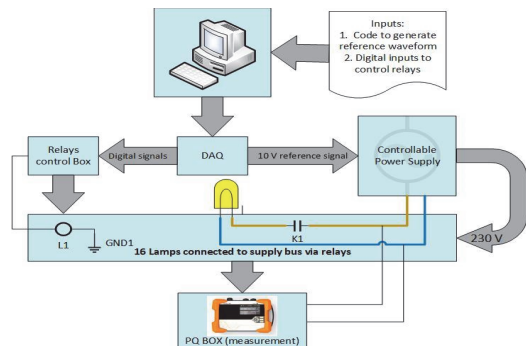

Fig. 1.   Measurement setup layout.

measurement A-Eberle PQ-BOX 200 device is used to record the measurement. It is capable of measuring harmonics with a 1-second interval. This interval is aggregated from a 200-millisecond measurement.

V. POWER QUALITY OF INDIVIDUAL LAMPS

The measurement has been performed by turning each lamp ON for 1 hour. The measurement data is analyzed to extract information about individual current harmonics. For each lamp, fundamental component and odd current harmonics from 3rd to the 13th are analyzed. Fig. 2, shows the per unit (PU) values of the fundamental and odd harmonics. The values are plotted over 1-hour for each second measurement. It is clear from the figure that all lamps take some time to get thermally stable. In the thermally stable state, the harmonic RMS and phase are almost stable. The time required by the lamps to get thermally stable is independent of the lamp power ratings. For example, the time taken by two 7 W lamps was 15 minutes and 50 minutes respectively to get fully thermally stable. Both lamps are from different manufacturers. However, lamp 9 and 13 have the same power ratings and are from the same manufacturer. But, the lamp 13 takes only 15 minutes to get thermally stable, but lamp 9 requires almost 40 minutes. Out of all 16 lamps, four lamps have taken more than 50 minutes to get stable. Three lamps required less than 15–20 minutes to get stable. For all the remaining lamps, 20-40 minutes were required for thermal stability.

For the individual harmonics, each lamp behaved differently in terms of the difference between RMS and phase values of the thermally stable and cold state condition. Here the term cold state means when the lamp is initially turned ON and not thermally stable. The maximum difference for the fundamental component was 9.7% between cold and stable state. For 60% of the lamps, the difference in the fundamental

component was less than 5%. Similarly, for 3rd harmonic, the maximum RMS difference was 8.7% and 60% of lamps shown less than 5% difference between cold and stable state. For the higher order harmonics, the maximum difference has increased even more and its 19% for 9th harmonic. For the 5th, 7th, 11th, and 13th harmonic the maximum RMS difference between cold and stable state is 13.60, 15.50, 12.50, and 12.25 percent, respectively. However, the average difference is from 3.6% to 4.9% in the odd harmonics for all 16 lamps.

For the phase angles, the change in the angle increases radically for higher order harmonics when the lamp goes from the cold state towards the stable state. For the 3rd harmonic, 80% of the lamps have less than 3-degree variation, and the average variation is only 2.25 degrees. The maximum and average phase difference got double for the 5th harmonic with a maximum value of 6.67 degrees and an average value of 4.25 degree. This difference increases even more for the 7th harmonic as the average, and the maximum difference is 8 and 17.90 degrees, respectively. For 9th, 11th, and 13th harmonics, the average difference is between 11 to 14 degrees. The max-imum phase deviation is 20 to 26 degrees for these harmonics between cold and stable state. The phase angle deviation for all 16 lamps over 1 hour of measurement is shown in Fig. 3.

VI. POWER QUALITY ASSESSMENT OF THE REAL TIME SCENARIO

Lighting load has a substantial share of total power consumption in the residential sector. It is therefore interesting to study the impact of total harmonic content added by all the lamps in a large building or houses in the distribution network. To evaluate this aspect, we have made a lighting usage model for the residential building based on real-time measurement.
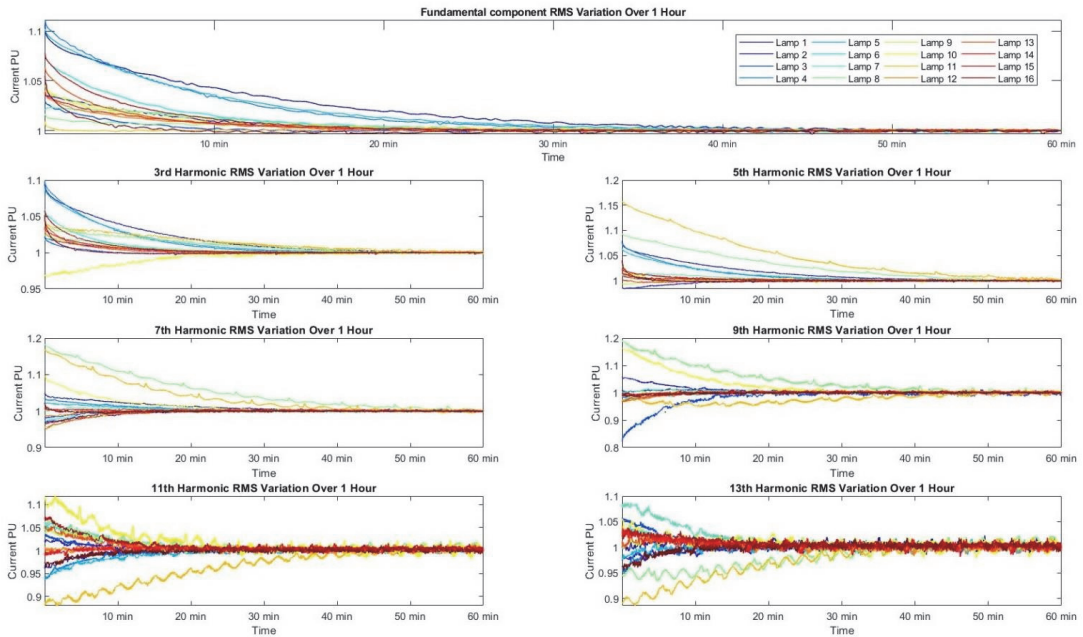

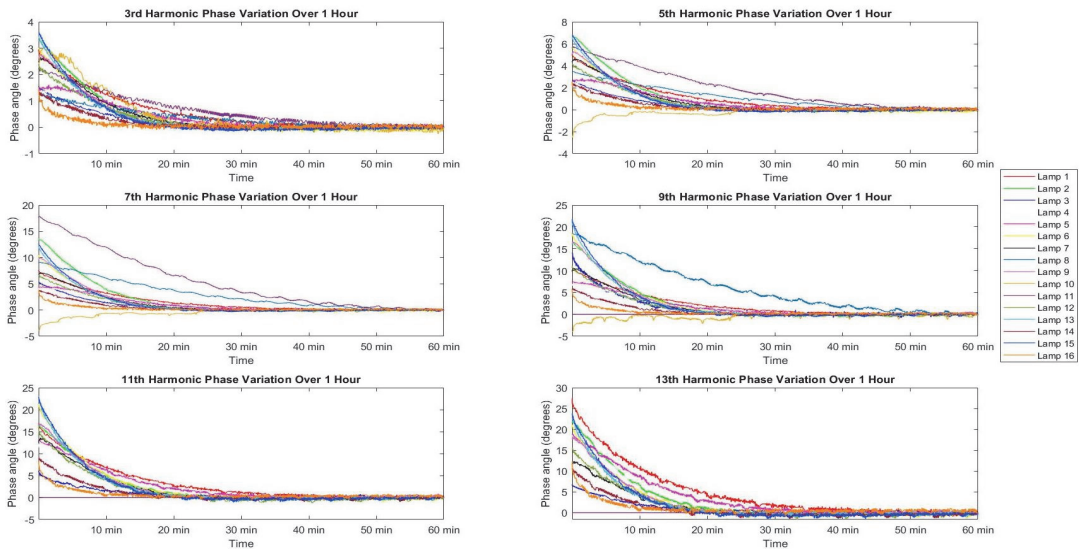Fig. 2. Harmonic current RMS (Per Unit) variation over 1 hour for LED lamps.

Fig. 3. Phase angle variation of current harmonics over 1 hour for LED lamps.

A residential building is measured using sub-meters for a month. The lighting load is then analyzed and compared with the lamps and their power ratings in the building. Lighting load is highly variable and depends on many variables. Occupancy in the building, weather conditions, solar radiance are some of the variables that can affect the lighting usage in the building [17].

We have used occupancy data in the building and usage pattern of each lamp in the house to create a lighting usage model for the residential building [18]. The measurement data is converted into the usage patterns of each lamp in the house. The lighting demand is divided into morning, evening, and day usage intervals. Each interval is simulated separately. Depending on the occupancy profile, the start time of each interval is estimated from its empirical cumulative distribution function (ECDF). The usage pattern for each lamp is divided into switching events and noise events. Each time when a lamp is used for more than 10 minutes, it is considered as a switching event. Noise events are less than 10-minutes in duration. During each interval, the first switching interval is estimated for each lamp based on the respective ECDF. Afterward, noise events and the gap from the next switching events are predicted based on their respective ECDF. Based on the occupancy

Fig. 4. Lighting usage in a typical house with 5 lamps.

profile and number of lamps in each house, the lighting demand can be simulated for any number of days for a house. The output of the model is the ON and OFF times of all light switches in the house [19].The advantage of this model is that the type of lamps can be selected at the later stage. Fig. 4 shows simulated results of the lighting usage in a house on a typical day with 5 lamp switches.

Based on this model, we have created a real-world scenario to estimate the power quality of the lighting load of 10 houses. Each house is populated with a random number of lamps from the measured 16 lamps. Each lamp usage is then compared with the measurement results. All the harmonics are added to assess the total power quality of the house at the point of common coupling. This process is extended to calculate the total harmonic RMS and phase values for all 10 houses for 5 days. To study the impact of thermal stability, we have created three different scenarios. In the cold state scenario, we have added the measurement results of the lamp during the cold state when they are not thermally stable. RMS and phase values for each house and a total of 10 houses are calculated for the cold state. In the second scenario, we have used the normal values of 1-hour measurement. When a lamp is turned ON in any house, its output is replaced with the measurement data from the cold state towards the hot sate. For example, if a lamp is used for 2 hours, starting from the 1st minute, we used the measurement data also at the 1st minute and then continue using it until the 60th minute. Afterward, each minute is compared only with the 60th-minute data as all lamps were thermally stable after 50 minutes. In the third scenario, we have used only measurement values when the lamps are thermally stable. Therefore, starting from 1st minute, we used measurement data at recorded at 60th minute.
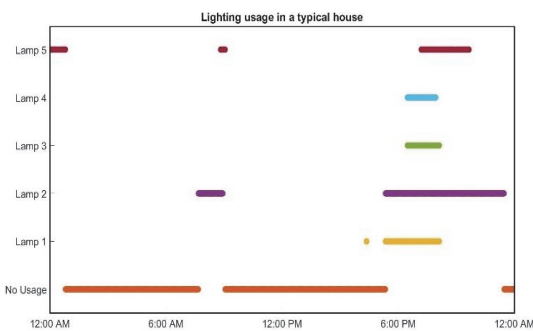
In the residential area, each house may have a different kind of lamp selection. It is probable that initially, residents buy the same lamps or lamps with different power ratings form the same manufacturer. After usage, they replace the broken or old lamps with new lamps of different power ratings from a different manufacturer. Therefore, the power quality
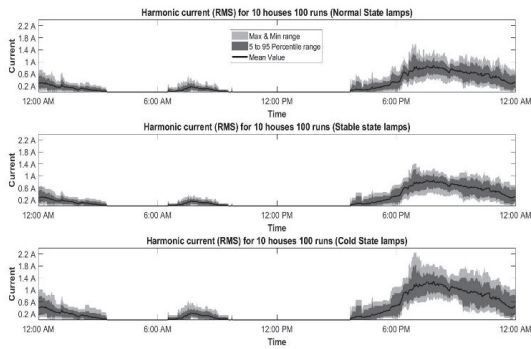
Fig. 5. Mean, 5–95 percentile range for normal, cold, and stable state.

rating could be different when the lamps have the same power rating from the same manufacturer or different power ratings from the same or different manufacturer. The harmonic cancellation effect is more noticeable when different types of lamps are used in combinations. Therefore, we have run the above scenario 100 times. Each time, every house is populated with different types of lamps selected randomly. The total harmonic content added by each house is calculated at the point of common coupling. Subsequently, the combined effect is observed by adding harmonic content generated by all 10 houses. This process is repeated 100 times and means values, 95 percentile values, 5 percentile values, maximum values, and minimum values are calculated for the harmonic content added by the 10 houses for 5 days in 100 different combinations of different lamps selected in each house.

Fig. 5 shows the mean, 5 to 95 percentile, maximum and minimum of total harmonic RMS of 10 houses estimated for 100 different combinations. The bold black line indicates the mean value of total harmonic current RMS of 10 houses. The dark grey band indicates 5 to 95 percentile value range for total harmonic current. The upper light grey area indicates the

maximum values and lower light grey area indicate minimum values of total harmonic current. It is clear from the figure that the difference between a stable state and the normal state is negligible. However, a significant difference between the normal state and cold state is evident from Fig. 5. Although, the RMS difference for each lamp between the cold and stable state on average is less than 5% for odd harmonics. But when a larger picture is considered for many houses, a significant difference is evident between cold state and normal or stable state lamps in terms of total harmonic current. Fig. 6 represents a clearer picture. In the top graph, a comparison between the normal state and stable state lamps is shown for mean values, 5 percentile and 95 percentile values. The results are very close. On the other hand, a significant difference can be observed from the graph of normal state lamps comparison with cold state lamps. Both results are taken after calculating the total harmonic current for 10 houses over 5 days run in 100 different combinations of lighting in each house.

VII. Conclusions

A detailed power quality study for LED lamps is presented in this paper. In section V, measurement results of 16 different LED lamps from different manufacturers and of different ratings were presented. The results indicate the average difference in the harmonic current RMS from 3rd to 13th harmonic between cold state, and stable state was less than 5%. However, the maximum difference was 19% for 9th harmonic and 15.5% for 7th harmonic. For the remaining harmonics, the maximum difference lies in the range of 9.5% to 12.5%. Similarly, the phase angle variation between cold sate and thermally stable state was more significant for higher order harmonics. The average difference for 3rd harmonic is 2.25 degrees but increases to 14 degrees for the 13th harmonic. In section VI, 10 houses were populated randomly with different LED lamps, and the total harmonic current was calculated by using our lighting demand model. The difference between the normal state and stable state lamps was negligible. However,
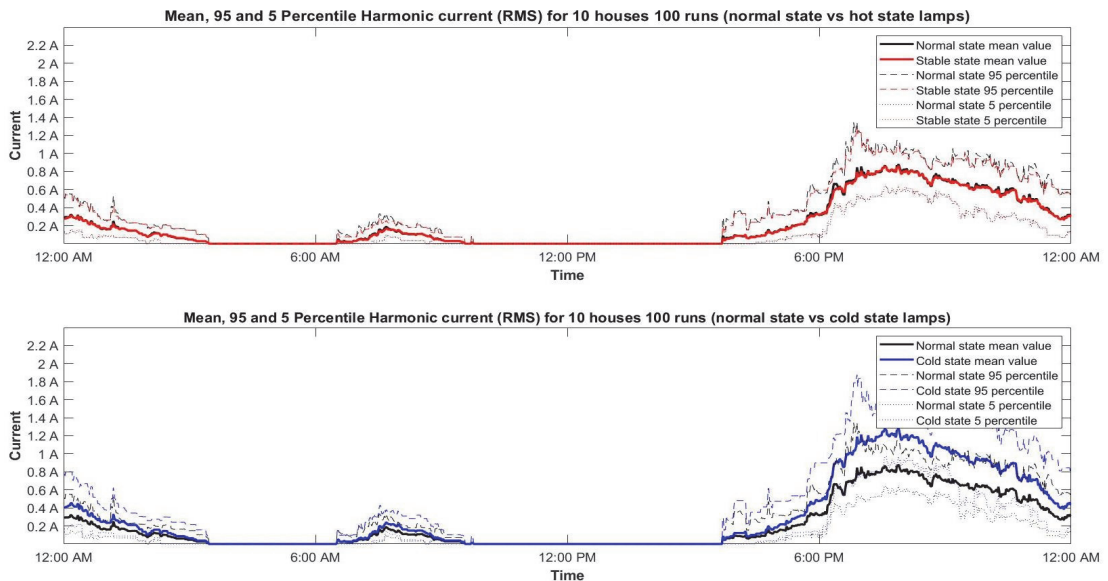

Fig. 6. Total harmonic current difference between the normal state and the stable/cold state in real time scenario.

there was a significant difference when cold state results are compared with normal sate. It could be concluded that individual LED lamp power quality measurement should be carried out when the lamps become thermally stable. However, if the measurement is taken for longer runs in the real-time scenario of a residential building, the results are not much different. Therefore, we can use the normal value of power quality measurement.

REFERENCES

[1] J. Trifunovic, J. Mikulovic, Z. Djurisic, M. Djuric, and M. Kostic, "Reductions in electricity consumption and power demand in case of the mass use of compact fluorescent lamps," Energy, 2009.

[2] M. Bladh and H. Krantz, "Towards a bright future? Household use of electric light: A microlevel study," Energy Policy, 2008.

[3] European Commission, "Regulation EU 1194/2012 - implementing Directive 2009/125/EC of the European Parliament and of the Council with regard to ecodesign requirements for directional lamps, light emitting diode lamps and related equipment," no. 3, pp. 1–22, 2012.

[4] "Guidelines accompanying Regulation (EU) No 874/2012 with regard to the energy labelling of lighting products, and Regulations (EC/EU) No 244 & 245/2009 and 1194/2012 with regard to ecodesign requirements for lighting products – July 2015."

[5] N. Khan and N. Abas, "Comparative study of energy saving light sources," Renewable and Sustainable Energy Reviews. 2011.

[6] A. Nardelli, E. Deuschle, L. D. de Azevedo, J. L. N. Pessoa, and E. Ghisi, "Assessment of Light Emitting Diodes technology for general lighting: A critical review," Renewable and Sustainable Energy Reviews. 2017.

[7] M. M. Aman, G. B. Jasmon, H. Mokhlis, and A. H. A. Bakar, "Analysis of the performance of domestic lighting lamps," Energy Policy, 2013.

[8] E. J. Brunner, P. S. Ford, M. A. McNulty, and M. A. Thayer, "Compact fluorescent lighting and residential natural gas consumption: Testing for interactive effects," Energy Policy, 2010.

[9] N. Chen and H. S. H. Chung, "A driving technology for retrofit LED lamp for fluorescent lighting fixtures with electronic ballasts," IEEE Trans. Power Electron., 2011.

[10] F. K. Yam and Z. Hassan, "Innovative advances in LED technology," Microelectronics J., 2005.

[11] H. Fengze, Y. Daoguo, and Z. Guoqi, "Thermal analysis of LED lighting system with different fin heat sinks," J. Semicond., vol. 32, no. 1, p. 14006, 2011.

[12] A. Dolara and S. Leva, "Power quality and harmonic analysis of end user devices," Energies, 2012.

[13] S. Uddin, H. Shareef, and A. Mohamed, "Power quality performance of energy-efficient low-wattage LED lamps," Meas. J. Int. Meas. Confer., 2013.

[14] A. Gil-de-Castro, S. K. Rönnberg, and M. H. J. Bollen, "Light intensity variation (flicker) and harmonic emission related to LED lamps," Electr. Power Syst. Res., 2017.

[15] S. Uddin, H. Shareef, A. Mohamed, and M. A. Hannan, "An analysis of harmonics from dimmable LED lamps," in 2012 IEEE International Power Engineering and Optimization Conference, PEOCO 2012 – Conference Proceedings, 2012.

[16] A. Gil-De-Castro, A. Moreno-Munoz, A. Larsson, J. J. G. De La Rosa, and M. H. J. Bollen, "LED street lighting: A power quality comparison among street light technologies," Light. Res. Technol., 2013.

[17] M. N. Iqbal and L. Kütt, "End-user electricity consumption modelling for power quality analysis in residential building," 2018.

[18] M. N. Iqbal, L. Kutt, and A. Rosin, "Complexities associated with modeling of residential electricity consumption," 2018 IEEE 59th Int. Sci. Conf. Power Electr. Eng. Riga Tech. Univ., pp. 1–6, Nov. 2018.

[19] M. N. Iqbal, L. Kutt, and N. Shabbir, "Modeling of lighting load in residential buildings," International Journal of Engineering and Advanced Technology (IJEAT), ISSN: 2249 − 8958, Volume-8, Issue-2S, pp. 232–236, 2018.

Publication IV

Jarkovoi, M.; Iqbal, M. N.; Kütt, L. (2019). Analysis of harmonic current stability and summation of LED lamps. 2019 Electric Power Quality and Supply Reliability Conference & 2019 Symposium on Electrical Engineering and Mechatronics: 2019 Electric Power Quality and Supply Reliability Conference, June 12 to 14, 2019 in Kärdla, Hiiumaa Island of Estonia. IEEE, 1–8.

Analysis of Harmonic Current Stability and Summation of LED Lamps

Marek Jarkovoi, M Naveed Iqbal, Lauri Kütt
Department of Electrical Power Engineering and Mechatronics
Tallinn University of Technology (TalTech)
Tallinn, Estonia
marek.jarkovoi@taltech.ee, miqbal@taltech.ee, lauri.kutt@taltech.ee

Abstract—**Harmonic load currents in distribution networks are to be closely observed, in particular, when connecting high number of non-linear loads and/or other sources to the grid. In order to accurately assess and estimate their impact on the network, it is essential to determine how the harmonic currents behave when various loads are connected to the point of common coupling (PCC). This paper presents an overview and variance of the harmonic currents of LED lamps and the harmonic current summation uncertainty when calculating resulting currents when estimating resulting harmonic currents.**

Keywords—power quality, harmonic currents, harmonic distortion, harmonic analysis, harmonic phasors, current measurement, LED lamps

I. Introduction

For the year 2030, there are energy efficiency targets set, for example by the EU, to have overall improvements by at least 32% compared to the year 1990 [1]. One aspect to achieve this is by using specialized power supply units, which convert the distribution network voltage to the desired parameters using power electronic circuitry with highest efficiency even for small-power loads. These units would provide a contribution to the harmonic currents in the network. Since energy efficiency is becoming a more central topic in residential households, and with the requirements of nearly net-zero energy buildings (NZEB) by the European Union directive on energy performance of buildings, it is not surprising that more energy-efficient LED lamps are rapidly replacing traditional incandescent and fluorescent lamps. The popularity and success of LED lighting was foreseen over 15 years ago, whereby we are now seeing ratings proposed in [2], that by 2020, the luminous efficacy will reach 200 lm/W and lifetime will increase to 100 000 hours, while the prices will drop to 2 $/klm.

Since LEDs operate on direct-current (DC), some type of power conversion is required from alternating current (AC) to DC. This means that a typical LED light bulb has a built-in AC/DC power converter, usually a simple rectifier circuit, which draws current with non-sinusoidal waveform form the power supply network. When distorted current is drawn from the power supply distribution network, it may cause additional losses in transformers and due to the impedance of the transformer and long distribution lines, the voltage drop caused by non-sinusoidal current may distort the voltage waveform and introduce harmonics to the supply voltage, which in turn may affect other devices connected to the same network. This primarily affects power quality in low voltage (LV) distribution networks.

A time-invariant non-sinusoidal waveform can be described using harmonic components of the fundamental frequency, also known as Fourier series. Such methods of measurement and harmonic component calculation of voltage

and current can be found in IEC standards 61000-4-30 [3] and 61000-4-7 [4].

One of the parameters that is commonly used to describe distortion extent of a waveform is total harmonic distortion (THD), which is the ratio of the root-mean-square (RMS) value of a set of harmonic components to the fundamental component. However, using only this parameter means that the information about individual harmonics is lost. In addition to the (RMS) values, harmonic components are also described by a phase angle, which is often not reported during power quality surveys. This means that a harmonic component can be described as a rotating vector quantity, a phasor, on a complex plane having real and imaginary components, illustrated in (1). In order to describe a current or voltage waveform precisely, the information about both the RMS values and phase angles are required.

$$\begin{cases} i_h = \sqrt{2}I_h \sin(h\omega t + \theta_{ih}) \\ i_{hx} = Re(i_h) = \sqrt{2}I_h \cos(\theta_{ih}) \\ i_{hy} = Im(i_h) = \sqrt{2}I_h \sin(\theta_{ih}) \end{cases} \quad (1)$$

In theory, if many loads are connected to a PCC they obey Kirchhoff's current law (KCL), which states that, at any point in time, the sum of the currents toward or from a single node is equal to zero. If each load draws current with a non-sinusoidal waveform, according the superposition principle, it should be possible to add up all the harmonic component phasors of all the loads and get a resulting current flowing at the PCC. For example, if two 5th harmonic phasors have a 180-degree phase angle difference, but equal magnitude, sum would be zero. This effect is called harmonic cancellation. When the cancellation conditions are not met, there will be a resulting phasor at the PCC that is the geometric sum of the harmonic current phasors. For example, if the phase angle difference between the phasors would be zero, the result would be double the magnitude with the same phase angle. And if the difference is exactly 45 degrees, then the result will be $\sqrt{2}$ times the magnitude with a phase angle precisely in the middle of the two components.

In a study on harmonic summation [5], data from individual load measurement was used to analyze summation and possible cancellation. The same authors have been using the term "prevailing phasor", which is a resulting phasor due to aggregated harmonic components. The harmonic current prevalence has been closely studied in [6]. The paper presents a methodology to assess prevalence and found that the prevailing harmonic currents largely depend on the consumer configuration types. A study on prevalence has also been performed in [7], which found that low levels of prevalence are an indication of the dynamic nature of multiple non-linear loads.

The possibility of harmonic cancellation has also been studied in [8]. The research showed a slight decrease in THDi when choosing the best combination of loads. A study from [9] analyzed how adding different types of loads can lead to cancellation effect due to the harmonic current spread of the phasors. However, a study from [10] analyzed the statistical distribution of harmonics and phase angles in medium voltage (MV) and LV residential networks and found that there is almost no cancellation present.

Although research has been published on measurement results from various distribution networks, households and products, significantly less discussion can be found on the harmonic summation and cancellation effect itself. While it is expected that the summation of harmonic currents occurs predictably, in real scenarios, due to measurement and calculation limits of the measurement methods and equipment, the actual results may vary from theoretical by some margin. This paper focuses on the harmonic component summation effect of randomly selected LED lamps in controlled laboratory conditions by varying the combinations. The scale, accuracy and deviation of harmonic component summation are measured and compared to theoretically obtained values from single measurements. It is relevant to assess the uncertainty when developing models for non-linear loads at the PCC that may be active at the same time.

II. MEASUREMENT SETUP AND METHODS

The setup for the study consists of a personal computer (PC) with a National Instruments data acquisition (DAQ) module with digital-to-analog arbitrary waveform generation capability, a Chroma 61505 4 kVA programmable power supply used as an amplifier to achieve LV distribution network voltage of 230 V, a 16-load combination array with two-pole double throw relays (DPDT or 2P2T), which are controlled using digital binary signals, and a measurement device A-Eberle PQ-Box 200 which is capable of recording harmonic magnitude and phase angles with a minimum measurement interval of 1 second that are aggregated from internal 200 ms or 10-cycle measurements according to Class-A measurement equipment.

The system was controlled using MATLAB software. The reference waveforms were generated with a sampling frequency of 100 kHz, which equates to 2000 samples per single 50 Hz cycle. The software also controlled the load relays to achieve different load combinations that were supplied by the amplified waveforms. Ideal 50 Hz sine waveform with an RMS value of 230 V was selected for the test.

16 randomly selected LED lamps found on the market in the year 2018 were used as loads. The power rating ranged from 7 W to 13 W with luminous flux between 500 lm and 1521 lm. Since there are 2^{16} or 65536 load permutations using 16 different LED lamps, specific patterns were chosen to reduce the number of combinations and duration of testing. A running group of consecutive lamps was powered by the amplified waveform at the same time with a grouping of 1 to 16 lamps. That means, for example, with a three-lamp grouping, loads number 1, 2, 3 were powered at first, then 2, 3, 4, then 3, 4, 5, and so on. This produced a total of 137 combination per waveform, including a combination where all lamps were off to measure voltage stability. Each combination was run for one minute, which means that using 1-second measurement intervals there were 60 values per combination. The first and last values were ignored because of time uncertainty of switching of the relays. For stability and

reproducibility, the first 10 seconds were also ignored due to any possible settling time caused by relay switching discontinuity. This setup and method resulted in about 50 stable values per one load combination.

Since it was previously found that LED lamps have a warm-up period, all lamps were powered for at least 60 minutes before the start of the test. The amplifier was also running for at least 30 minutes before testing to achieve its working temperature. To keep the LED lamps at working temperature, the continuous running was achieved using the double-throw relays which provided power to the lamps from the power outlet in the laboratory when the relays were unengaged. When relays were engaged, both phase and neutral line were routed to the amplifier circuit. The complete overview of the setup is presented in Fig. 1.
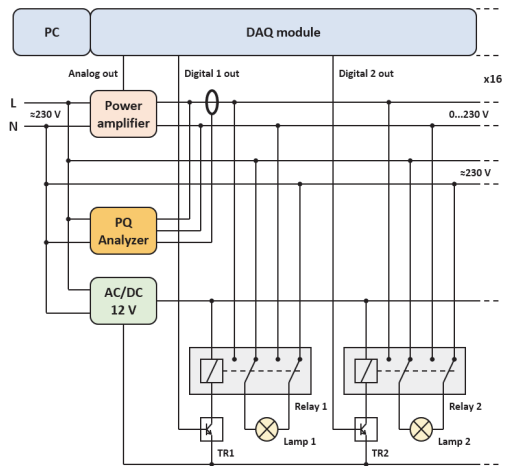

Fig. 1. Measurement setup diagram.

For each combination, the harmonic currents and their phase angles were recorded for every 1-second measurement interval. The phase angles of harmonic currents that are presented in this paper are always related to the fundamental voltage component.

From the measurement data of each combination, the RMS mean values, standard deviation (SD) and coefficient of variation (CV) were calculated according to (2), including the 1st order, or fundamental component. Mean and SD of the phase angles were also calculated. The wrapping of the phase angle around 180 degrees was taken into consideration.

$$\begin{cases} I_h = \frac{1}{N}\sum_{n=1}^{N} I_{h,n} \\ \varphi_h = \frac{1}{N}\sum_{n=1}^{N} \varphi_{h,n} \\ SD_{I,h} = \sqrt{\frac{1}{N}\sum_{n=1}^{N}\left(I_{h,n} - I_h\right)^2} \\ SD_{\varphi,h} = \sqrt{\frac{1}{N}\sum_{n=1}^{N}\left(\varphi_{h,n} - \varphi_h\right)^2} \\ CV_{Ih} = \frac{SD_{I,h}}{I_h} \end{cases} \quad (2)$$

Since harmonic components are essentially phasors, just the RMS and phase angle data separately might not provide enough information about its dispersion. To assess the actual spread or dispersion of the phasors, the RMS and phase angle data was converted to real (x) and imaginary (y) complex counterparts using the following formula:

$$\begin{cases} I_{h,x} = \sqrt{2}I_h \cos(\varphi_h) \\ I_{h,y} = \sqrt{2}I_h \sin(\varphi_h) \\ I_{h,xy} = \sqrt{I_{h,x}^2 + I_{h,y}^2} = \sqrt{2}I_h \end{cases} \quad (3)$$

From real and imaginary orthogonal components $SD_{I,h,x}$ and $SD_{I,h,y}$ the spatial harmonic current standard deviation $SD_{I,h,xy}$ values are calculated for the complex plane. The resulting $SD_{I,h,xy}$ shows the possible dispersion or "spread" from the mean harmonic phasor value $\underline{I}_{h,xy}$. Since spatial deviation is related to phasors, it is compared to the amplitude of the phasor, instead of RMS value, to obtain spatial coefficient of variation. It could also be viewed as a probability circle, which includes at least 95% of the measured values. The spatial CV for $\underline{I}_{h,xy}$ is calculated using the following formulas:

$$\begin{cases} I_{h,x} = \frac{1}{N}\sum_{n=1}^{N} I_{h,x,n} \\ I_{h,y} = \frac{1}{N}\sum_{n=1}^{N} I_{h,y,n} \\ SD_{I,h,x} = \sqrt{\frac{1}{N}\sum_{n=1}^{N}(I_{h,x,n} - I_{h,x})^2} \\ SD_{I,h,y} = \sqrt{\frac{1}{N}\sum_{n=1}^{N}(I_{h,y,n} - I_{h,y})^2} \\ SD_{I,h,xy} = \sqrt{SD_{I,h,x}^2 + SD_{I,h,y}^2} \\ CV_{I,h,xy} = \frac{SD_{I,h,xy}}{I_{h,xy}} \end{cases} \quad (4)$$

To assess the harmonic summation accuracy, for each combination, the respective individual harmonic phasors from single-unit measurement data were summed to obtain the resulting harmonic current, including magnitude and phase angle. The calculated harmonic phasors were compared to the phasor data obtained from real measurement of the respective combination by assessing the difference of the mean values for magnitude and phase angle and the absolute spatial difference between the two phasors.

Due to the measurement limit of the current clamps used in the setup, the minimum measurable harmonic current RMS value with phase angle data was 1 mA. If the harmonic current was below this value, the measurement data was ignored and not used in the summation algorithm. If the load combination had at least one single unit with an unmeasurable harmonic component, then the harmonic summation was flagged and excluded from the statistical analysis. DC component was also not measured because of the inductive current clamp type.
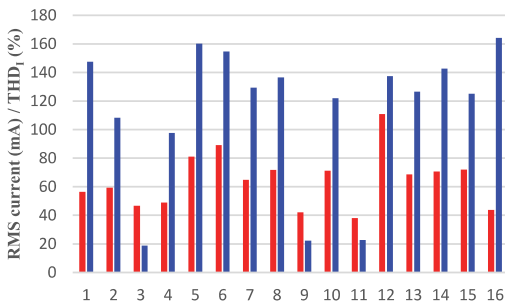
III. HARMONIC CURRENT VARIATION

For all 16 lamps the measured RMS current and total harmonic current distortion (THD$_I$) are presented in Fig. 2. The measured current was in the range of 40 mA to 110 mA. Harmonic distortion can be separated into two groups: the first group had a THD$_I$ in the range of 100% to 160% and the second group around 20%. This kind of low harmonic content is most probably due to the presence of a power factor correction (PFC) circuit.

Fig. 3 shows the harmonic current component distribution relative to the fundamental in percent for all 16 LED lamps, where each line represents the harmonic content of a single lamp. Almost all 16 lamps follow a similar pattern: harmonics drop almost linearly from 80–90% for 3rd order to 20–30% for the 13th order. The higher harmonic orders are between 10 and 25% up to 19th. However, a few lamps have a noticeably smaller harmonic contribution: Around 20% for the 3rd order, 5–15% for the 5th and below 10% up to 11th order. From 13th order up to 19th the levels were at unmeasurable levels. These are the laps that that possibly had PFC.

The results of 137 LED lamp combinations are shown separately in Fig. 4 and Fig. 5. The CV of the harmonic current RMS values is presented in percent with respect to the measured mean values. Each point represents measurement result from one combination. The continuous line represents the mean value of all combinations and the dashed lines represent the 5 and 95 percentile values respectively. This data representation is used in all the following data plots. The variation of the harmonic RMS current component is increasing with the harmonic order, with 19th harmonic CV reaching around 6% with a few exceptions ranging between 12% to 19%. The variation of harmonics up to 11th order with CV under 1%. Mean values from the combinations reach 0.4% for 11th and 2% for 19th harmonic order.

Since at higher harmonic orders, the measured harmonic currents were minimal, variation was expected to be large due to the measurement limits. To put the values into perspective, Fig. 6 shows the SD of the harmonic current RMS values relative to the mean fundamental component. The relative variations are very small, being up to 0.1% until 9th harmonic order and reaching only 0.2% for 19th order. The mean values are only up to 0.07%. This means that although the higher order harmonic current components have quite high variation themselves, the magnitude variation compared to the fundamental component is very small. If, for example, most lamps had the 19th harmonic content between 10% and 20%, then the deviation of 0.1% is marginal.

Fig. 2. RMS current (red) and THD$_I$ (blue) for all lamps used in the testing.
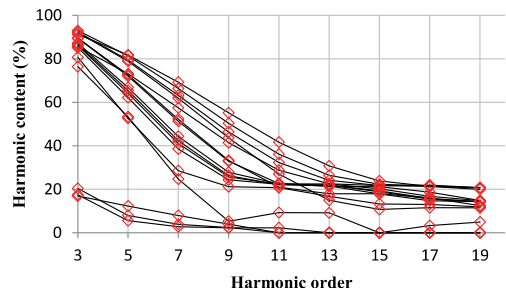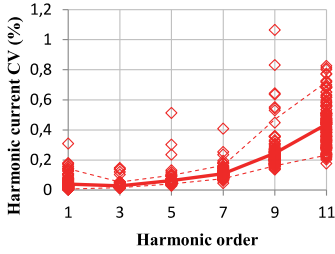
Fig. 3. Harmonic content of 16 LED lamps.

Fig. 4. Coefficient of variation of low-order harmonic current magnitude.
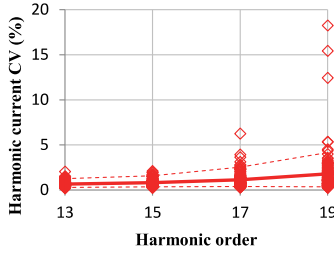

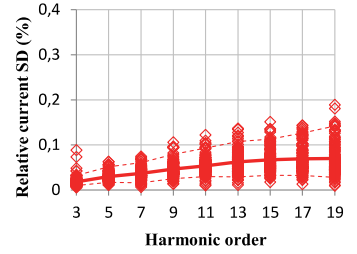Fig. 5. Coefficient of variation of high-order harmonic current magnitude.

Fig. 6. Relative standard deviation of harmonic current magnitude compared to the fundamental component.

The SD of the harmonic current phase angles is presented as degrees in Fig. 7 and Fig. 8. The phase angles follow a similar pattern as the magnitude values. The deviation of the harmonic component phase angles increases with the harmonic order, having SD mostly under 4 degrees, but also with a few exceptions ranging between 7 and 9 degrees. Up to 11th harmonic order, the phase angle SD was under 1 degree. The maximum mean value for phase angle deviation is up to 0.2% for low-order harmonics and up to 1% for high-order harmonics.

The spatial variation results from the spatial phasor spread data are presented in Fig. 9 and Fig. 10. Compared to the results obtained from the RMS data alone, the deviation is more significant, which is expected, as the phase angle variance is inclusive in the spatial data. Up to 11th harmonic order, the spatial variation reaches 1.2% and higher harmonics reach 5–10% with a few exceptions over 20% for 19th harmonic order. The mean spatial CV is quite low: only about 0.5% for low-order harmonics and below 3% for high-order harmonics.

As with harmonic current magnitude values, a relative comparison has also been made for spatial data. The relative spatial standard deviation of harmonic current compared to the fundamental component amplitude is presented in Fig. 11. The relative spatial deviation is below 0.25% for all harmonics with a mean of only 0.1%.

While both magnitude and phase information are useful for describing phasor changes, the spatial phasor deviation can be used to estimate the multi-dimensional probability distribution of the phasors. Depending on the load type, it should be possible to estimate where each harmonic component phasor would be located on the complex plane with given uncertainty and determine the most probable corresponding magnitude and phase angle from the results. However, since the spread directionality is not known, looking at magnitude and phase deviation helps to determine if the phasor tends to rotate, change in magnitude, or both.
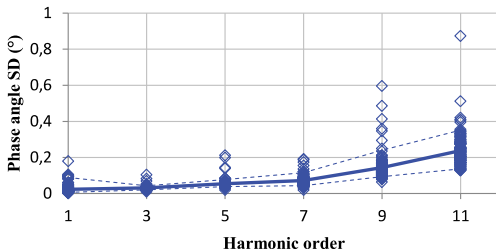

Fig. 7. Standard deviation of low-order harmonic current phase angles.
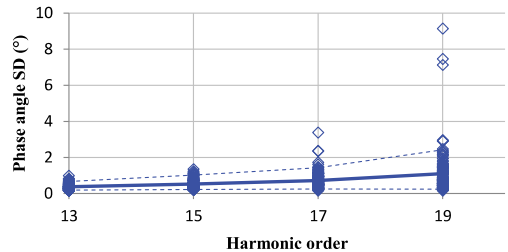

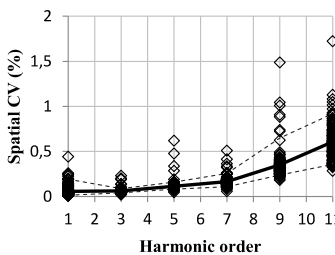Fig. 8. Standard deviation of high-order harmonic current phase angles.

Fig. 9. Coefficient of variation of low-order harmonic current real (red); imaginary (blue) and complex (black) values.
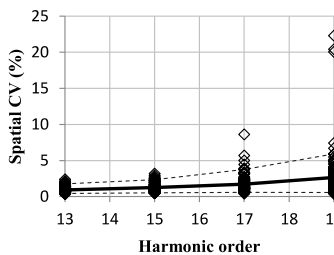

Fig. 10. Coefficient of variation of high-order harmonic current real (red); imaginary (blue) and complex (black) values.
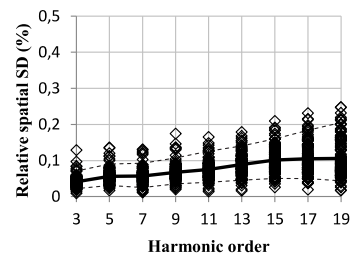

Fig. 11. Spatial relative standard deviation of harmonic current phasors compared to the fundamental component.
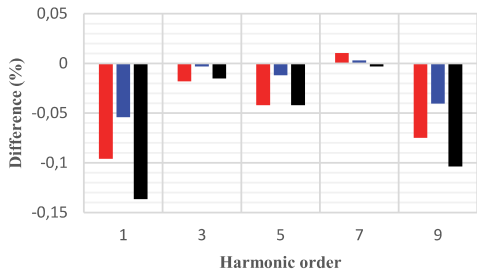
Fig. 12. Difference of low-order harmonic current CV (red), phase angle SD (blue) and spatial phasor CV (black) between single and maximum number of lamps from linear regression in relation to the number of lamps in combination
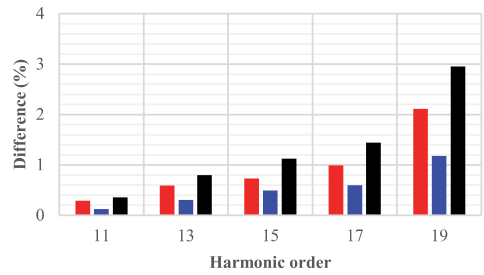
Fig. 13. Difference of high-order harmonic current CV (red), phase angle SD (blue) and spatial phasor CV (black) between single and maximum number of lamps from linear regression in relation to the number of lamps in combination.

To analyze how the number of lamps in a combination affects the harmonic current variation parameters, a linear regression, or trend, was composed and evaluated in relation to the number of lamps in a single combination. The difference of harmonic current CV, phase angle SD and spatial phasor variation from the regression between single and maximum number of lamps is presented in Fig. 12 and Fig. 13.

For low-order harmonics, the differences for harmonic current CV, phase angle SD and spatial CV are very minimal and slightly tend to decrease as the number of lamps increases. For high-order harmonics, the differences are more visible and the higher the harmonic order, the more strongly the harmonic current variation parameters depend on the number of lamps in a combination. The difference in average harmonic current CV is over 2% for the 19th harmonic, and the difference in average phase angle SD is just over 1 degree, but the average spatial phasor variation reaches 3%. This means that there is a relationship between the number of lamps and the variability

of the harmonic current for harmonic orders 11th and up. This uncertainty should be considered when estimating harmonic currents using mathematical summation of load models.

Fig. 14 shows an overview of relative harmonic current SD compared to the fundamental component for all measured harmonics and combinations. As in the statistical analysis, the variation compared to the fundamental is very small, being less than 0.2% even for high-order harmonics.

A few examples of various types of harmonic current spatial distribution on a complex plane are presented in Fig. 15, Fig. 16, and Fig. 17. Each point represents a single 1-second measurement result for a specific harmonic current phasor. The red ellipse is constructed from real and imaginary axis standard distributions $SD_{I,h,x}$ and $SD_{I,h,y}$ with the central line showing the prevailing phase angle direction. The blue circle is the spatial standard deviation $SD_{I,h,xy}$, which includes at least 95% of the measurement samples.
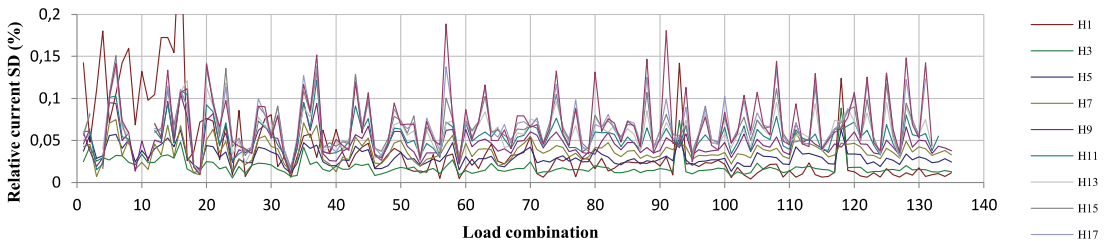

Fig. 14. Relative standard deviation of harmonic current to the fundamental component for all load combinations.
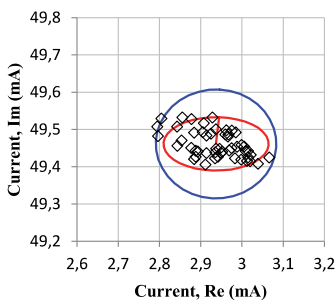

Fig. 15. Spatial spread example of harmonic current with phase variation (h5, L5).
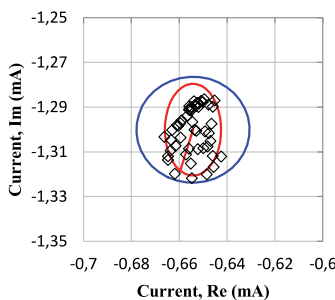
Fig. 16. Spatial spread example of harmonic current with magnitude variation (h11, L4).
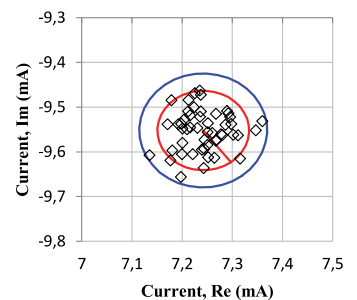
Fig. 17. Spatial spread example of harmonic current with even spatial variation (h15, L15).

Harm. order	Number of lamps in combination																
	1	*2*	*3*	*4*	*5*	*6*	*7*	*8*	*9*	*10*	*11*	*12*	*13*	*14*	*15*	*16*	*Total*
1	16	15	14	13	12	11	10	9	8	7	6	5	4	3	2	1	**120**
3	16	15	14	13	12	11	10	9	8	7	6	5	4	3	2	1	**120**
5	16	15	14	13	12	11	10	9	8	7	6	5	4	3	2	1	**120**
7	16	15	14	13	12	11	10	9	8	7	6	5	4	3	2	1	**120**
9	16	15	14	13	12	11	10	9	8	7	6	5	4	3	2	1	**120**
11	14	11	9	7	5	3	2	1	–	–	–	–	–	–	–	–	**38**
13	13	9	6	4	2	–	–	–	–	–	–	–	–	–	–	–	**21**
15	12	8	5	3	1	–	–	–	–	–	–	–	–	–	–	–	**17**
17	13	9	6	4	2	–	–	–	–	–	–	–	–	–	–	–	**21**
19	13	9	6	4	2	–	–	–	–	–	–	–	–	–	–	–	**21**

IV. HARMONIC CURRENT SUMMATION

The calculated sum of harmonic currents for all usable combinations was compared to the actual measurement data with the corresponding load combination. The resulting difference between mean magnitudes is presented in percent and difference between mean phase angles in degrees. It should be noted that the number of data points for higher-order harmonics is reduced due to the exclusion of data which would have otherwise included individual harmonic current data that was at unmeasurable levels. Only those harmonic current combinations were used that had all the individual harmonic currents successfully recorded in a combination. The summary of data used in this paper is presented in Table I. Due to this exclusion, from 11th harmonic order, there is little to none combination data available for over 6 lamps in a combination.

To assess the statistical phasor accuracy of the summation in general, looking at the magnitude and phase angle separately does not provide adequate comparison as the result will depend on the initial phasor angle itself. The spatial phasor difference is obtained by calculating the distance between calculated and measured phasors. The diagram for determining the magnitude, phase and spatial phasor difference is shown in Fig. 18.
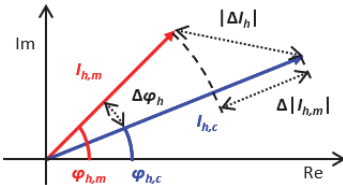

Fig. 18. Diagram for determining the magnitude ($\Delta|I_h|$), phase angle ($\Delta\varphi_h$) and phasor ($|\Delta I_h|$) difference between measured (red) and calculated (blue) values.

Fig. 19 and Fig. 22 present the resulting relative magnitude difference for the combinations. For low-order harmonics, the difference has 9- to 95-percentile values between ±2.5% and +0.5% with a slight tendency to underestimate the magnitude by up to +1%. For high-order harmonics, the difference is in range of –5% and +2.5% with a tendency to underestimate the magnitude by almost +2%. A few exceptions have a magnitude difference of around +10%.

The results for the harmonic phase angles are presented in Fig. 20 and Fig. 23. For low-order harmonics, the difference is between –0.5 and +2 degrees, with 9th harmonic order having the largest difference. The mean phase angle difference is very low, about +0.5 degrees. For high-order harmonics, the difference increases up to 0 to +3 degrees, with a few exceptions at –2 and +7 degrees. The mean calculated phase angle difference tends to be rotated up to +2 degrees in the positive direction.

The phasor difference between calculated and measured harmonic currents are presented in Fig. 21 and Fig. 24. For low-order harmonics, the mean difference is below 1.5%, while the maximum is around 4%. For high-order harmonics, the mean difference reaches 4% for 19th harmonic with maximum values of around 6%. Only two combinations had a difference of about 12% for 17th harmonic order and 16%.

The calculated total current RMS and THD values were also compared to the measured data for different number of lamps in a combination, as shown in Fig. 27. The RMS difference remains very small, between –0.2% and +0.4%. As for the THD$_I$, the difference increases visibly with number of lamps up to –1% for 16 lamps. This means that as the number of loads used in summation increases, the THD$_I$ has a probability of being underestimated. Since higher-order harmonics are at very low levels compared to the fundamental, they do not have a significant impact on the current RMS.
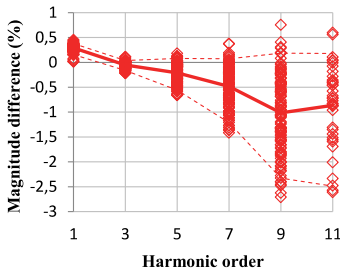

Fig. 19. Relative magnitude difference for low-order harmonic current.
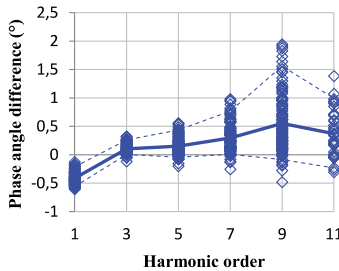

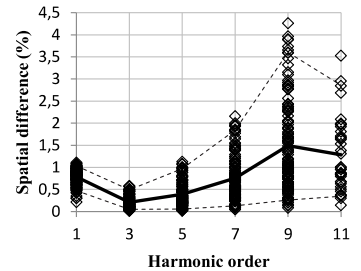Fig. 20. Phase angle difference for low-order harmonic current.

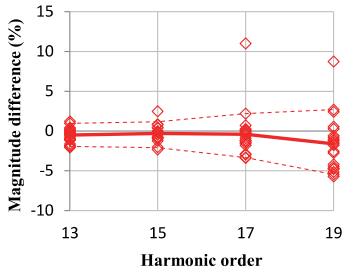Fig. 21. Phasor difference for low-order harmonic current.

Fig. 22. Relative magnitude difference for high-order harmonic current.
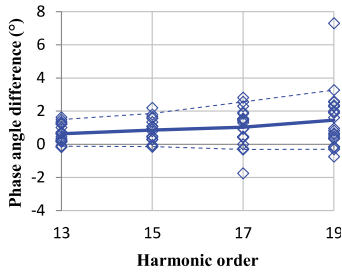
Fig. 23. Phase angle difference for high-order harmonic current.
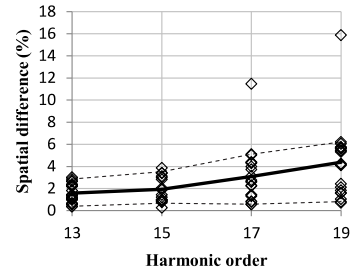
Fig. 24. Phasor difference for high-order harmonic current.

Fig. 25. Harmonic current content for 3rd to 11th harmonic order in relation to the number of lamps in a combination.

Fig. 26. Harmonic current content for 13rd to 19th harmonic order in relation to the number of lamps in a combination.

Fig. 27. Total current RMS and THD$_I$ difference depending on the number of lamps in a combination.

Fig. 28. Measured (red) and calculated (blue) THD$_I$ depending on the number of lamps in a combination.

V. Harmonic Cancellation

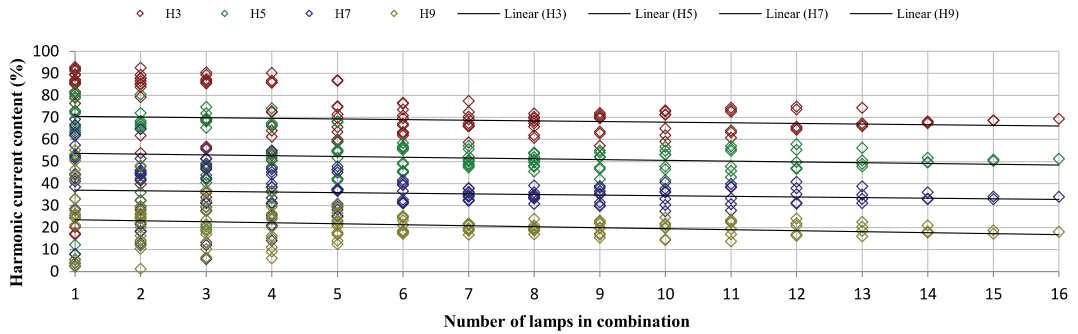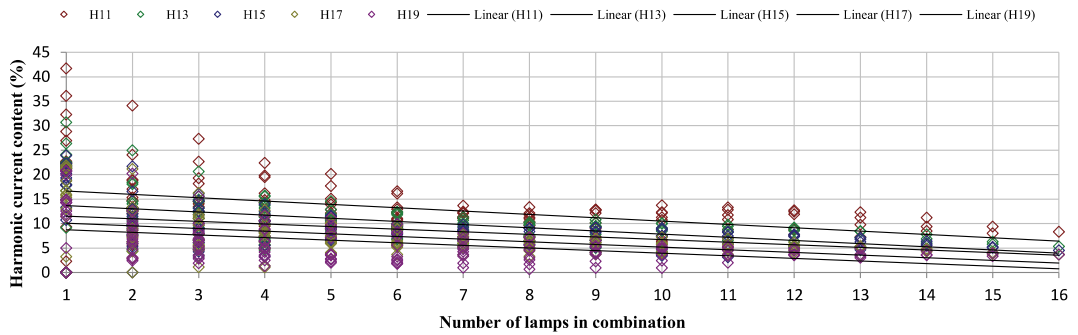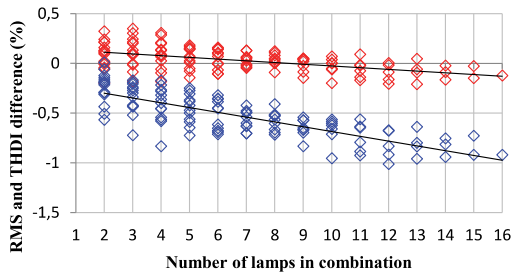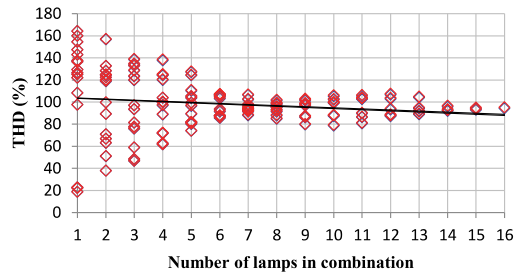In addition to the assessment of stability and summation accuracy, the harmonic cancellation effect has also been briefly investigated.

Fig. 25 and Fig. 26 show the harmonic current content in % relative to the fundamental component for each number of lamps in a combination. For lower-order harmonics, as the number of lamps increases, the individual harmonic current components tend to average out, and the average harmonic levels are reduced, as can be seen from the linear regression lines. The average reduction of harmonic content for 16 lamps is only about 6.7% for 9th order compared to single lamp results. For lower order harmonics, the reduction is only around 4–5. For high-order harmonics, a more visible drop in harmonic content can be clearly distinguished from the measurement results. The average reduction is between 8 and 10%. This means that the low-order harmonic currents have high directivity and harmonic phasors are aligned in a similar direction on the complex plane. As for high-order harmonic currents, phasors tend to be more spread out on the complex plane, thus resulting in a possible cancellation effect.

The THD_I for each number of lamps in combinations is presented in Fig. 28 and compared to the calculated values from single-unit measurement results. As with the individual harmonics, the values tend to average out as the number of lamps in combination increases. The average reduction of the THD_I is 14.7% for measured results and 15.5% for calculated results. This 1% difference is in line with the harmonic summation results from the previous chapter.

Conclusions

The measurement setup and methods described in this paper provide an adequate overview of the harmonic current stability and assessment of the harmonic summation accuracy. The measurement results and specific conclusions are based on 16-LED lamp study and may or may not apply to other types of loads. Odd harmonics only up to 19th were considered for the study.

For each harmonic current, it is possible to determine the coefficient of variation of harmonic magnitude, the standard deviation of phase angle and the spatial deviation or spread of harmonic phasor on the complex plane. For stable loads like LED lamps, especially when previously warmed up to the thermal stability, the spatial variations compared to the fundamental component almost negligible. But individual harmonics can achieve a variation of 5–10% for higher harmonics and in rare cases, even 20%, but this might be because of the low levels. Looking at harmonic current magnitude and phase angle variation separately might provide a more simplified overview, but the information about the spatial spread is not considered.

Relationship between harmonic current variation and number of lamps has been observed for higher-order harmonics. As the number of simultaneously connected loads increases, the average variation of harmonic current also increases by some margin. Low-order harmonic currents below 11th do not seem to be affected by the number of loads. The number of lamps also does not seem to affect the relative deviation compared to the harmonic current fundamental.

The harmonic current summation accuracy and comparison for various possible combinations of LED lamps between calculated and measured results has also been studied. The data and thorough analysis were somewhat limited due to some high-order harmonic current levels of several being at unmeasurable using the described measurement setup. As a result, it was not possible to use them in the summation calculation and the affected combinations had to be excluded from statistical analysis.

Despite the limited number of combinations, it was found that the difference for higher-order harmonics is more significant and varies more combination by combination. The harmonic current magnitude could be underestimated by up to 2.5% and 5% and the phase angle difference was up to 2 and 3 degrees for low-order and high-order harmonics, respectively. The spatial difference for harmonic currents, which incorporates both magnitude and phase by using phasors, was up to 4% for low-order harmonics, with 9th harmonic being the most inaccurate and up to 6% for high-order harmonics. Although the estimated total current RMS was accurate, there was a difference of −1% when estimating THD_I.

Harmonic cancellation effect was also briefly examined, and a clear relationship had been found between the extent of cancellation and harmonic order and lamp number. Since high-order harmonics have more phasor spread from device to device on the complex plane, it means that the resulting harmonic current will be less because of summation. Average reduction up to 10% was observed. Due to the harmonic cancellation of the high-order harmonics, an average decrease of about 15% for THD_I was observed. Low-order harmonic current phasors from devices are more grouped together and thus do not experience cancellation.

References

[1] European Commission, "A policy framework for climate and energy in the period from 2020 to 2030," 2014.

[2] J. M. Gee, J. Y. Tsao, and J. A. Simmons, "Prospects for LED lighting," in Third International Conference on Solid State Lighting, 2004.

[3] Electromagnetic compatibility (EMC) - Part 4-30: Testing and measurement techniques - Power quality measurement methods. IEC 61000-4-30:2015, 2017.

[4] Electromagnetic compatibility (EMC) - Part 4-7: Testing and measurement techniques - General guide on harmonics and interharmonics measurements and instrumentation, for power supply systems and equipment connected thereto. IEC 61000-4-7:2002, 2009.

[5] J. Meyer, P. Schenger, and K. Heidenreich, "Harmonic summation effects of modern lamp technologies and small electronic household equipment," in 21st International Conference on Electricity Distribution (CIRED), 2011.

[6] J. Meyer, A. M. Blanco, M. Domagk, and P. Schegner, "Assessment of prevailing harmonic current emission in public low-voltage networks," IEEE Trans. Power Deliv., 2017.

[7] B. Peterson, J. Rens, and J. Desmet, "Harmonic emission assessment on a distribution network: the opportunity for the prevailing angle in harmonic phasors," CIRED – Open Access Proc. J., 2017.

[8] A. Abd El-Mageed Elhenawy, M. Mohamed Sayed, and M. Ibrahim Gilany, "Harmonic cancellation in residential buildings," in 2018 20th International Middle East Power Systems Conference, MEPCON 2018 – Proceedings, 2019.

[9] A. Gil-De-Castro, S. K. Rönnberg, M. H. J. Bollen, and A. Moreno-Muñoz, "Harmonic phase angles for a domestic customer with different types of lighting," Int. Trans. Electr. Energy Syst., 2015.

[10] Y. Wang, J. Yong, Y. Sun, W. Xu, and D. Wong, "Characteristics of harmonic distortions in residential distribution systems," IEEE Trans. Power Deliv., 2017.

Probabilistic bivariate modelling of harmonic current

Marek Jarkovoi, Lauri Kütt, M Naveed Iqbal
Department of Electrical Power Engineering and Mechatronics
Tallinn University of Technology
Tallinn, Estonia

Abstract—Modeling modern non-linear loads with varying current poses a significant challenge. While the traditional numeric models provide an adequate representation of stable loads, when a device or a group of devices operate at different modes with varying harmonic currents, a statistical approach is more practical. This paper provides an overview of probabilistic modeling methods for harmonic currents and presents a novel method for empirical nonparametric harmonic current modeling.

Index Terms—current measurement; gaussian mixture model; power system harmonics; probability density function; probability distribution

I. Introduction

As the share and complexity of non-linear loads connected to the public network is rapidly increasing, it is becoming more challenging to model the load currents. Since non-linear loads exhibit significant harmonic current distortion, one of the most practical ways is to decompose the load current into its harmonic components and model the harmonic content individually. During the early years of non-linear load growth, mostly the harmonic current magnitude was considered. However, it is now evident that the harmonic phase angles have a substantial impact on the harmonic summation and estimation where possible cancellation can occur due to load and harmonic current diversity [1], [2].

A modern household device can also exhibit different states of operation, e.g., a variable load, which means the current, even at a constant voltage, will vary due to the supply circuit topology and operation, control processes and various algorithms. This kind of variation cannot be easily modeled with simple electrical parametric models. Even probabilistic models can run into difficulties, depending on the scope and characteristics of the harmonic current variation. The accuracy of any model also depends on where it is applied. For example, modeling a single device can produce different results than a group of devices, point of common coupling (PCC), or a feeder in a distribution network.

Several types of models have been proposed in the literature for modeling harmonic loads. This paper presents an overview of common load harmonic current modeling methods, including their benefits and drawbacks, and analysis of several parametric and nonparametric probabilistic approaches.

The paper also proposes a novel nonparametric method for bivariate harmonic current modeling. The probabilistic model describes the harmonic current with sufficient accuracy while maintaining low data usage and high simulation speed, even with various types of variation characteristics.

II. Deterministic harmonic load models

Among various proposed deterministic harmonic load models, several types have been mainly described and used [3].

A. Constant current source

The simplest harmonic model is a constant current source model (CCS), which represents a harmonic current as a quantity having a constant magnitude and phase. The current for each harmonic order is independent of the input voltage and does not vary in time. This model can be used if the load is stable and is insensitive to any external parameters.

B. Norton model

A more detailed model is the Norton model. For each harmonic order, in addition to the harmonic current source, the model includes a parallel impedance. The model presents a relationship between voltage and current harmonics, which can be used to model the harmonics in conjunction with the network voltage distortions. However, this approach assumes the superposition of the harmonics and ignores the possibility of cross-dependency.

C. Crossed-frequency admittance matrix

One of the most detailed deterministic models of a harmonic load is the crossed-frequency admittance matrix (CFA) model. It was proposed in [4] and [5], although, slightly modified versions exist [6]–[8]. The CFA model consists of a complex admittance matrix, which considers interactions between voltage and current harmonics of different orders. For example, a 3rd order voltage harmonic can affect 3rd harmonic current, but also 5th harmonic current at the same time.

D. Harmonic coupled Norton equivalent model

By combining the CFA and Norton model, it was later developed into Harmonic Coupled Norton Equivalent (HCNE) model [9]–[11]. This approach increased accuracy and reduced errors for harmonic load modeling by defining harmonic coupling around a set Norton point.

III. PROBABILISTIC APPROACHES

Deterministic models are capable of modeling static loads that do not exhibit variations in load current depending on factors like time, operating modes, usage cycling, etc. When these variations are present, a probabilistic approach should be considered. The most direct way to construct a model is based on the empirical data, e.g. measurement results. Both harmonic current magnitudes and phase angles should be measured to produce meaningful models. The probabilistic approach can be divided into two categories. Parametric models describe probability using a fixed set of parameters that fit a certain kind of distribution function. Nonparametric models describe the probability as empirical distributions calculated from the observed data set.

E. Parametric models

The most common parametric method used for probabilistic modelling is Gaussian distribution, also known as the normal distribution. It can be applied for both the harmonic current magnitude and phase angle and it also takes into account their variation. This approach would be acceptable if a load current had only one operating point and the variation approximated a normal distribution. The advantage of the normal distribution is that it can be described with only two variables: mean (expected) value and variance.

Because of the magnitude-phase or similarly, real-imaginary component co-dependency, a more appropriate method would be to use bivariate (joint) distribution. A bivariate normal distribution is defined by the covariance matrix, which describes both mean values, their variance, and the covariance between the two values. Since a harmonic current can have a large magnitude, but a small phase angle variation, or similarly, large real component, but a small imaginary component variation, the resulting probability distribution would be elliptical, not circular, thus describing the possible values more accurately.

Fig. 1a and 1c present an example of measured fundamental current, including normal distributions for both complex components separately and a joint bivariate normal distribution surface an ellipse with radii of 2 standard deviations (two-sigma or 2σ ellipse), which includes about 95% of the values.

The drawback of the normal distribution approach is that it is a generalization, and if a harmonic current phasor variation has a distinctive non-Gaussian shape, as it is often with variable non-linear loads, using the normal distribution to describe the probability results in missing points or points which do not exist. When a load has multiple stable operating points, the effect is even more evident, as the normal distribution approach encompasses both operating points as a single distribution. Fig. 1b and 1d present an example of a joint normal distribution of 5th harmonic current of a load with three distinct operating points. The normal distribution treats the individual operating points as one with a considerable variation.

To deal with the issue of multiple operating points, cluster analysis can be used. There are many different algorithms like k-means, expectation-maximization (EM), etc. The primary purpose of these algorithms is to group the data into separate clusters. To describe the probabilistic behavior of a cluster, a probabilistic model would still be applied after the clustering.
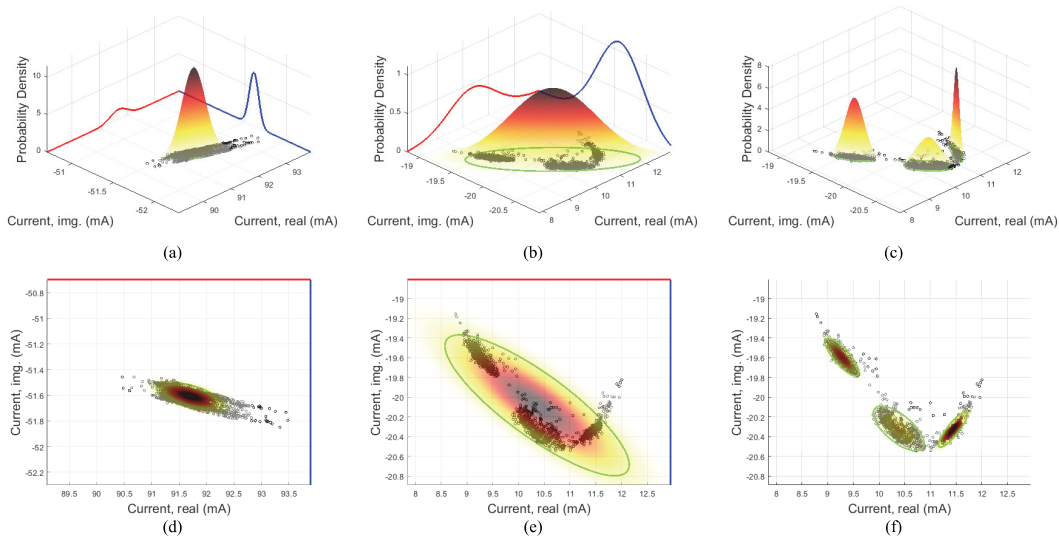
Figure 1. Comparison of parametric probabilistic distributions from measurement data. (a) and (d) represent the side and top view of a bivariate normal probability distribution of fundamental current phasor components of a PC monitor during video playback. (b) and (e) represent a bivariate normal probability of 5th harmonic current of a PC during a stress test and (c) and (f) represent a gaussian mixture model of the same data. Black markers are the 1-second measurement results during 1 hour of measurement. Red and blue curves represent the probability distributions of each component respectively. The green ellipse represents the area of two standard deviations (2σ), and the warm-colored surface represents the joint normal distribution

An example of such a technique is the Gaussian mixture model (GMM). Such an approach has been reported in the case of modeling power quality parameters [12]. The data is clustered using, for example, the EM algorithm and then the probabilities described using a set of bivariate Gaussian distributions with specified proportions. The EM method is iterative and convergent, which means that the result can depend on the initialization condition selection. The convergence can also be optimized, but this procedure is rather complicated and requires more iterations. An example of GMM from the previous data is presented in Fig. 1c and 1f. In this example, the resulting probability distribution is composed of three distinct normal distributions, which fits the data quite well. One drawback of the GMM is that the standard algorithm requires the number of Gaussian components to be specified beforehand, although algorithms are available to estimate the best combination.

F. Nonparametric (empirical) models

One of the most used nonparametric approaches is kernel density estimation (KDE). The usage of this approach under certain conditions to model harmonic current magnitudes and phase angles has been published in [13], [14]. However, analyzing the components separately will only provide information about the probability of both parameters separately, and reconstructing phasors from the said probabilities can result in inaccurate data.

In order to eliminate such errors, a bivariate method is required due to magnitude-phase or real-imaginary codependency. A bivariate KDE model can represent the distribution of a harmonic current quite well, but it has some drawbacks. The KDE algorithm requires assumptions about the bandwidth in both dimensions, which will affect the shape of the final distribution. The probability itself is stored as curve (univariate) or a surface (bivariate) of predefined points, thus resulting in a large amount of data, in quantity which depends on the resolution that is required [15], [16]. Fig. 2 presents an example of a bivariate kernel density estimation for the 5th harmonic current of a load, including KDEs for both complex components separately and a KDE surface. The amount of data required to describe the KDE depends on the number of points on the surface.

Compared to the computation-intensive KDE method, a simple nonparametric way of representing the harmonic current is to create an empirical bivariate histogram of probability. A histogram is simply a grouping of data into bins by counting how many data points fall inside the bin. The number of bins must be specified beforehand. The histogram data can then be normalized to represent probability density by using (1) for the bivariate histogram:

$$p_{i,j} = \frac{c_{i,j}}{N \cdot w_i \cdot w_j} \tag{1}$$

Fig. 3 presents an example of a bivariate probability histogram with their corresponding complex components. The number of bins, or resolution, is the essential factor in determining the shape of the probability distribution.
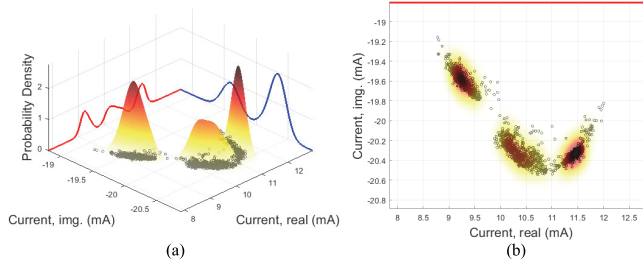

Figure 2.   Side (a) and top (b) view of bivariate kernel density estimates of 5th harmonic current of a PC during a stress test.
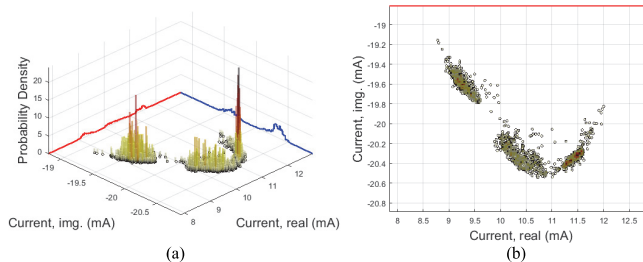

Figure 3. Side (a) and top(b) view of bivariate histograms of 100x100 bins of 5th harmonic current of a PC during a stress test.
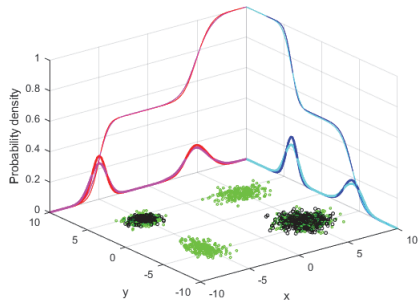
Figure 4. Example of simulated data from KDE using only CDF of both variables separately. Black and green markers represent the original and simulated data points. The red and blue curves represent the PDF (thick) and CDF (thin) of original data, magenta and cyan curves represent the respective probability distributions of the resulting simulated data.

IV. PROPOSED NONPARAMETRIC MODEL

The main issue with non-parametric bivariate distributions is that generating probabilistic data can be complicated since both components of the bivariate data have to be treated as codependent variables, otherwise, data points can be generated that were not part of the original data set. Traditionally, simulated data is generated by sampling points from cumulative distribution function (CDF) by using random numbers between 0 and 1 and matching them to the function. However, due to the joint properties of the bivariate data, using CDFs separately is not suitable for realistic simulations. Fig. 4 shows how this method leads to the creation of false samples while the distribution functions remain the same. Since there is little documentation on bivariate nonparametric probabilistic data sampling, an alternative method is proposed.

By using bivariate component modeling (amplitude-phase or real-imaginary components), it is possible to produce a sum of the harmonic emission from any simultaneously connected loads. When only rms values are used, depending on the variation of harmonic phasors, it is not possible to get adequate results, as often the sum of phasor magnitudes is not equal to the vector sum of said phasors. For example, the higher current harmonics of LED lamps exhibit a high amount of variation between different lamp models that can cause partial cancellation of harmonics if connected simultaneously [17].

This paper presents an empirical approach to nonparametric probabilistic bivariate harmonic current modeling. The model describes the probabilistic distribution of load harmonic current and maintains a decent compromise between data size and accuracy. The data representation is similar to a histogram, but instead of using a PDF bivariate mesh to store the data, a set of linked CDFs arrays are used. This method reduces the data size required to represent harmonic current and it requires a minimal amount of recalculation when used in simulations since CDF is readily available. One of the benefits of this type of empirical model is that extreme values can also be represented. It means that using this model in simulations can lead to the detection of potential problems in harmonic distortion levels which other models might miss.

A compromise between data size and resolution is necessary to reduce the number of points required to define the model. The resolution can be defined by the accuracy required to represent the current harmonics, which can be based on the harmonic current phasor magnitude. Often, a value of less than 1% is rarely needed and it is unnecessary to have too much detail of the variation because some of it can be caused by noise or the measurement setup itself. After the model is calculated, the resolution can be reduced by aggregation, where necessary. To store a very detailed representation of the harmonic load current, a resolution can be chosen that is comparable to the measurement accuracy of the system used in obtaining the measurement data, or by a specific set of rules. However, the data increases exponentially with resolution and at some point, storing the complete measurement data is less data-consuming.

To construct a model for each current harmonic, a stepped empirical cumulative distribution function (ECDF) is created from first the variable (for example, the real component of the harmonic current) with predefined resolution. The data used for the distribution can be from any fixed-interval measurement results. Then, for each said resolution group, an ECDF of the second variable (for example, the imaginary component) is constructed. This results in N+1 distribution curves, where N is the number of resolution groups. The resulting ECDFs can be stored as a cell structure, for example, in MATLAB as a variable, or as a text file with comma-separated values (CSV), which requires more data storage. The algorithm for model construction is presented in Fig. 5.

Figure 5. The algorithm for proposed model construction.
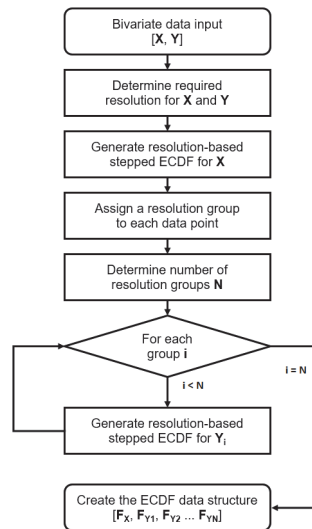
One crucial factor for constructing the harmonic current model is time. A load has to be measured for a duration long enough to obtain a sufficient amount of data points and extreme values that can change with different operating modes or with time. For example, for a battery charging device that takes two hours to charge, it is not feasible to measure only 5 minutes

because, if the harmonic load variation caused by the processes itself, it will not represent the charging cycle accurately.

Measuring harmonic emissions at different scenarios will produce an "image" or a "fingerprint" for each harmonic current of a specific load or load combination for each scenario. The measured data is then converted to the probabilistic representation with a defined resolution. When enough scenarios are obtained, the harmonic current model for the specific scenario can be chosen based on the situation.

It is important to distinguish if the harmonic variations are caused by the internal operating modes or by user selection. For a static load, the time required should be enough to record any internal variations, which are usually small. For variable loads, a typical usage cycle can be recorded and then represented. If some operating modes can be distinguished based on the purpose of the operation, it could be viewed as a separate scenario. However, a single electrical device usually performs a specific task for a specific purpose. There are models available [18] that can simulate when and how often a device is used, i.e. when it is on and when it is off. This is not considered as an operating cycle and it is usually influenced by the external factors and should be viewed separately.

Coupled with the load usage models and network state models, it is possible to use Monte-Carlo simulation to produce an estimation of harmonic emission levels at any PCC based on different scenarios.

Another benefit of this type of model is that is universal and can be used on many different layers of the distribution network. It is possible to represent current harmonics for a single load, group of loads, residential PCC, network feeder or even a transformer. However, this model is mainly suitable for a single load or a group of loads as other factors such as usage patterns, time of day, week and seasonal changes are present at higher layers. By aggregating the model in time, e.g., by measuring longer intervals, which results in loss of resolution and phasor accuracy due to averaging, it would be possible to represent a longer time cycle, such as a day or a week.

One other drawback of the model is that it can only represent a specific scenario, which means that it cannot distinguish the effects of outside factors such as voltage levels, voltage distortion, network failures, etc. In order to determine the effects of outside variables, a measurement should be performed for each specific scenario that represents the corresponding network situation. However, it is possible to group the network situations with similar specific parameter ranges as one scenario and create sub-models for different scenarios. For example, where the voltage level is high, the voltage distortion is high, or both. To simulate a network scenario, a measurement can be carried out using a predefined voltage magnitude and waveform. When enough scenarios are modeled, the opportunity arises to choose the correct scenario model for simulating harmonic emission levels.

V. SIMULATIONS

During the research, several types of household loads, including LED lamps, PCs, PC monitors, etc. were measured for an hour by supplying them with pure sine voltage with the rms value of 230 V.

The measurement was set up using a data acquisition device (DAQ) for signal generation from MATLAB, a low-noise and low-distortion linear amplifier, and a power quality measurement device with the capability of measuring harmonic components' magnitude and phase angles with a 1-second interval. The complete measurement setup is described in [17].

Simulations were carried out for comparing the normal distribution, gaussian mixture model and the proposed nonparametric model by sampling data from the corresponding bivariate probability distributions. In total, 1000 random points of bivariate data was generated for each model and then compared to the original data. To assess the model accuracy, full ECDFs for the original and simulated data were constructed for both bivariate components.

All the models had no problem reproducing harmonic currents with a simple variation pattern. However, with the most intricate variations, the differences between the results of the modeling techniques started to develop. Fig. 6 and Fig. 7 present the simulation results for the 5th and 9th harmonic of a PC during stress tests respectively. The current in these examples had clusters with variations in magnitude, phase angle, and in case of 9th harmonic, also quadrant variations.

Figure 6. Simulation results for 5th harmonic current of PC under a stress test with (a) normal distribution, (b) Gaussian mixture, (c) proposed model. Black markers represent the original data, green markers represent simulated data. Red and blue curves represent the CDF of original data, magenta and cyan curves represent CDF of simulated data.
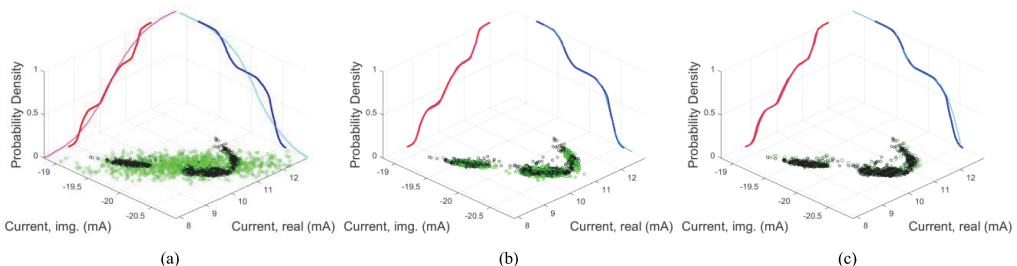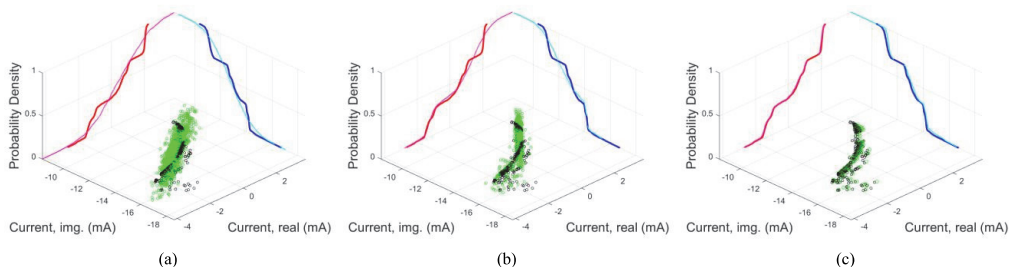
Figure 7. Simulation results for 9th harmonic current of PC under a stress test with (a) normal distribution, (b) Gaussian mixture and (c) proposed model.

By comparing the original and simulated data ECDFs, the results show that the proposed nonparametric model matches and, in some cases, outperforms the parametric GMM. When the harmonic current variation is not easily defined, the nonparametric models can sometimes perform better in these situations due to the GMM model not converging properly. The bivariate normal distribution is not suitable for such variations since it cannot follow the shape of the variation.

Although the nonparametric resolution-based approach, having a discrete distribution, generates less data point diversity, the resulting ECDF still matches the original one, thus proving that even though the very small variations are aggregated, the model is still able to represent the harmonic current variation sufficiently.

VI. CONCLUSIONS

Based on the simulation results, the best parametric approach for bivariate harmonic current modeling is the gaussian mixture model, which could simulate harmonic current accurately while maintaining the shape of the variation in most cases. The proposed nonparametric model, which uses bivariate empirical cumulative distribution arrays (BECDA) could also match, and in some cases outperform the GMM.

The purpose of this kind of models and simulations is to develop a methodology to simulate harmonic currents probabilistically, which can be used in summation for PCC harmonic current estimation. Because of the variations present in modern non-linear loads, aggregating or averaging harmonic current phasors has no meaning as these. Combined with the usage models and large enough database of measured loads, it could be possible to estimate the harmonic current levels by presenting a probability distribution of each harmonic current present in the low-voltage network.

REFERENCES

[1] J. Meyer, P. Schenger, and K. Heidenreich, "Harmonic summation effects of modern lamp technologies and small electronic household equipment," in *21st International Conference on Electricity Distribution (CIRED)*, 2011.

[2] J. Meyer, A. M. Blanco, M. Domagk, and P. Schegner, "Assessment of Prevailing Harmonic Current Emission in Public Low-Voltage Networks," *IEEE Trans. Power Deliv.*, 2017.

[3] M. E. Balci, D. Ozturk, O. Karacasu, and M. H. Hocaoglu, "Experimental verification of harmonic load models," in *Proceedings of the Universities Power Engineering Conference*, 2008.

[4] M. Fauri, "Harmonic modelling of non-linear load by means of crossed frequency admittance matrix," *IEEE Trans. Power Syst.*, vol. 12, no. 4, pp. 1632–1638, 1997.

[5] J. A. Fuentes, A. Gabaldón, F. J. Cánovas, and A. Molina, "Harmonic model of electronically controlled loads," in *Proceedings of the IEEE Power Engineering Society Transmission and Distribution Conference*, 2000, vol. 3, pp. 1805–1810.

[6] Y. Sun, G. Zhang, W. Xu, and J. G. Mayordomo, "A harmonically coupled admittance matrix model for AC/DC converters," *IEEE Trans. Power Syst.*, vol. 22, no. 4, pp. 1574–1582, 2007.

[7] J. Yong, L. Chen, and S. Chen, "Modeling of home appliances for power distribution system harmonic analysis," *IEEE Trans. Power Deliv.*, vol. 25, no. 4, pp. 3147–3155, 2010.

[8] J. Molina, J. J. Mesas, N. Mesbahi, and L. Sainz, "LED lamp modelling for harmonic studies in distribution systems," *IET Gener. Transm. Distrib.*, vol. 11, no. 4, pp. 1063–1071, 2017.

[9] A. B. Nassif, J. Yong, and W. Xu, "Measurement-based approach for constructing harmonic models of electronic home appliances," *IET Gener. Transm. Distrib.*, vol. 4, no. 3, pp. 363–375, 2010.

[10] C. F. M. Almeida and N. Kagan, "Harmonic coupled norton equivalent model for modeling harmonic-producing loads," in *ICHQP 2010 - 14th International Conference on Harmonics and Quality of Power*, 2010.

[11] A. S. Fölting, J. M. A. Myrzik, T. Wiesner, and L. Jendernalik, "Practical implementation of the coupled norton approach for nonlinear harmonic models," in *Proceedings - 2014 Power Systems Computation Conference, PSCC 2014*, 2014.

[12] J. Meyer and P. Schegner, "Characterization of power quality in low voltage networks based on modeling by mixture distributions," in *2006 9th International Conference on Probabilistic Methods Applied to Power Systems, PMAPS*, 2006.

[13] F. Nasrfard-Jahromi and M. Mohammadi, "Probabilistic harmonic load flow using an improved kernel density estimator," *Int. J. Electr. Power Energy Syst.*, vol. 78, pp. 292–298, 2016.

[14] M. Chen, C. Roberts, P. Weston, S. Hillmansen, N. Zhao, and X. Han, "Harmonic modelling and prediction of high speed electric train based on non-parametric confidence interval estimation method," *Int. J. Electr. Power Energy Syst.*, vol. 87, pp. 176–186, 2017.

[15] T. Duong, "ks : Kernel density estimation for bivariate data," *October*, no. October, pp. 1–4, 2009.

[16] S. Węglarczyk, "Kernel density estimation and its application," *ITM Web Conf.*, 2018.

[17] M. Jarkovoi, M. N. Iqbal, and L. Kutt, "Analysis of Harmonic Current Stability and Summation of LED Lamps," in *2019 Electric Power Quality and Supply Reliability Conference (PQ) & 2019 Symposium on Electrical Engineering and Mechatronics (SEEM)*, 2019, pp. 1–8.

[18] M. N. Iqbal, L. Kutt, and A. Rosin, "Complexities associated with modeling of residential electricity consumption," in *2018 IEEE 59th Annual International Scientific Conference on Power and Electrical Engineering of Riga Technical University, RTUCON 2018 - Proceedings*, 2018.

Curriculum vitae

Personal data

Name:	Marek Jarkovoi
Date of birth:	07.07.1988
Place of birth:	Tallinn, Estonia
Citizenship:	Estonian

Contact data

E-mail:	marek.jarkovoi@taltech.ee

Education

2013–2019	Tallinn University of Technology, PhD
2010–2013	Tallinn University of Technology, MSc, *cum laude*
2007–2010	Tallinn University of Technology, BSc, *cum laude*
1995–2007	Tallinn Secondary Science School, Secondary education, *silver medal*

Language competence

Estonian	Fluent
English	Fluent
Russian	Basic level

Professional employment

2008	Tallinn Lilleküla Gymnasium, Physics teacher
2009	Energiatehnika OÜ, Consultant (practice)
2013-2016	Tallinn University of Technology, Engineer
2016-2017	Tallinn University of Technology, Junior researcher
2018…	Tallinn University of Technology, Engineer

R&D related managerial and administrative work

2007-2011	Tallinn University of Technology Student Council, member of the educational committee
2009	TTÜ Student Research Competition and Conference, project manager and organizer
2014	Physics Olympiad Tallinn regional round, member of the committee

Honours & awards

2007	International Physics Olympiad, honourable mention
2016	Olev Liik grant for doctoral studies
2017	Best presentation in Electrical Engineering session (16. International Symposium "Topical Problems in the Field of Electrical and Power Engineering"

Elulookirjeldus

Isikuandmed

Nimi:	Marek Jarkovoi
Sünniaeg:	07.07.1988
Sünnikoht:	Tallinn, Eesti
Kodakondsus:	Eestlane

Kontaktandmed

E-post:	marek.jarkovoi@taltech.ee

Hariduskäik

2013–2019	Tallinna Tehnikaülikool, PhD
2010–2013	Tallinna Tehnikaülikool, MSc, *cum laude*
2007–2010	Tallinna Tehnikaülikool, BSc, *cum laude*
1995–2007	Tallinna Reaalkool, Keskharidus, *hõbemedal*

Keelteoskus

Eesti keel	Kõrgtase
Inglise keel	Kõrgtase
Vene keel	Suhtlustase

Teenistuskäik

2008	Tallinna Lilleküla Gümnaasium, Füüsikaõpetaja
2009	Energiatehnika OÜ, Konstultant (praktika)
2013-2016	Tallinna Tehnikaülikool, Insener
2016-2017	Tallinna Tehnikaülikool, Nooremteadur
2018…	Tallinna Tehnikaülikool, Insener

Teadusorganisatsiooniline ja -administratiivne tegevus

2007–2011	Tallinna Tehnikaülikooli Üliõpilasesindus, haridustoimkonna liige
2009	TTÜ Üliõpilaste Teadustööde Konkurss ja Konverents, projektijuht ja korraldaja
2014	Füüsikaolümpiaadi Tallinna piirkonnavoor, komisjoni liige

Teaduspreemiad ja tunnustused

2007	Rahvusvaheline Füüsikaolümpiaad, aukiri
2016	Olev Liigi nimeline doktoriõppe stipendium
2017	Parim ettekanne Elektrotehnika sessioonis (16. Rahvusvaheline Sümpoosion "Topical Problems in the Field of Electrical and Power Engineering"